A STUDY OF OPTICALLY STIMULATED LUMINESCENCE IN Al_2O_3 FIBERS FOR THE DEVELOPMENT OF A REAL-TIME, FIBER OPTIC DOSIMETRY SYSTEM

By
JERIMY CLIFFORD POLF

Bachelor of Science
Oklahoma State University
Stillwater, OK
1998

Masters of Science
Oklahoma State University
Stillwater, OK
2000

Submitted to the Faculty of the
Graduate College of the
Oklahoma State University
in partial fulfillment of
the requirements for
the Degree of
Doctorate of Philosophy
August, 2002

A STUDY OF OPTICALLY STIMULATED

LUMINESCENCE IN Al_2O_3 FIBERS

FOR THE DEVELOPMENT OF A

REAL-TIME, FIBER OPTIC

DOSIMETRY SYSTEM

Thesis Approved:

Thesis Adviser

Dean of the Graduate College

ACKNOWLEDGEMENTS

I would like to think a number of people for helping me to realize my potential and helping me to reach this point in my life. First of all, I would like to thank Dr. McKeever for giving a clueless, slow-to-comprehend undergraduate a job. Over the years working in Dr. McKeever's research group, I have learned so many things, many of which have nothing to do with my research. Everything I have learned from everyone in the research group, I believe will prove to be invaluable to me in the future. I would also like to think all of my professors that gave me too much homework, and test questions that seemed next to impossible to solve. It was during the long nights of problem solving and studying that I gained an understanding of Physics and an understanding to approach and solve any possible problem that I will ever face. Also, I would like to thank Dr. Mark Akselrod for all providing us with all the samples we could ever study and then some, as well as for all the guidance he gave me as an undergrad and a graduate student. I would like to thank Mr. Art Lucas for all the insightful stories, and for his amazing ability of always knowing the answer to those tough questions that nobody else could answer.

I owe a lot of thanks to Dr. Paul Westhaus for all of his work to get the Photonics program at OSU started, and helping to make sure that I was a part of it. I would like to thank the NSF and the Integrated Graduate Education for Research and Technology (IGERT) program for the financial support. I would like to thank Dr. Lars Bøtter-Jensen for the opportunity to live and work in Denmark at the Risoe National Laboratories.

Next I would like to thank every member of my family for supporting me even when I was less than appreciative of it. I believe that without my father's example of hard work, determination, and perseverance, I never would have had the bull-headed, refusal to quit needed to reach this point in my life, and thanks mom for always being a mom. Thank you mom for always making sure I was eating right and always telling me (and anyone that would listen) how proud you were of me. Thank you to Trey, Hunter, Lyndsey, Carissa, Jessica, and Amanda for being there to give me someone to try and inspire to work hard for what they want. Whenever I was feeling beaten, I knew that if I worked harder and succeeded at what I was doing, that it might show my cousins and nieces that they can have whatever they if want they work hard and never quit. Also, I would like to think my two nieces, Scooter (Jessica) and Chubs (Amanda) for always loving their uncle Jerimy entirely too much and for always helping to laugh and have fun.

Finally, I would very much like to thank a group of men that may have just saved my life. To my brothers at the Beta Kappa chapter of the Phi Kappa Tau Fraternity, THANK YOU. You came into my life when I was headed in the wrong direction. Thanks to you guys, I had a reason to work hard and stay in school. You helped me when the classes were a little too hard, and taught me how to be a successful college student.

Also, I think that it is important to mention the importance of the 3M corporation for their continued production of Duct Tape, black electrical tape, and double sticky tape. Without these three items I believe that none of my experiments would have been

possible. Whenever an experiment was not aligned correctly or light from an outside source was leaking into the sample chamber, the best fixes always involved some the use of some combination of these three items.

TABLE OF CONTENTS

LIST OF FIGURES

Chapter 1

1. Introduction

1.1 General History of Luminescence Radiation Dosimetry

Radiation dosimetry is the measurement of the absorbed dose of radiation resulting from the interaction of radiation with matter.[1] The absorbed dose is the energy imparted per unit mass to a target, where the energy imparted is essentially the energy removed from the radiation field. In practice, however, radiation dosimetry is the determination of absorbed dose in the medium of interest – i.e. the dosimeter. The dose measured in the dosimeter is then related to the absorbed dose in the target. Typically, this involves the detection of some quantity, (such as temperature, electronic charge or, in the present case, luminescence intensity) which is proportional to the absorbed dose in the medium of interest.

The field of modern luminescence radiation dosimetry had its beginnings in the late 1940's and early 1950's with the work of Randall & Wilkins, Garlick & Gibson, and Daniels, Boyd, and Saunders as well as many others.[2,3,4] Research on luminescence produced during thermal stimulation of materials following their irradiation led Daniels and his research group at the University of Wisconsin to the observation that the intensity of luminescence produced by a material during heating increased with the dose of radiation absorbed by the material. This led them to suggest the use of the luminescence signal produced during heating as a tool for radiation dosimetry.

Since that time the application of luminescence techniques to the field of radiation dosimetry has grown immensely. Luminescence dosimeters have been produced for the

measurement of heavy particles such as neutrons and alpha particles as well as high-energy photons such as X-rays and gamma rays.[5] This work has led to the advancement of two types of luminescence as dosimetry techniques. These are thermally stimulated luminescence, more popularly known as thermoluminescence (TL), and optically stimulated luminescence (OSL). These two techniques differ in the form of stimulation used to read out the luminescence signal from the dosimeter. For TL the dosimeter is heated, and for OSL the dosimeter is illuminated. Both TL and OSL have been widely used in the field of commercial radiation dosimetry and shall be discussed in greater detail in later chapters. For now we simply note the particular importance of TL and OSL to the field of radiation dosimetry as well as to the work presented in this thesis.

1.2 General History of Thermoluminescence

The first reported observation of thermoluminescence was by Sir Robert Boyle in 1663, and observations of naturally occurring thermoluminescence were reported by many others throughout the period from the late 1600s to the late 1800s.[6] The term thermoluminescence (TL) was not coined until 1895 by Weidman and Schmidt, who pioneered the study of "artificial" TL, since the luminescence was induced by an intentional exposure to radiation, by irradiating their samples with an electron beam to induce the TL signal.[7] Artificial TL induced by exposure to X-rays was studied by Trowbridge and Burbank in 1898.[7] These authors drained the TL from several naturally occurring phosphors, and then restored the signal by exposing the phosphors to X-rays. The study of TL focused on signals from natural and synthetic phosphors after exposure to many different kinds of irradiation, such as X-rays, β rays, UV light, and electron beams.[8,9,10] However, a theory of the TL process was not formalized until Randall and

Wilkins published their papers in 1945. Randall and Wilkins considered the thermal release of electrons from traps, and assumed that the released electrons did not retrap, but instead recombined to produce luminescence. From this they developed the standard expressions for first-order TL kinetics.[2] This was followed by the work of Garlick and Gibson, who assumed that the retrapping process dominated the recombination process to produce the so-called second-order TL kinetics.[3] The kinetic equations considered by Randall and Wilkins and Garlick and Gibson were generalized in 1964 by May and Partridge to develop the general order kinetic equations for TL.[11] From these expressions many techniques were developed to obtain information about trap distributions by analyzing the TL from a sample.

Daniels and colleagues first used LiF as a dosimeter in 1953, in order to measure the radiation resulting from an atomic weapons test and to measure the internal radiation dose received by a patient during cancer treatments.[4,12] LiF became the first widely used material as a thermoluminescence dosimeter (TLD) when a version of the material doped with titanium and magnesium (LiF:Mg,Ti) was developed. This material was marketed commercially by Harshaw Corp. (later Bicorn, and currently Saint-Gobain) and quickly became, and remains, the industry standard. However, the complicated nature of the luminescence signal from this material and the various handling techniques for employed during the readout of the material has fueled the ongoing search for better materials for use as TLDs. Over the years numerous materials have been suggested as alternatives. These materials include beryllium oxide (BeO), calcium sulphate doped with Dy and Tm ($CaSO_4$:Dy, $CaSO_4$:Tm), and calcium fluoride (CaF) doped with several different types of impurities, just to name a few of the more popular ones.[13] In particular, an

increasingly popular material is aluminum oxide (Al_2O_3) which is the material used in the research presented in this thesis.

1.3 General History of Optically Stimulated Luminescence

OSL has become a common dosimetric measurement method for several different types of applications. The first modern use of OSL for dosimetry was by Huntley *et. al.* to determine environmental radiation doses received by geological samples in order to determine the age of the sample.[14] This is typically done by continuously stimulating grains of natural quartz or feldspars from the geological sample with light and measuring the luminescence signal produced. This type of measurement is known as continuous wave or CWOSL. For quartz grains the color of the stimulation light typically used is green with the measured emission wavelengths in the ultra-violet (UV). For feldspars, the stimulation wavelengths used are usually in the infra-red (IR), and the emission wavelengths again are in the UV. Thus a distinction has been made in the literature depending upon what wavelength of stimulation light is used. Stimulation with visible light is known as OSL, and stimulation with infra-red light is known as IRSL.[15] Since the mid 1980's OSL and IRSL dating methods have been used to date a variety of different types of geological samples including wind and water deposited sediments.

The use of OSL for personal dosimetery is a relatively young field developing mostly in the 1990s, but the idea of OSL as a dosimetry technique has been around for a long time. OSL was first suggested as a possible dosimetry technique by Anatov-Romanovskii et al. in the 1950s.[16] The first experimental use of OSL for radiation dosimetry was presented in 1967 by Braunlich et al. and Sanborn and Beard[17,18].

Many different OSL measurement techniques have been studied over the years in an attempt to develop a usable OSL dosimeter. Many tried using CW-OSL to develop a dosimeter with different phosphors such as MgS, CaS, SrS, and SrSe doped with different rare earth elements.[12,13,19] These materials possessed a high sensitivity to irradiation, but suffered from a fading of the optical signal at room temperature. This led to the development of a measurement system in which the trapped charge induced during irradiation is optically transferred to trapping states that are unstable at room temperature. The optical signal is then measured after stimulation as the charge leaks away from the unstable traps. Since the optical signal is measured after the optical stimulation this methods is known as delayed optically stimulated luminescence (DOSL).[20] This method is also called cooled OSL (COSL) when the sample is cooled below room temperature making the unstable traps thermally stable. Charge is then optically transferred into them, and the luminescence signal is read as the sample is warmed to room temperature[21]. DOSL and COSL methods were tried with several phosphors, but showed to be an insensitive method for measuring dose. A more recently developed method named pulsed optically stimulated luminescence (POSL) has proven to be the most sensitive OSL method to date[22]. This method stimulates the material with a train of light pulse and synchronously measures the luminescence from the dosimeter between the light pulses. This method has been developed into a commercial optical dosimetry system using an Al_2O_3:C dosimeter that is marketed by Landauer Inc.

1.4 General Background of Fiber Dosimeters

Optical fiber dosimeters offer a unique capability for remote monitoring of radiation in difficult-to-reach and/or hazardous locations. Optical fiber sensors can be located in the

radiation hazardous areas and optically interrogated from a safe distance. A variety of remote optical radiation dosimetry methods have been developed. All of these methods are based on some form of radiation-induced change in the optical properties of materials such as: radiation induced darkening (optical attenuation) or luminescence from radiation-induced or natural defects in crystals, phosphors, and glasses.

1.4.1 Optical Attenuation Fiber Dosimeters

It is well known that when glasses are exposed to relatively high radiation doses, the color of the glass changes due to the formation of color center defects, and the degree of darkening can be correlated to the dose absorbed by the glass.[23] When a length of optical fiber is exposed to radiation, the radiation-induced darkening in the core of the fiber causes the optical transmission to be reduced. A light source, such as a laser, LED, or spectrally filtered lamp can be used to measure the transmission characteristics of the fiber. A photodetector, such as a photodiode or photomultiplier tube is used to measure the intensity of the transmitted light. One of the earliest applications for this type of dosimeter was on the Navigational Technology Satellite 2 (NTS-2) that was launched in June, 1977.[24] The goal of this mission was to measure radiation doses in space for comparison with predictive models for the outer radiation zone electron environment.

In practice, the determination of the absorbed dose from an optical attenuation dosimeter is complicated by the fact that the radiation-induced darkening fades over time and that the darkening is wavelength dependent.[23,24,25,26] Following exposure, the degree of darkening tends to decrease with time and approaches a steady-state value. This is due to the presence of thermally unstable defects and trapping states. These traps thermally anneal at room temperature over time leaving only stable traps and defects. The

wavelength dependence of the darkening is more pronounced at shorter wavelengths and falls off sharply for wavelengths greater than 800 nanometers.[27] Based on these characteristics, it is seen that for high-dose dosimetry applications, probes utilizing longer wavelengths are preferable.

The sensitivity of the fiber probe may be adjusted simply by choosing a suitable length of fiber. The lower the dose to be measured, the longer the length of the fiber needs to be. However, it has also been shown that changing the elemental composition of the fiber can also change its radiation sensitivity. Pure silica core fibers have the lowest sensitivity to radiation and therefore offer the best choice for transmitting information through high radiation environments. Incorporation of various dopants into the fiber core such as B, Ge, P, or Pb provides a significantly higher level of darkening per unit radiation. A given length of Pb-doped silica fiber can be more than 4 orders of magnitude more sensitive than a pure silica core fiber.[25] A silica fiber containing 60 % PbO by weight has been developed for use in radiation therapy.[28] A twenty millimeter length of fiber is capable of measuring a 1 Gy dose with a precision of about 2 %. This type of dosimeter has been developed to measure and verify the dose given to a patient during radiotherapy cancer treatment.

1.4.2 Radioluminescent Fiber Dosimeters

Practically all glass and crystalline materials yield prompt luminescence, or radioluminescence (RL), when exposed to ionizing radiation due to the presence of native impurities or defects. In some cases, radiation-induced defects are also luminescent and may be monitored as a function of dose. In general, the intensity of radioluminescence signals is proportional to the dose rate.

The radiation-induced radioluminescence properties of silica core fibers were studied as early as 1981.[28] The pure silica fiber showed two distinct luminescence bands at 450 and 650 nm. The intensity of the 450 nm has been shown to increase linearly up to a dose of about 140 kGy, and continues to increase (sublinearly) up to a saturation dose of about 340 kGy. The 650 nm band is seen to decrease with increasing dose due to radiation-induced darkening at longer wavelengths.[29] Using this fact to calculate the effect of the radiation-induced darkening, the 450 nm band can be corrected to compensate for radiation-induced transmission losses. With correction, the dose response of the 450 nm luminescence band is linear up to 340 kGy.

The level of the radiation-induced attenuation is clearly more severe for shorter wavelengths than for longer wavelengths.[27] To exploit this, several efforts have been made to design a radioluminescenct fiber dosimeter with red or near infrared emission. One approach was to attach a luminescent phosphor at the end of the fiber. Phosphors such as $Gd_2O_2:Pr^{3+}$ have been used due to their highly structured emission bands at 650, 765, and 900 nm.[30] When corrections for darkening were made, the dose measurements made with the 900 nm emission were able to measure a dose with a precision of about ±5%. An alternative to attaching phosphors is to directly dope the glass with impurities. The dopant ions are typically rare earth ions such as Pr^{3+} or Eu^{3+}, but other ions have also been used such as Cu^{+}, Cu^{2+}, and Mg^{2+}, to produce long wavelength emission bands.[30,31] The efficiency of the radioluminescence produced in the doped glass dosimeters was seen to be greatly reduced due to the presence of charge traps in the material. Radiation-induced free charge in the material is trapped at a thermally stable charge trap and therefore not be available for recombination required to produce luminescence.

1.4.3 Thermoluminescent Fiber Dosimeters

Thermoluminescent fiber dosimeters operate on the same principles as TLDs. The radiation sensitive element is located at one end of the fiber dosimeter.[32] A high power laser light is coupled into the fiber to heat the dosimeter producing the luminescence. The resulting thermoluminescence is directed back down the same fiber where it is readout using a photomultiplier tube.

A typical TL fiber dosimeter consists of a phosphor directly attached to the end of the fiber optic cable followed by a thin layer of black absorbing material to transfer heat to the phosphor. The phosphors used for TL fiber optic dosimeters are typically $CaSO_4$:Mn, $CaSO_4$:Dy, or CaF_2:Tm. The heating of the dosimeter is accomplished by an infrared diode laser with a typical output power of greater than 400 mW. Laser heating with this method is very efficient and with just 400 mW of power, the phosphor can be heated to several hundred degrees in less than a second, and in fact, heating rates as high as 1200 °C/sec. have been recorded.[32] The luminescence is directed back down the fiber optic cable and separated from the laser stimulation light by a beam splitter and optical filters. The resulting TL is detected by a PMT interfaced with a computer to record the resulting glow peak. TL fiber dosimetry systems are sensitive enough for environmental monitoring applications, and the sensitive dosimeter can be located up to 200 meters from the stimulation and detection sources.[33] Multiplexed systems have been developed so that several TL fiber dosimeters can be measured by a single stimulation and detection system.[32]

1.4.4 Optically Stimulated Fiber Dosimeters

OSL fiber dosimeters operate on the same principles of optically stimulated luminescence dosimeters. Laser light is directed down the fiber optic cable to stimulate the radiation sensitive element attached to the other end. The laser light stimulates trapped charges to recombine producing luminescence. The luminescence is directed back down the fiber optic cable where it is detected by a PMT.

OSL fiber dosimeters are constructed by attaching a radiation sensitive element to the end of a fiber optic cable. The radiation-sensitive element may be a phosphor such as, MgS or BaS doped with Sm, Ce, or Eu. Also, the sensitive element may be made of radiation-sensitive glasses, such as Cu and Eu doped glass, or single crystals, such as Al_2O_3 grown in fiber form.[31]

OSL fiber dosimetry systems are similar to TL fiber dosimetry systems in that a laser is used to stimulate the sample, and the luminescence is separated from the stimulation and filtered before being detected by a PMT. For OSL fiber dosimeters, the laser power may be much lower since heating of the dosimeter is not required (and in general discouraged). The stimulation light must, therefore, be more energetic to obtain efficient stimulation of the trapped charges, and this results in use of visible light.

OSL fiber dosimeters have been, and are currently, being developed for a wide variety of applications. They have been demonstrated using a MgS:Sm,Ce phosphor, which have shown a linear dose response over a range from 8×10^{-5} to 4×10^{-2} Gy making it suited for monitoring in environmental applications.[34,35] Also, an OSL fiber dosimeter has been developed showing a linear dose response over the range from 1×10^{-2} to 1×10^{2} Gy for use in dose measurement in radiotherapy treatment. This dosimeter is

made by attaching a length of Cu^{+}-doped glass to a fiber optic cable.[31] The OSL dosimeter has been tested with a variety of types of radiation as used for radiotherapy including protons, electrons, and gamma rays, and shows a good response to several types of particles, and for a broad range of particle energies.[36] Further development of this fiber dosimeter is currently underway including clinical testing.

1.5 This Thesis

OSL fiber dosimeters show enormous potential for the remote monitoring of radiation doses in a variety of different environments. In particular, the ability for a fiber dosimeter to read the dose received by a patient during radiotherapy in real time during the irradiation procedure is an attractive application for the medical community. Currently the dose received by a patient is measured by dosimeters placed outside the body close to the region of exposure. The dosimeters must then be retrieved and read out after the treatment. Therefore any information about the radiation dose received by the patient is only known after the treatment. Also, many times the patient is being treated for a tumor that is located in areas that are not suitable for the placement of dosimeters. In this instance, the dose is calculated from models developed through the irradiation of phantoms used to mimic the human body. Therefore, no actual dose to the patient is ever measured. The radiation exposure that the patient receives is based on what exposure time was needed to deliver the desired dose to a human phantom. In light of this, a method of measuring the actual dose received by a patient while the patient is being exposed is a very desirable tool.

For this project, Al_2O_3:C in fiber form was used for the purpose of attachment to a fiber optical cable in order to produce an OSL fiber dosimeter. The excitation/emission

properties and radiation-induced luminescence of the Al_2O_3:C fibers were studied to determine the most desirable properties for development of an OSL fiber dosimeter. Also, the real-time luminescence signal produced from the fibers during irradiation was measured. This included the characterization of both the radioluminescence and the real-time OSL. Methods of coupling the Al_2O_3:C fiber to fused silica fiber optic cables in order to maximize transmission of both the stimulation light and the luminescence signal were studied. Next, a real-time readout system for the dosimeters was developed. The readout system was developed to be portable and capable of measuring the absorbed dose and dose rate from the Al_2O_3:C fiber probes in real-time over the dose range of interest.

Chapter 2

2. Thermal and Optical Luminescence Processes in Solids

2.1 Basic Concepts

Luminescence from a solid is described as the emission of light after the absorption of energy from an external source. The emission can be categorized as either fluorescence or phosphorescence depending on the process in the solid that occurs after the absorption of energy. The two processes can typically be distinguished by the amount of time between the absorption of the energy and the emission of the luminescence.[37] Fluorescence is the emission following the excitation of an electron from its ground state energy level to an excited state and its subsequent relaxation back to the ground state. Therefore the delay between absorption of energy and emission is determined by the lifetime of the excited state. This can be very short, on the order of picoseconds, or in the case of spin or parity forbidden transitions, may be as long as several milliseconds. The process of excitation and emission involved in production of fluorescence is shown in figure 2-1. Phosphorescence occurs when the relaxation to the ground state, after the absorption of energy, is delayed by the transition of the excited electron into and out of a metastable energy state. This metastable state may be defined as a localized energy state other than the ground or excited states of the electron. The metastable state is a localized energy state, possibly at some defect site, in the solid where the electron will be "trapped." The electron will remain in this state until it is stimulated with sufficient energy to overcome the potential well of the localized state.

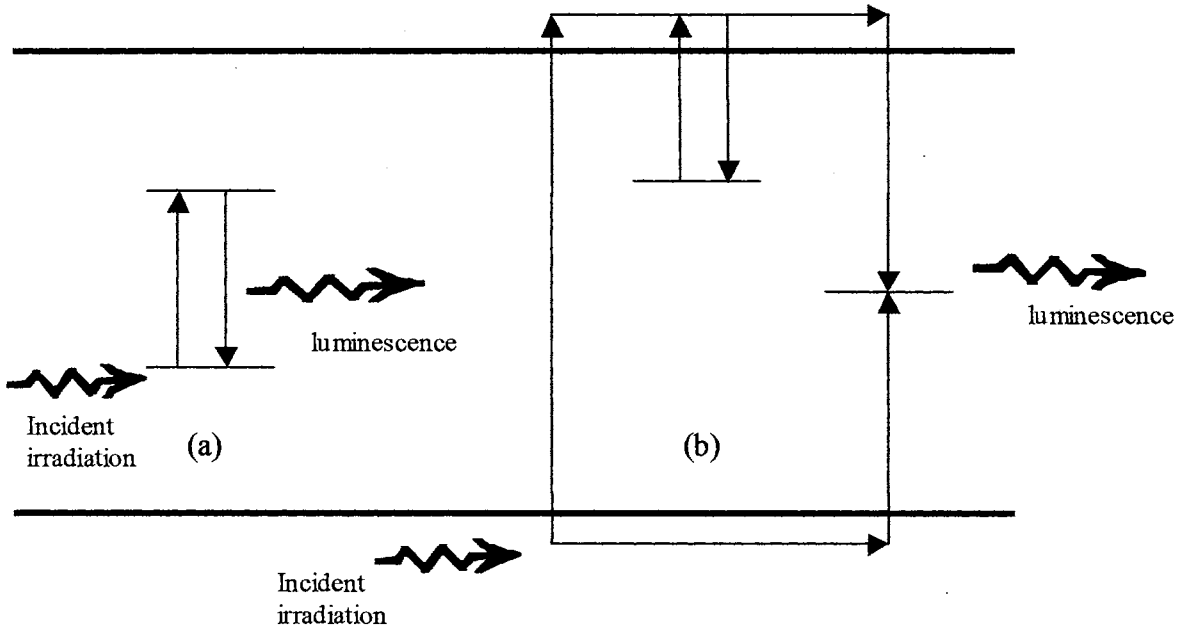

Figure 2-1: A schematic energy level diagram showing (a) the excitation and relaxation of a localized charge in the production of fluorescence, and (b) the excitation, trapping and release of charge from defect sites, and recombination of charge in the production of phosphorescence.

For this type of process, where the return of the electron to the ground state is delayed for a finite time by the lifetime of the electron in a metastable state, the resulting emission is known as phosphorescence. In the case of phosphorescence, the emission of luminescence will be delayed for an amount of time equal to the lifetime of the electron in the metastable state. For the purpose of radiation dosimetry, the lifetime in the trap needs to be long, with the luminescence only being seen after stimulation. The luminescence from the dosimeter is measured a finite period of time after the dosimeter has been irradiated with the production of luminescence being initiated by the stimulation of the dosimeter during readout.

Irradiation of a solid can result in the ionization of an electron into the conduction band leaving a delocalized hole in the valance band (ionizing radiation), or can excite charge that is already trapped into its respective delocalized band for the case of nonionizing radiation. Typical types of ionizing radiation are gamma rays, x-rays, beta and alpha particles, protons, and neutrons, and some types of nonionizing radiation include UV and visible light, depending of the band gap of the material. Ionized electrons and holes may move through the crystal in their respective delocalized bands where they may be trapped at a localized metastable energy level at a defect site in the solid, or recombine with a charge of opposite sign already trapped at a localized defect site. A schematic of the charge ionization, trapping, release, and recombination process is shown in figure 2-2. The energy level of the charge trapped in the metastable state will be less than that of the charge (electron/hole) in its respective delocalized band by an amount known as the activation energy (ΔE) of the trap. The charge may be released

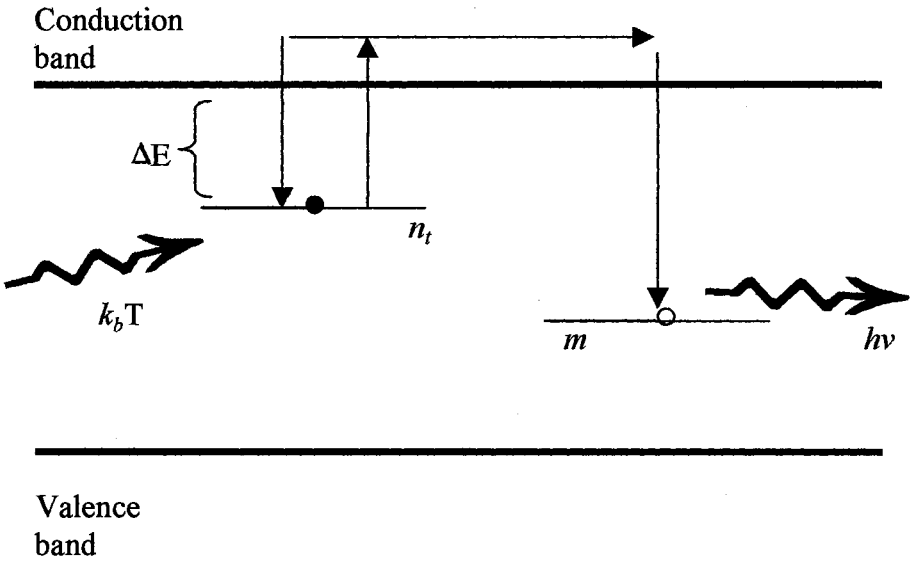

Figure 2-2: A schematic of the TL process in a one trap-one recombination center model. The trap is an electron trap with activation energy ΔE and the electron is released into the conduction band where it recombines with a trapped hole at a recombination center.

from the traps by stimulation with energy comparable to the activation energy of the trap. A delocalized charge may recombine if it encounters an oppositely charged defect in the solid, which is known as a recombination center. Recombination occurs when a charge encounters, and is localized by the coulombic potential of an oppositely charged defect site in the solid. This creates an excited defect center, which then can relax to its ground state via the emission of a photon.[38]

The localized energy levels created by defects in solids can play two roles in the production of luminescence. These are named either charge traps or recombination centers. Charge traps are those sites at which the probability of the release of a localized charge when stimulated into its respective delocalized band is greater than the probability of recombination of the trapped charge with a charge of opposite sign.[37] Conversely, a recombination center is defined as one in which the probability of recombination with a delocalized opposite sign charge carrier is greater than that of the charge being released from the localized state when stimulated.

2.2 *Theoretical Model of Thermoluminescence*

A model of thermoluminescence will be developed using the flow of charge in the crystal during heating. This simple model will use only one trapping state and one recombination center, but will then be expanded to include additional shallow and deep trapping centers.

2.2.1 Simple Model of TL

In this section, a simple model known as the one trap-one recombination center model will be discussed for the processes of thermoluminescence and optically stimulated

luminescence. A schematic of the TL process for the one trap-one recombination center model is shown in figure 2-2. In order to describe the TL process mathematically, several assumptions will be made to allow analytical equations to be written for the processes involved in the model. First, it is assumed, that only electrons are released from traps during the TL process. It should be noted that a model can just as easily be described using the release of holes during the TL process. Second, we make the assumption that all transitions out of localized traps take place via the conduction band. Next, that all transitions of electrons into localized traps are nonradiative producing only phonons, and that all transitions into recombination centers (trapped holes) are radiative producing photons. Finally, for this model, we assume that the sample is heated at a linear rate during readout.

From the above assumptions that no trapped holes are released during heating, we see that the only way that the trapped hole concentration (m) changes is through recombination. Therefore, we see that the luminescence intensity is proportional to the change in the concentration of trapped holes. The luminescence intensity can then be given by the equation

$$I_{TL} = -\eta \frac{dm}{dt}, \tag{2.1}$$

where η is a proportionality constant known as the luminescence efficiency. The luminescence efficiency is defined as the ratio of the number of recombinations that result in the production of a photon, to the total number of recombinations and is not constant for most materials. The TL process can be modeled in terms of a series of rate equations that describe the flow of charge into and out of the delocalized bands and

charge traps during thermal stimulation. The change in concentration of trapped electrons and holes and electrons in the conduction band can be given by

$$\frac{dn_c}{dt} = sn_t \exp[-\frac{\Delta E}{k_b T}] - n_c A_n (N - n_t) - n_c m A_{mn} \tag{2.2}$$

$$\frac{dn_t}{dt} = n_c A_n (N - n_t) - sn_t \exp[-\frac{\Delta E}{k_b T}] \tag{2.3}$$

$$\frac{dm}{dt} = -n_c m A_{mn} \tag{2.4}$$

where n_c, n_t, and m are the concentrations of electrons in the conduction band, trapped electrons, and trapped holes respectively, s is the attempt to escape frequency measured in units of s^{-1}, k_b is Boltzmann's constant, T is the temperature in Kelvin, N is the total concentration of electron traps, A_n is the trapping probability expressed in units of volume per unit time, and A_{mn} is the recombination probability measured in units of volume per unit time. The trapping and recombination probabilities are defined as the products of the thermal velocities of the electrons (v_n) and the capture cross sections of the centers (σ_n, σ_{mn}) as given by the equations

$$A_n = v_n \sigma_n \tag{2.5}$$

$$A_{mn} = v_n \sigma_{mn}. \tag{2.6}$$

It is also noted that electrons and holes are created in pairs in the sample during irradiation, and therefore the total number of electrons and holes taking part in the trapping and recombination process will be equal. Assuming that all holes created during irradiation are trapped, the equal number of electrons and holes can be expressed by the equation

$$n_c + n_t = m. \tag{2.7}$$

Equation 2.7 is known as the charge neutrality condition. Differentiating with respect to time and solving for the change in the concentration of electrons in the conduction band gives the expression

$$\frac{dn_c}{dt} = \frac{dm}{dt} - \frac{dn_t}{dt}. \tag{2.8}$$

Equations 2.2-2.4 and 2.8 represent the system of rate equations describing the movement of electrons during the heating cycle of the TL measurement. These equations are coupled, first-order, nonlinear differential equations that are, in general, analytically insoluble. It should be noted that n_c, n_t, and m are all functions of both time (t) and temperature (T) linked by the heating function T=T(t). To develop an analytical expression for the TL intensity as a function of temperature ($I_{TL}(T)$), several assumptions must first be made to further simplify the above differential equations.

One important assumption is that of "quasi-equilibrium" (QE). This assumption requires that the number of electrons in the conduction band be changing much slower than the number of trapped charges. This assumption is expressed by the equation

$$\frac{dn_c}{dt} \langle\langle \frac{dn_t}{dt}, \tag{2.9}$$

or if the above expression is integrated,

$$n_c \langle\langle n_t. \tag{2.10}$$

Applying the QE approximation made in equation 2.9, to equation 2.8 yields the relation

$$\frac{dm}{dt} \approx \frac{dn_t}{dt}. \tag{2.11}$$

Next, substituting equations 2.3 and 2.4 into equation 2.11 and solving for n_c gives

$$n_c = \frac{sn_t \exp[\frac{-\Delta E}{k_b T}]}{A_{nm}m + A_n(N - n_t)}. \tag{2.13}$$

Substituting this result into equation 2.8 and using equation 2.1 for the TL intensity is obtained to be

$$I_{TL} = -\frac{dm}{dt} = sn_t \exp[\frac{-\Delta E}{k_b T}]\left(\frac{A_{nm}m}{A_{nm}m + A_n(N - n_t)}\right) \tag{2.14}$$

which can be rewritten in the form

$$I_{TL} = -\frac{dm}{dt} = sn_t \exp[\frac{-\Delta E}{k_b T}]\left(1 - \frac{A_{nm}(N - n_t)}{A_{nm}m + A_n(N - n_t)}\right). \tag{2.15}$$

Equations 2.14 and 2.15 are known as the general-one-trap (GOT) expression for TL emission.[39,40] In equation 2.15, the term in round brackets represents the probability that the thermally released electrons will not be retrapped, and the ratio $A_n(N\text{-}n_t)/A_{nm}m$ is the ratio of the retrapping probability to the recombination probability.

To find a first-order solution to equation 2.15, another approximation is often made regarding the size of the retrapping probabilities and the recombination probabilities. One assumption, that was first proposed by Randall and Wilkins that is often made is $mA_{nm} \rangle\rangle (N - n_t)A_{nm}$.[2] That is, the recombination probability is much greater than the retrapping probability. With this assumption equation 2.14 becomes

$$I_{TL} = -\frac{dm}{dt} = sn_t \exp[\frac{-\Delta E}{k_b T}]. \tag{2.16}$$

This equation can now be integrated over the temperature range of the TL measurement. For a measurement in which the temperature is ramped linearly according to the expression $T = T_o + \beta t$, where T_o is the initial temperature and β is the heating rate.

Applying the quasiequilibrium condition of equation 2.11 to equation 2.16, it is seen that $n_t \propto -dn_t/dt$. Substituting dn_t/dt into equation 2.16 and integrating using a linear heating rate, the expression for the concentration of trapped electrons is given by

$$n_t = n_o \exp[\frac{-s}{\beta}\int_{T_o}^{T} \exp[\frac{-\Delta E}{k_b \theta}]]d\theta \tag{2.17}$$

where n_o is the initial concentration of trapped electrons and θ is a dummy variable of integration. Substituting this value back into equation 2.16, the TL intensity is found to be

$$I_{TL} = sn_o \exp[\frac{-\Delta E}{k_b \theta}]\exp[\frac{-s}{\beta}\int_{T_o}^{T} \exp[\frac{-\Delta E}{k_b \theta}]]d\theta. \tag{2.18}$$

This equation for the TL intensity is known as the Randall-Wilkins equation.[2] This expression represents a first-order expression for the TL intensity since it depends on the first power of the carrier concentration. This first-order expression for the TL intensity produces asymmetric peaks with the peak position depending on the activation energy and frequency factor. The shape of the first order TL peak is shown figure 2-3.

The Randall-Wilkins expression was derived using the assumption that recombination dominated over retrapping of the electrons during heating. For the opposite case, when retrapping dominates over recombination ($A_{nm} m \langle\langle A_n (N - n_t)$), along with the assumption that the number of electrons traps is much larger than the number of trapped electrons ($N \rangle\rangle n_t$) and the number of trapped electrons equal the number of trapped holes ($n = m$), we see that equation 2.16 becomes

$$I_{TL} = \frac{dn}{dt} = s(\frac{A_n}{A_{nm} N})n^2 \exp[\frac{-\Delta E}{k_b T}]. \tag{2.19}$$

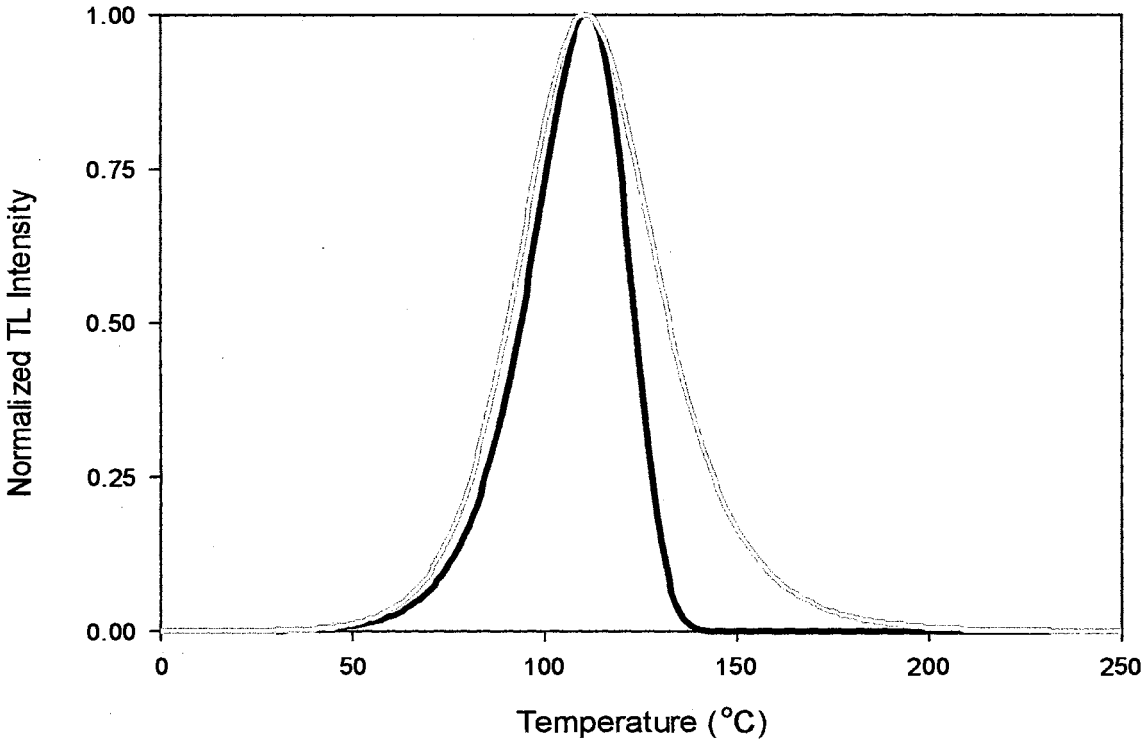

Figure 2-3: First order Randal-Wilkins TL peak generated using equation 2.18 (black) and second order Garlick-Gibson TL peak generated using equation 2.20 (gray).

Note that equation 2.19 depends on n^2 and represents a second-order expression for the TL intensity. Considering the additional assumption that $A_n = A_{nm}$, equation 2.19 can be integrated to yield the expression

$$I_{TL} = (\frac{n_o^2}{N}) \exp[\frac{-\Delta E}{k_b T}] \{1 + (\frac{n_o s}{\beta N}) \int_{T_o}^{T} \exp[\frac{-\Delta E}{k_b \theta}] d\theta\}^{-2}. \tag{2.20}$$

This is the Garlick-Gibson TL expression for second-order kinetics.[3] The second-order expression produces a more symmetric peak shape as shown in figure 2-3. This can be understood from the assumption that retrapping dominates over recombination. Therefore large numbers of electrons are being retrapped and released before recombining spreading out the luminescence over a large temperature range.

The Randall-Wilkins and Garlick-Gibson equations were both derived using specific assumptions about the relative recombination and retrapping probabilities. From the forms of equations 2.18 and 2.20, Rasheedy proposed an equation for TL intensity of general-order with the form of

$$I_{TL} = -\frac{dn}{dt} = s(\frac{n^b}{N_t^{b-1}}) \exp[\frac{-\Delta E}{k_b T}] \tag{2.21}$$

which clearly reduces to the first-order case for $b \rightarrow 1$.[41]

2.2.2 Adding to the TL Model

The one trap-one recombination presented in the previous section describes the main features of a TL glow peak, such as shape of the glow peak, and dependence on the trapped charge concentration, heating rate, and trap depth. Despite the usefulness of the model, we realize that there is no actual material for which one can accurately claim that there is only one trap and one recombination center. Many other methods of solving

equation 2.2-2.4 for cases of multiple traps and multiple recombination centers have been investigated. Methods of numerically solving the rate equations using a mixture of first-order, second-order, and general-order kinetics have been used to fit experimental data and extract information about the parameters of the glow peaks.[42,43] Also, numerical analysis of TL glow peaks has been carried out testing the validity of the quasi-equilibrium approximation and the assumption of a single valued activation energy of the charge traps.[42,44,45]

In most materials, there are several charge traps with different thermal activation energies and several different recombination centers. For a given temperature range over which a TL glow peak appears for a material, there are inevitably traps in the material for which the thermal stability of the trapped charge is greater than that for the TL signal being monitored. That is to say, that there are likely to exist deep traps which retain their trapped charge during a heating cycle that empties the shallower traps for readout of the TL signal. From this, we see that the charge neutrality condition becomes

$$n_t + n_D = m \tag{2.22}$$

where n_D is the concentration of electrons trapped in the deep traps. For a more complete analysis of the TL glow peak, the deep traps can be added to the one trap-one recombination center model.[46] With the addition of deep traps, the charge neutrality condition from equation 2.8 becomes

$$\frac{dn_c}{dt} = \frac{dm}{dt} - \frac{dn_t}{dt} - \frac{dn_D}{dt} \tag{2.23}$$

and the rate equation for the flow of charge into and out of the deep traps is given by

$$\frac{dn_D}{dt} = n_c A_D (N_D - n_D) - sn_D \exp[-\frac{\Delta E_D}{k_b T}] \tag{2.24}$$

where A_D is the trapping probability of the deep traps, N_D is the total concentration of the deep traps, and ΔE_D is the activation energy of the deep traps. This equation is now added to equations 2.2-2.4 for the analysis of the TL glow peak. If the deep trap is considered to be "thermally disconnected," that is, if the charge in the traps is not released during readout of the shallower traps, then the second term of equation 2.24 can be neglected and the rate equation for the deep traps becomes

$$\frac{dn_D}{dt} = n_c A_D (N_D - n_D). \tag{2.25}$$

Including equation 2.25 in the analysis with equation 2.2-2.4 takes into account that the deep traps may capture electrons released from the shallower traps during heating. Therefore the deep traps compete with the recombination centers for the capture of electrons freed from the shallow traps. Using the assumption that the deep traps are full ($N_D \cong n_D$) then a "general-one-trap" equation can be written.[47] The expression for the general-one-trap equation that includes the deep traps becomes

$$I_{TL} = -\frac{dm}{dt} = sn_t \exp[\frac{-\Delta E}{k_b T}]\left(\frac{A_{nm}(n_t + n_D)}{A_{nm}(n_t + n_{D)} + A_{nm}(N - n_t)}\right). \tag{2.26}$$

With the assumption of slow retrapping, this equation reduces to the first-order Randall-Wilkins equation. However, if the assumption of fast retrapping is applied, along with the assumption that $N \rangle\rangle n$, equation 2.26 reduces to

$$I_{TL} = -\frac{dm}{dt} = \left(\frac{s}{(N+n_D)}\right)\left(n_t n_D \exp[\frac{-\Delta E}{k_b T}] + n_t^2 \exp[\frac{-\Delta E}{k_b T}]\right). \tag{2.27}$$

From this, it can be seen that with the competition of the deep traps, the glow peak intensity becomes a mixture of both first and second-order kinetics.

Of course if we continue to heat the sample past the active temperature range of the first traps, eventually the thermal threshold of the deep traps will be reached, and they will begin to release their trapped electrons producing a second TL peak. For a material with multiple recombination centers and traps with a distribution of thermal activation energies, the general-one-trap equation for TL intensity can be written as the summation of contributions from each individual trap.[48,49] The complex general-order equation for a distribution of traps of index j = 1 to v and recombination centers for index i = 1 to u can be written

$$I_{TL} = \sum_{j=1}^{v} E \frac{m_j A_{nmj}}{R+U} \tag{2.28}$$

where

$$E = \sum_{i=1}^{u} n_i s_i esxp[\frac{-\Delta E_i}{k_b T}], \tag{2.29}$$

$$R = \sum_{j=1}^{v} m_j A_{nmj}, \tag{2.30}$$

and

$$U = \sum_{i=1}^{u} A_{ni}(N_i - n_i). \tag{2.31}$$

In fact, for a material with multiple traps each with different thermal activation energies, the TL glow curve will exhibit multiple peaks corresponding to all of the electron traps

that were thermally emptied during heating. These peaks could be separate, or overlap depending on the difference in the thermal activation energies of each trap. An example of a TL glow curve from irradiated natural topaz is shown in figure 2-4. Topaz shows three distinct TL peaks in the temperature range from 25 to 350 °C. The 40 °C and 140 °C TL peaks are believed to arise from a discrete trapping state with a single thermal activation energy values and the 225 °C peak is a composite of two smaller peaks coming from two different traps of slightly different activation energies.[50]

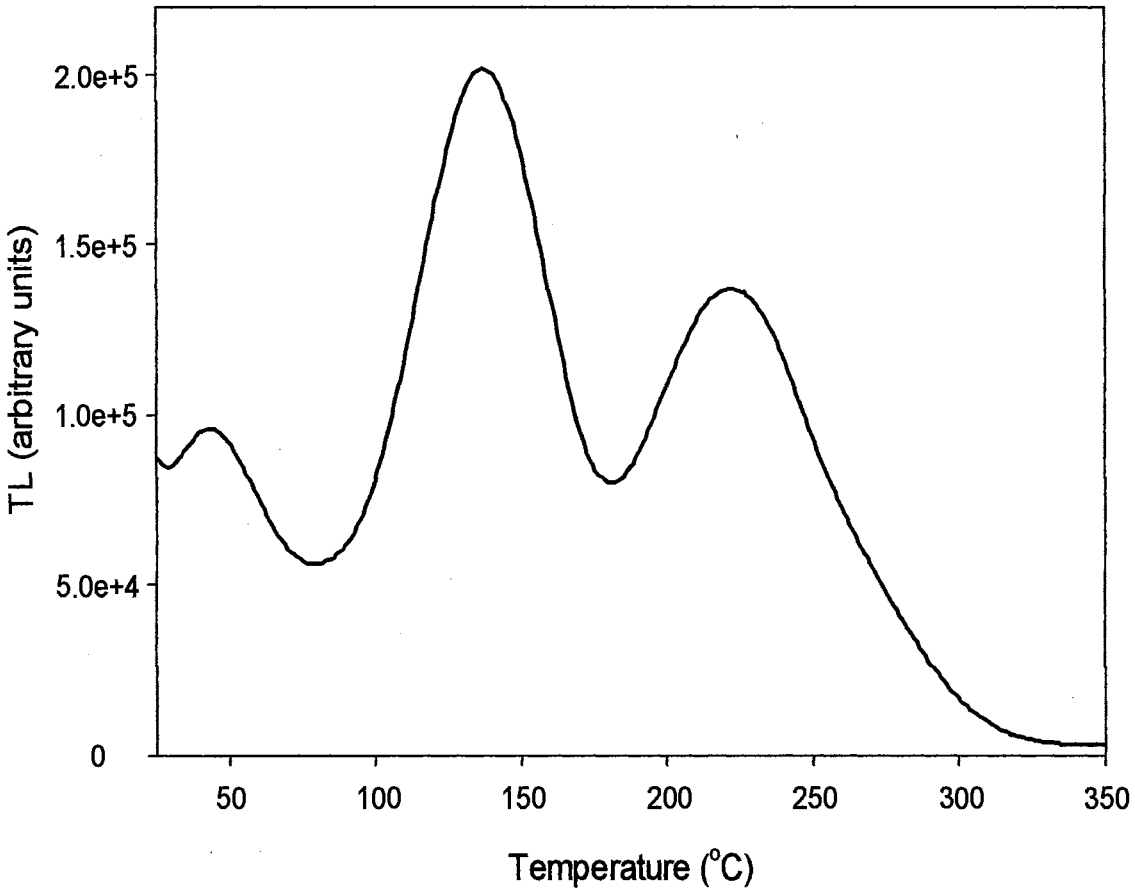

Figure 2-4: TL glow curve for irradiated natural topaz. Topaz has three distinct TL peaks in the temperature range from 25 to 350 °C corresponding to at least three different charge traps with different thermal activation energies.

2.3 Theoretical Model of Optically Stimulated Luminescence

A model of Optically Stimulated Luminescence will be developed using the flow of charge in the crystal during optical stimulation. A simple model will be developed using only one trapping state and one recombination center, and then will be expanded to include both shallow and deep trapping centers.

2.3.1 A Simple Model of OSL

In order to develop a simple one trap-one recombination center model of OSL, the same assumptions that were described in the previous section for TL will be used. Only electrons are considered in the trapping and recombination processes, and all charge transport will take place via the conduction band. The rate equations describing the flow of charge transfer during optical stimulation can be given by

$$\frac{dn_t}{dt} = -n_t f - n_c A_n (N - n_t) \tag{2.22}$$

$$\frac{dn_c}{dt} = n_t f - n_c A_n (N - n_t) - n_c A_{mn} m \tag{2.23}$$

$$\frac{dm}{dt} = -n_c A_{mn} m \tag{2.24}$$

where $f = \phi(\lambda)\sigma(\lambda)$ with $\phi(\lambda)$ defined as the photon fluence rate (photons/m^2/s^2) and $\sigma(\lambda)$ is known as the photoionization cross section (m^2). The wavelength dependence of f is stated explicitly with the wavelength dependence of all equations containing f understood. The photoionization cross section can be described as the efficiency of a given wavelength of light at ionizing trapped charge from a given trap.[51] The photoionization cross section can be given by the equation

$$\sigma = C\sqrt{\Delta E}\frac{(h\nu - \Delta E)^{3/2}}{h\nu(h\nu - \gamma\Delta E)^2} \tag{2.25}$$

where C is a constant, $h\nu$ is the energy of the incident photon, and γ is a constant dependent on the effective masses of the trapped electron and vacancy site (or trapped hole) that the electron occupies.[52] The OSL intensity can be expressed by the same condition as the TL intensity given by equation 2.1. Using these rate equations along with the condition of charge neutrality, the assumption of quasiequilibrium, and negligible retrapping, the expression for the OSL intensity is given by

$$I_{OSL} = -\frac{dm}{dt} = -\frac{dn_t}{dt} = n_t f . \tag{2.26}$$

This expression can be easily integrated to give a first-order solution for the OSL intensity of the form

$$I_{OSL} = n_o f \exp[-ft] = I_o \exp[\frac{-t}{\tau}] \tag{2.27}$$

where I_o is the initial luminescence intensity at $t = 0$ and $\tau = 1/f$ and is known as the decay constant.

For the case of optical stimulation, all traps in the sample are stimulated simultaneously instead of only stimulating traps with thermal activation energies comparable to the thermal energy of the material during readout. The efficiency of the stimulation light to stimulate charge out of a given trap depends on the size of the photoionization cross section of the trap at the given wavelength of stimulation. Therefore, for materials with a distribution of optically active traps ($\sigma > 0$), equation 2.27 is seen to be the sum of the luminescence stimulated from each individual trap.

Therefore, for a distribution of optically active traps (i = 1 to v), the OSL signal is sum of a series of decaying exponentials given by the equation

$$I_{OSL} = n_{o1} f_1 \exp[-f_1 t] + n_{02} f_1 \exp[-f_2 t] + \ldots n_{ov} f_v \exp[-f_n t] = \sum_{i=1}^{v} n_{oi} f_i \exp[-f_i t]. \quad (2.28)$$

The shape of the OSL curve will be the convolution of each individual decaying exponential, and the intensity and decay rate of each exponential will depend on the stimulation rate (f_i) of charge from each trap. An example of an OSL decay curve for quartz is shown in figure 2-5. The OSL curve from quartz is known to be composed of three exponential components from three distinct trapping states that have become known as the fast component with a lifetime ($1/\tau$) equal to about 2.5 seconds, the medium component with a lifetime equal to about 8.0 seconds, and a slow component with a lifetime equal to about 800 seconds.[53]

2.3.2 Adding to the OSL Model

The model of OSL can be extended to include multiple trapping states in much the same way as the TL model. Since all traps are stimulated simultaneously according to the relative size of their photoionization cross section, the additional trapping states that are considered are traps that are optically inactive (σ= 0) and thus act as competing traps. These optically inactive competitors are then classified according to their thermal stability. A trap that is not thermally stable at the OSL readout temperature is known as a shallow trap. As well as these shallow traps, deep traps of the type described in section 2.2.2 will contribute to the shape of the OSL curve along with the main traps considered in the previous section.

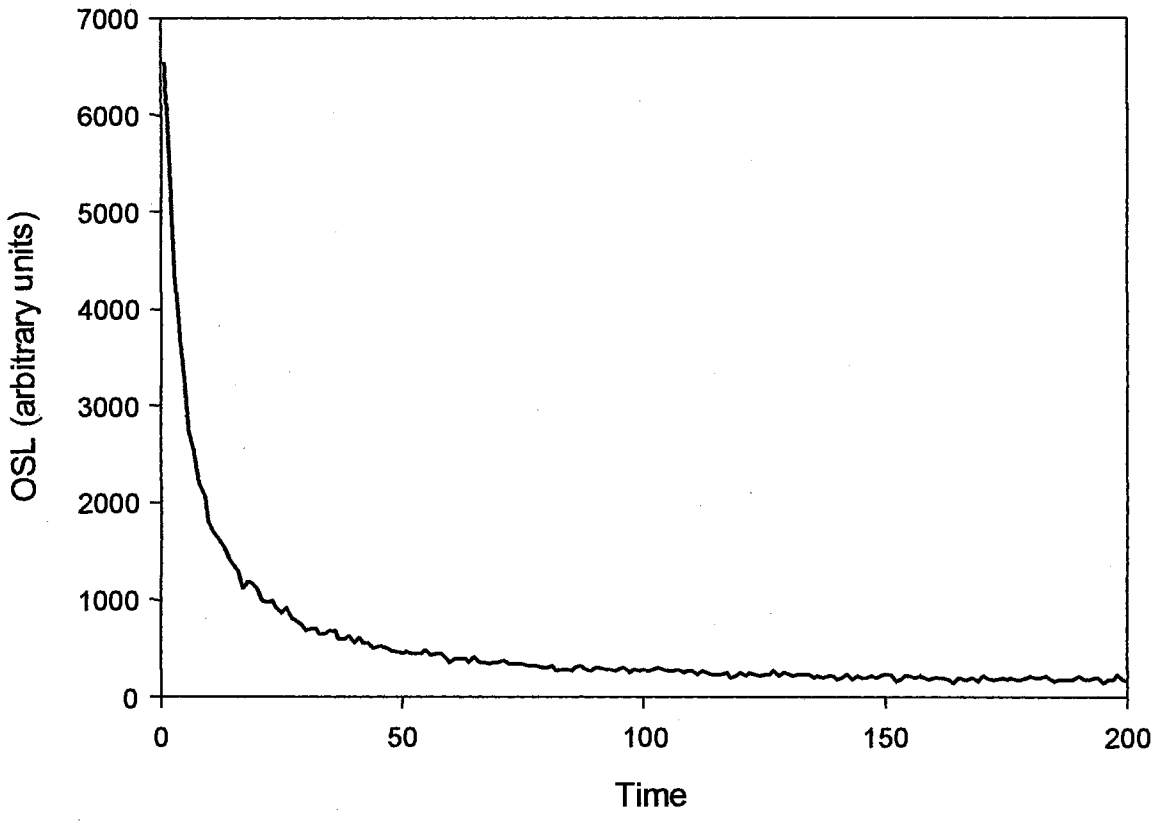

Figure 2-5: A typical OSL decay curve from a quartz sample. The curve is a convolution of three decaying exponential components with fast, medium, and slow lifetimes.[53]

If a trap in the material is optically inactive and thermally stable, this trap will act as a competitor for the main optically active traps. In this case, the OSL intensity can be written

$$I_{OSL} = n_{o1} f_1 \exp[-f_1 t] - n_c A_2 (N_2 - n_2) \tag{2.28}$$

where the second term represents a reduction of the OSL intensity due to the trapping of charge by the optically inactive trap. Making the initial assumption that $N_2 >> n_2$ then the second term of equation 2.28 becomes

$$n_c A_2 N_2 \approx C \tag{2.29}$$

where C is a constant and the term is therefore approximately constant. In the limit that $t \to \infty$, the concentration of charge in the conduction band will go to zero ($n_c \to 0$) as the charge trapped in the optically active traps is depleted, and therefore $C \to 0$. This means that C is in fact a very slowly varying function of time. Alternatively, if the competing traps are shallow traps, which are thermally unstable at the temperature of the OSL measurement, then a term that takes into account the thermal release of electrons from the competing trap is added to the equation for the OSL intensity and equation 2.28 becomes

$$I_{OSL} = n_{o1} f_1 \exp[-f_1 t] - n_c A_2 (N_2 - n_2) + n_2 s_2 \exp[\frac{-\Delta E}{k_b T}]. \tag{2.30}$$

The last two terms in equation 2.30 give rise to a long-lived, temperature dependent tail to the OSL decay curve. A comparison of the OSL decay from Al_2O_3 samples, one with a large concentration of competing traps, and one with a relatively low concentration of competing traps is shown in figure 2-6. The component from the competing traps will be in the form of an initial increase in the intensity followed by a decrease with a long-lived

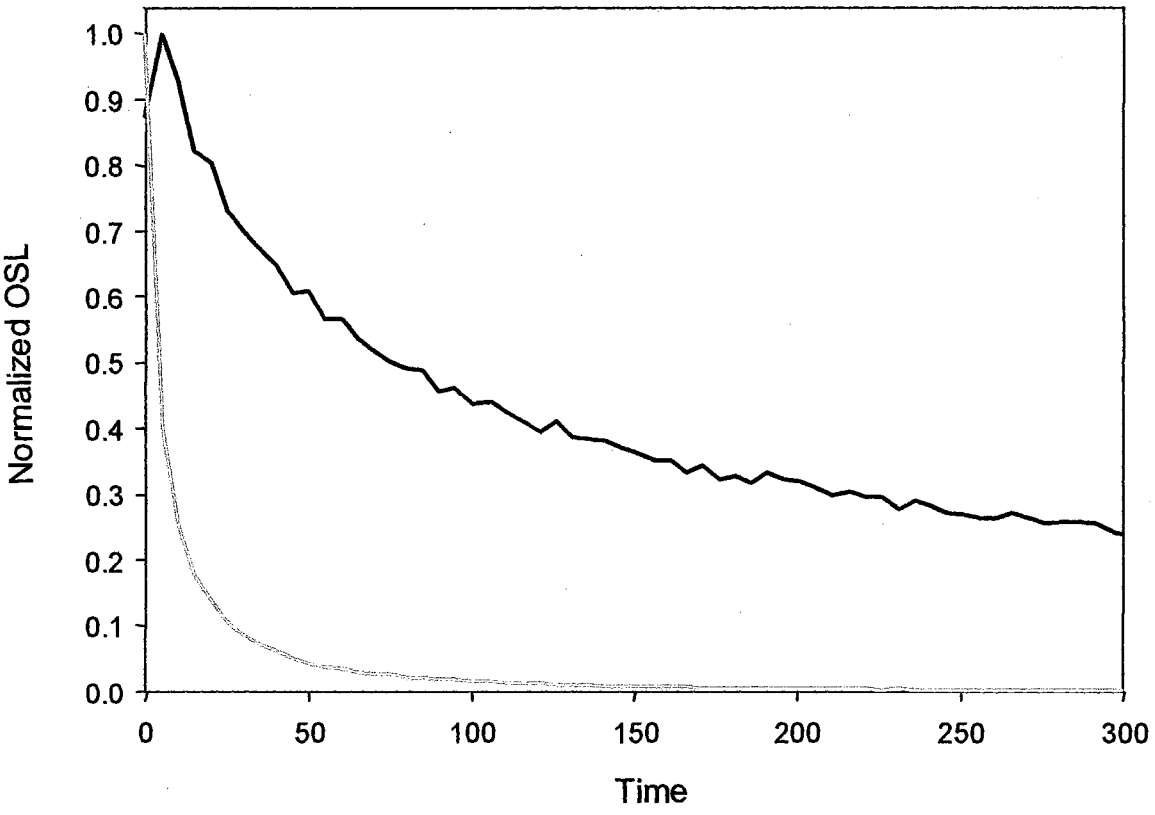

Figure 2-6: A comparison of the OSL decay for Al_2O_3 two different samples. The first sample (gray line) contains a relatively low concentration of competing deep and shallow trapping centers, and the second sample (black line) contains a relatively high concentration of competing trapping centers.

decay of the luminescence. Depending on the relative size of this component compared to the optical stimulation term, the OSL curve may exhibit an initial increase followed by the characteristic decay.[54]

2.4 Theoretical Model of Radioluminescence

Following the same development as for TL and OSL, a model of radioluminescence produced by a material during irradiation will be developed using the one trap-one recombination model and the influence of shallow and deep traps on the RL signal will be discussed.

2.4.1 A simple model of RL

Radioluminescence arises from the prompt recombination of electrons during irradiation of a material. Electrons excited into the conduction band by absorption of energy from the incident radiation can become trapped, or can immediately recombine at a recombination center to produce radioluminescence. The one trap-one recombination model for radioluminescence can be described with similar rate equations as for the OSL and TL models by noting that the stimulation of charge now is not out of the charge traps, but instead is due to the ionization of electrons into the conduction band from the valence band. The rate equations for this process are written as

$$\frac{dn_t}{dt} = n_c A_n (N - n_t) \tag{2.31}$$

$$\frac{dn_c}{dt} = \Gamma\Phi - n_c A_n (N - n_t) - n_c A_{mn} m \tag{2.32}$$

$$\frac{dm}{dt} = -n_c A_{mn} m \tag{2.33}$$

where Γ is the efficiency of electron-hole generation in the material for the incident Assuming quasistatic equilibrium ($dn_c/dt \approx 0$), equation 2.32 can be solved for the electron concentration in the conduction band

$$n_c = \frac{\Gamma\Phi}{A_n(N_t - n_t) + A_{mn}m}, \tag{2.34}$$

This can be substituted into equation 2.1 for the luminescence intensity to get the expression for radioluminescence intensity given by

$$I_{RL} = -\frac{dm}{dt} = \Gamma\Phi\frac{A_{mn}m}{A_n(N_t - n_t) + A_{mn}m}. \tag{2.35}$$

As the material is irradiated, the electron traps will continue to fill, in the absence of any stimulation source, to the point of saturation when all traps are filled. As the traps fill, the concentration of filled traps will approach the total concentration of traps ($n_t \cong N_t$) and $A_n(N_t - n_t) \to 0$. In the limit that all traps are full, the radioluminescence intensity will reduce to

$$I_{RL} = \Gamma\Phi. \tag{2.36}$$

Therefore, the RL intensity is seen to rise to a maximum level according to the filling characteristics of the electron traps in the material, and the dose rate, or incident flux of irradiation. An example RL intensity curve from Al_2O_3 is shown in figure 2-7. The RL intensity starts at and initial value that is greater than zero immediately after the irradiation is turned ($t=0$). This initial RL value depends on the ratio of the concentration of charge traps, to the concentration of recombination centers in the sample prior to the start of irradiation and the dose rate.

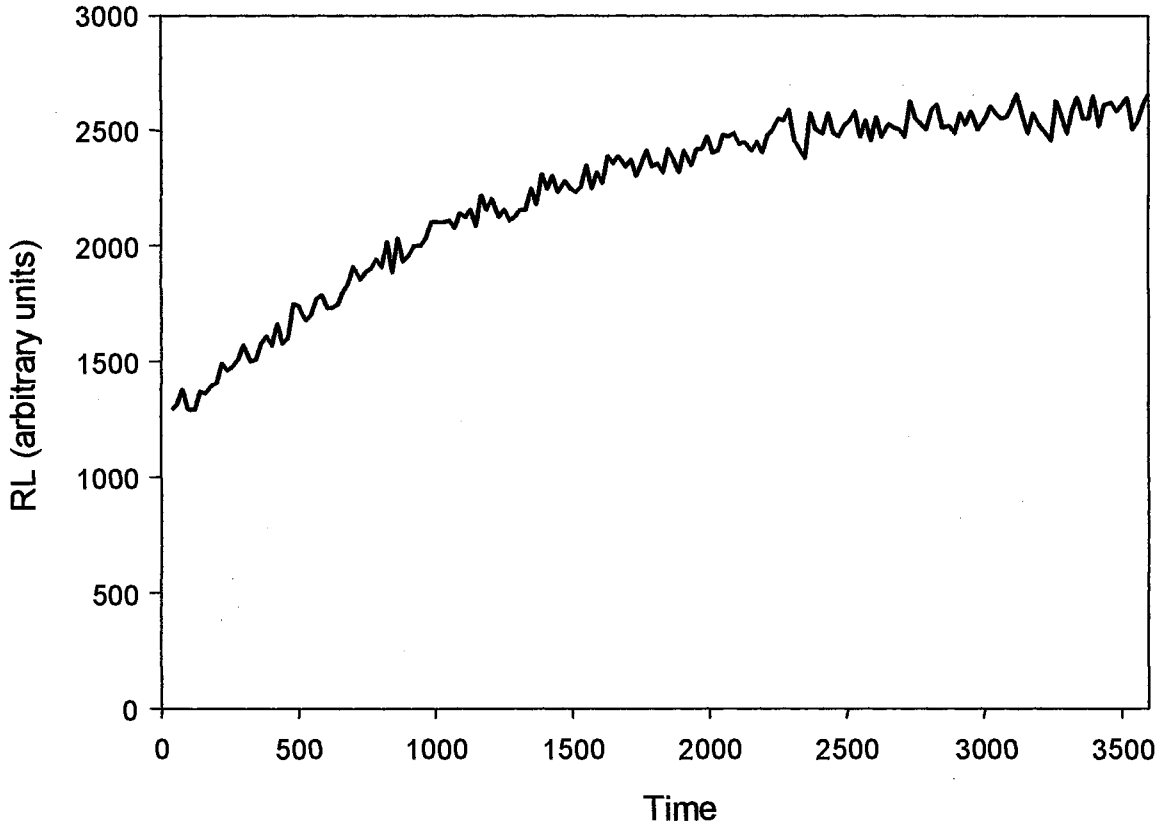

Figure 2-7: Radioluminescence signal from Al_2O_3 for a constant dose rate. The RL signal follows a rise to maximum signal as the electron traps in the sample are slowly filled by the incident radiation.

2.4.2 Adding to the RL Model

The rise to max of the RL will be slowed with the introduction of deep and shallow trapping states in the sample due to the longer amount of time need to fill a larger total concentration of traps in the sample. If a shallow, thermally unstable trap is added to the model, the equation for the RL intensity will be modified by the thermal release of trapped charge from the shallow traps into the conduction band. The modified rate equations for RL include the change in concentration of charge in the shallow traps given by

$$\frac{dn_2}{dt} = n_c A_{n2}(N_2 - n_2) - n_2 s_2 \exp[\frac{-\Delta E_2}{k_b T}]. \tag{2.37}$$

With the addition of equation 2.37 to the rate equations, the rise to maximum of the intensity of the RL is seen to be slowed down. Solving for the RL intensity with the addition of equation 2.37 give the expression

$$I_{RL} = \frac{-dm}{dt} = \left[\frac{A_{mn}m}{A_n(N_t - n_t) + A_{n2}(N_2 - n_2) + A_{mn}m}\right](\Gamma\Phi + n_2 s_2 \exp[\frac{-\Delta E_2}{k_b T}]). \tag{2.38}$$

The change in the shape of the RL curve due to the addition of a shallow trap is shown in figure 2-8. A computer simulation of the RL for the one trap-one recombination center model is compared to a modified version of the model to which a shallow trap has been added. From figure 2-8, the shape of the RL can be seen to change with the rise to maximum being slowed significantly.

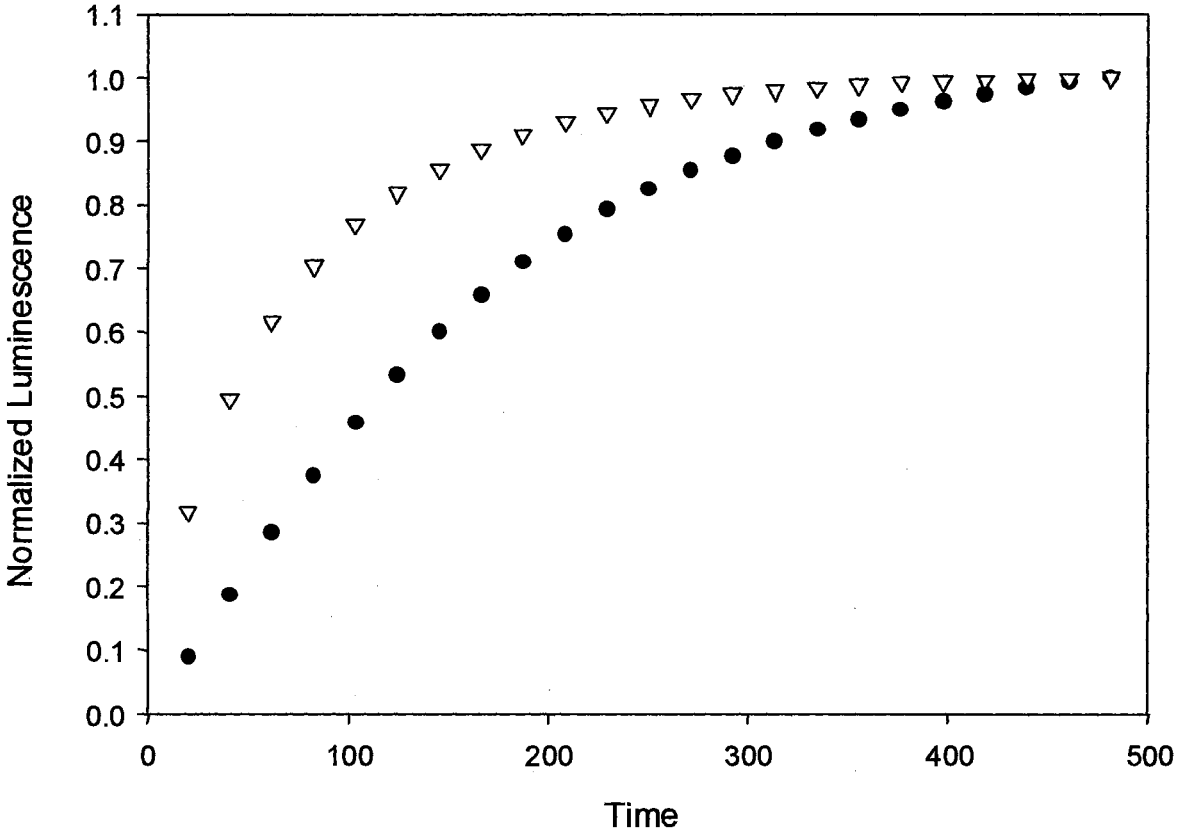

Figure 2-8: Comparison of Radioluminescence curve with only one-trap one recombination center (triangles) and Radioluminescence with shallow trap added to the one trap-one recombination center model.

2.5 Properties of Al_2O_3

This research is focused on the study of Al_2O_3 fibers for the purpose of developing a radiation dosimeter based on the OSL signal measurements from the fibers after irradiation. Therefore we now discuss the relevant properties of Al_2O_3. In particular, the properties of the F and F^+ center oxygen vacancies and their role in the production of luminescence. The discussed properties of these vacancies will be compared with the current characterization measurements of TL, OSL, and photoluminescence to determine useful properties of the fibers for use as OSL dosimeters.

2.5.3 Crystal Structure and Growth

The Al_2O_3:C crystal structure is shown in figure 2-9. It consists of a hexagonal close packed O^{2-} sublattice with Al^{3+} ions occupying two out of every three interstitial sites in the lattice. The O^{2-} ions occupy two equilateral triangles one above and one below the plane of the Al^{3+} ion. The Al-O bond lengths are 0.197 nm and 0.186 nm due to the slight distortion of the Al^{3+} sublattice.[55] Al_2O_3:C has a band gap of approximately 9.0 eV.[56]

Al_2O_3:C used in this research is typically grown from the melt at a temperature of approximately 2050 °C. The crystals are grown by the Stepanov method, and as a result have a relatively high concentration of carbon impurities (100-5000 ppm). Carbon is believed catalyze the production of F^+ centers in the material by substituting for aluminum in the crystal lattice. The increase in the concentration of F^+ centers due to carbon has been shown to increase the TL and OSL sensitivity of the material.[57] Along with carbon other intrinsic impurities occur in small amounts (Ca, Cr, Ti, Ni, Si, Cu, and

(a)

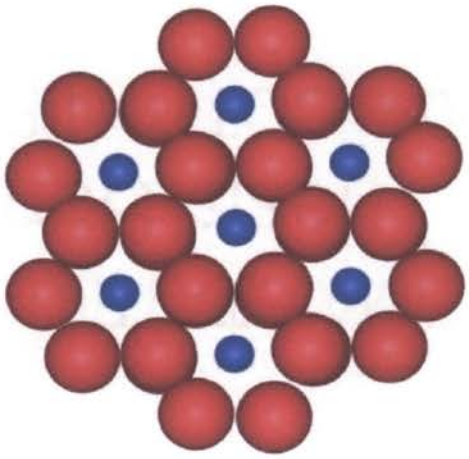

(b)

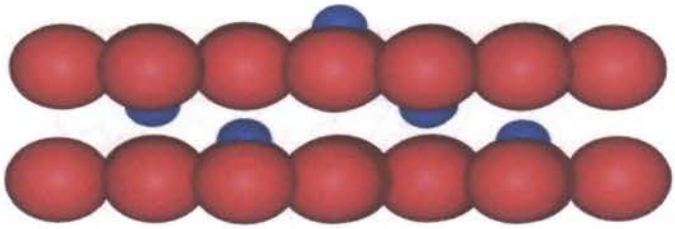

Figure 2-9: Schematic of the Al_2O_3 lattice with a top view (a) showing the hexagonal structure of the oxygen atoms (red) with the central Aluminum (blue). From the side view (b), the distortion of the aluminum sublattice due to varying bond lengths can be seen.

Fe).[58]

2.5.2 TL of Al_2O_3:C

TL glow curves for Al_2O_3:C (known as TLD-500 from commercial sales by the Harshaw Corportation) show several peaks over the temperature range from room temperature to ~700 °C as shown in figure 2-10. A strong peak is seen centered at ~175 °C (known as the main peak) and weaker peaks appear at ~325 °C and ~475 °C. The efficiency of the luminescence in Al_2O_3:C is shown to be strongly temperature dependent above ~200 °C. Akselrod et. al have shown that for Al_2O_3 the luminescence efficiency of the F center emission is given by the equation

$$\eta(T) = \frac{1}{(1 + \tau\nu * \exp[\frac{-W}{k_b T}])} \tag{3.1}$$

with $\tau\nu \approx (3.8\pm1.5) \times 10^{12}$, $W \approx 1.1\pm0.05$ eV, and W is the activation energy for a nonradiative transition.[56] As shown for the ~175 °C TL peak in figure 2-11, the intensity of the TL is reduced and the peak temperature is shifted to higher values. In this case the TL intensity would be given by the equation,

$$I_{TQ} = \eta(T) I_{TL} \tag{3.2}$$

where I_{TL} is given in general by equation 2.21. Along with this the shape of the TL peak is distorted producing a more symmetrical peak shape after correcting for thermal quenching. This has led to some conflicting analysis of the TL peaks when using the general-order equation for TL (equation 2.21). Kitis et. al. suggested that the uncorrected peaks appeared to fit to a TL peak with order parameter b ≈ 1.42 while Kortov suggested that the peaks fit to TL peaks with b ≈ 2.[55,59] However, when the peaks are

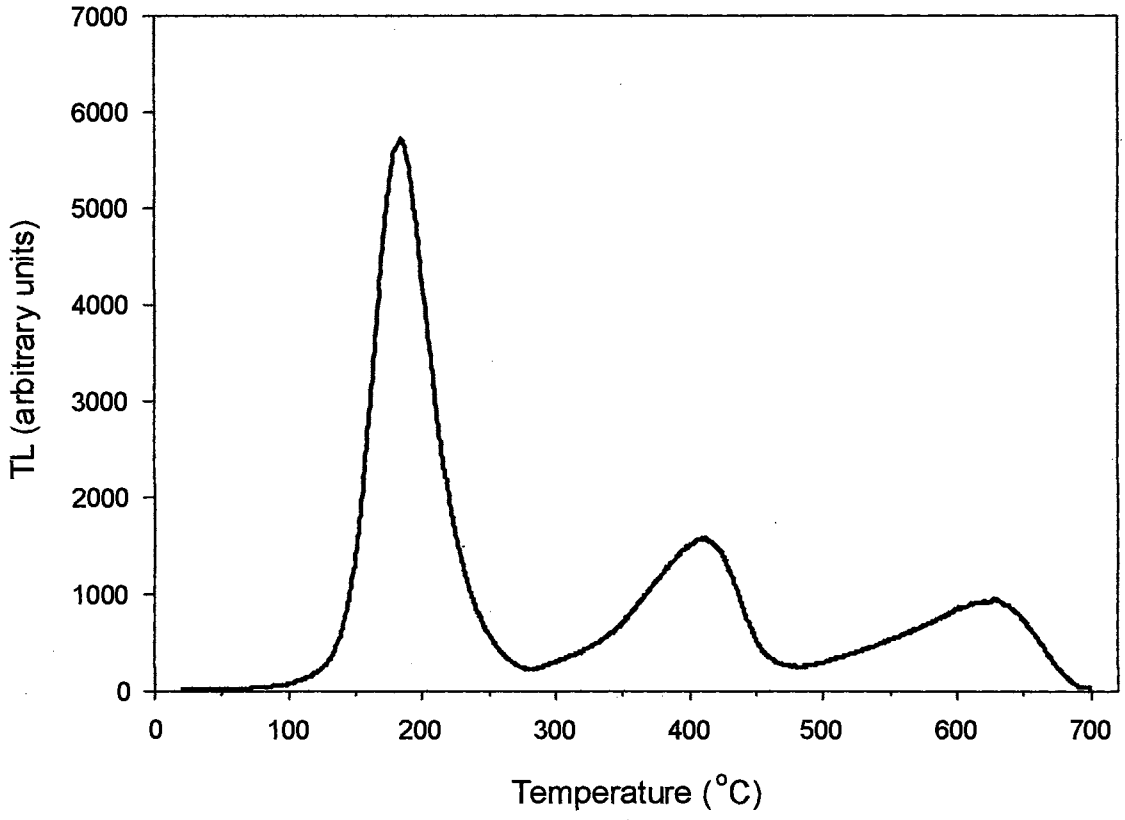

Figure 2-10: TL glow curve for Al_2O_3:C.

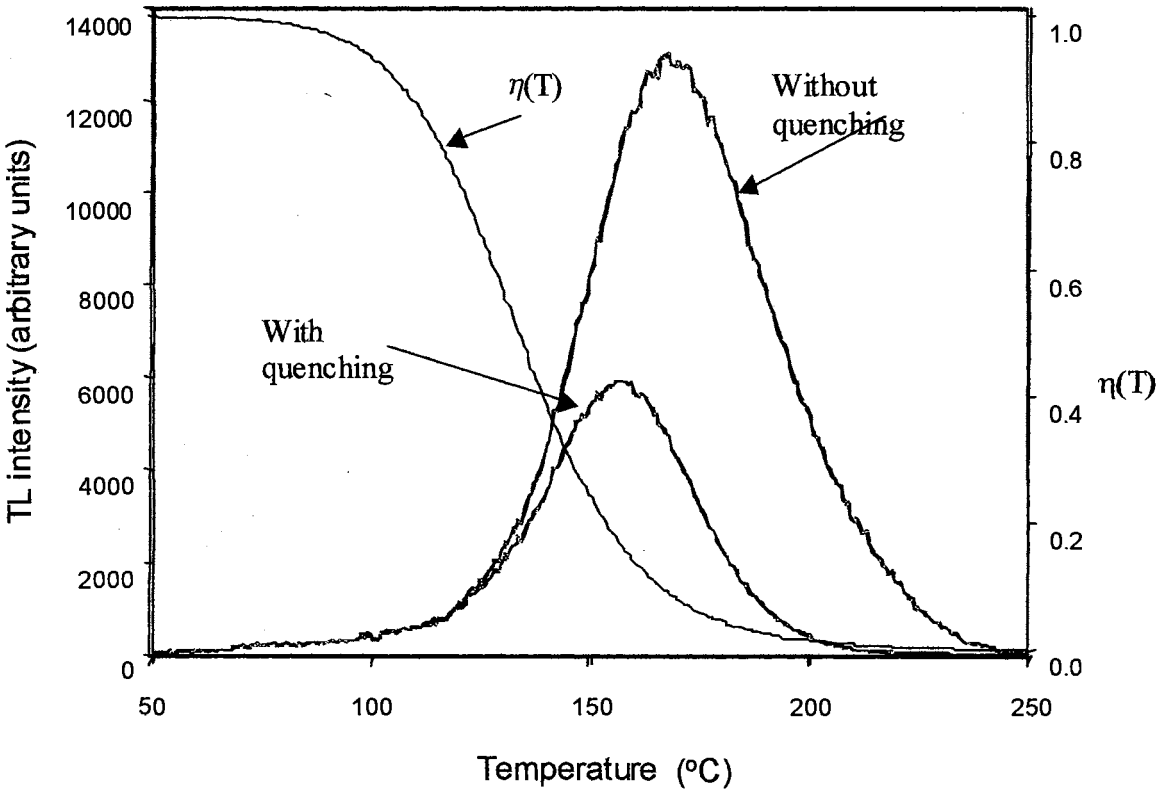

Figure 2-11: First order Randall-Wilkins glow peaks with and without the thermal quenching of luminescence intensity η(T).

corrected for thermal quenching, it is has been shown that the peaks are actually made up of several closely spaced first-order peaks that produce the overall TL peak.[60] Therefore the TL peaks in Al_2O_3:C are generally believed to be due to a distribution of traps that are thermally active over the temperature range of the peak. Along with the changes due to thermal quenching, the luminescence efficiency is affected by the heating rate of the measurement. According to the predictions of the kinetic analysis made earlier in chapter 2, the luminescence intensity will increase as the heating rate is increased. However, due to thermal quenching in Al_2O_3:C this has been shown not to be the case. Thus, the expression for TL intensity must be modified to include the expression for thermal quenching. As the heating rate is increased, the TL peak will shift to higher temperatures and the numerical value of the efficiency changes accordingly. Therefore due to the behavior of the thermal quenching term given by equation 3.1 the TL peaks decrease in intensity as the heating rate increases.[56]

2.5.3 F Center Defects in Al_2O_3:C

The main defects present in radiation sensitive Al_2O_3 are the F center oxygen vacancies. The neutral F center is an oxygen vacancy that has localized two electrons to leave the site neutral with respect to the lattice. Also present in this material is the F^+ center, which is an oxygen vacancy with only one localized electron leaving an overall 1^+ charge with respect to the lattice. For the F center, the prominent absorption band is centered near 6.0 eV (205 nm), and the associated luminescence band is centered at about 3.0 eV (420 nm).[61] The F center absorption band is due to a transition from the 1A ground state to the 3P excited state.[62] The lifetime of the F center emission has a reported lifetime of about 35 ms, and has been associated with a transition from the 1B excited state to the 1A

ground state.[13,63] Along with the main emission band observed at 420 nm, Caulfield and Cooper have reported a luminescence band centered at about 310 nm that they have attributed to the direct transition from the 1P excited state to the 1A ground state of the F center.[64] The absorption and emission transitions for the F and F^+ centers is shown in figure 2-12.[61,62] Absorption bands centered at about 4.8 (255 nm), 5.4 (235 nm), and 5.8 eV (210 nm) have been associated with transition from the 1A ground state to the 1B, 2B, and 2A excited sates of the F center respectively.[61,65] The main F^+ centered emission band is centered at about 3.8 eV (326 nm) and is associated with the relaxation of the center from the 1B excited state to the 1A ground state.[61] The production of F center emission is thought to be caused by the recombination of electrons with F^+ centers producing an excited F center that relaxes according to the process[13],

$$F^+ + e^- \Rightarrow F^* \Rightarrow F + h\nu_{420nm}. \tag{3.3}$$

In this process, the TL process would involve the release of a trapped electron that uses an F^+ center as a recombination center. Conversely, the production of F^+ center emission is believed to be caused by the recombination of a free hole with an F center according to the process[13],

$$F + h^+ \Rightarrow F^{+*} \Rightarrow F^+ + h\nu_{326nm}. \tag{3.4}$$

In this case, the TL or OSL process would involve the release of a trapped hole that uses an F center as a recombination center.

The F and F^+ center concentrations in Al_2O_3:C have been shown to exhibit a strong reciprocal relationship. That is to say photostimulation of the F center with 6 eV light has been shown to lower the concentration of the F center and increase the F^+ center concentration.[61,66,67] Also, when the crystal is exposed to ionizing radiation, the

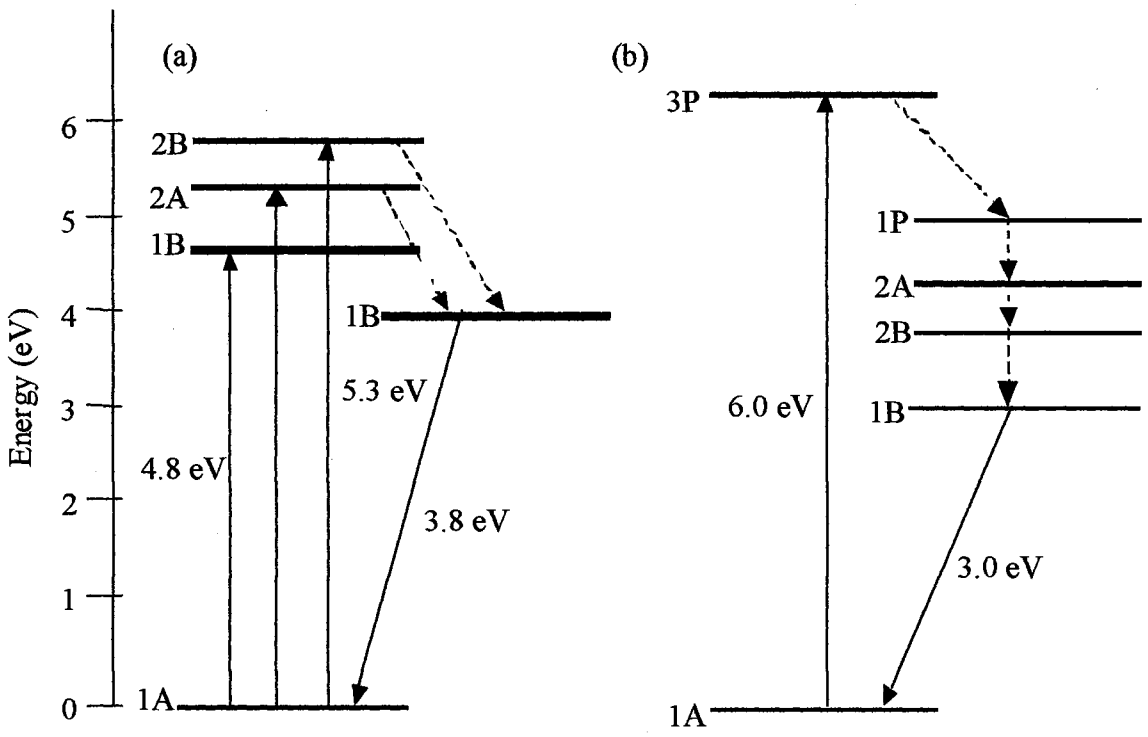

Figure 2-12: (a) F^+ center transitions at 4.84 eV and 5.27 eV and emission of 3.8 eV, and (b) F center transition at 6.01 eV and emission at 3.0 eV[61,62].

concentration of F centers is seen to increase and F^+ centers to decrease.[67,68] This supports the idea of the electrons being ionized into the conduction band by the irradiation are becoming trapped at the F^+ centers to produce F centers. Conversely, when the sample is illuminated with 205 nm (6 eV) light, the electrons are excited out of the centers to produce F^+ centers. This reciprocal relationship supports well the ideas for recombination and the production of F center emission during TL given by equation 3.3.

Along with the absorption and emission bands from the F and F^+ center vacancies, Al_2O_3 exhibits several other bands that are associated to the various charge states of aggregate oxygen vacancies. These aggregate centers, known as F_2 centers, are composed of next nearest neighbor anion vacancies with two, three, or four trapped electrons.[69,70] The F_2 center has four trapped electrons, and is neutral with respect to the lattice. The absorption and emission transitions of the F_2 aggregate centers are shown in figure 2-13. The F_2^+ is an aggregate oxygen vacancy with three trapped electrons, and has a $^+1$ charge with respect to the lattice. The F_2^{2+} is an aggregate center with 2 trapped electrons leaving a local $^+2$ charge with respect to the lattice. The F_2 center is reported by Pogatshnik et. Al to display an absorption band centered at about 300 nm (4.09 eV), and a corresponding emission band centered at 322 nm (3.85 eV).[70] The F_2^+ has an associated absorption band at 355 nm (3.46 eV) with a corresponding emission centered at 378 nm (3.28 eV).[70] The F_2^{2+} centered absorbs in a band centered at about 450 nm (2.75 eV) with a broad emission band reported to be centered at about 560 nm (2.21 eV).[70]

Furthermore, photostimulation with 4.09 eV light can ionize the F_2, thus reducing the F_2 concentration causing a reduction in the F_2 emission at 3.85 eV.[71] The reduction in

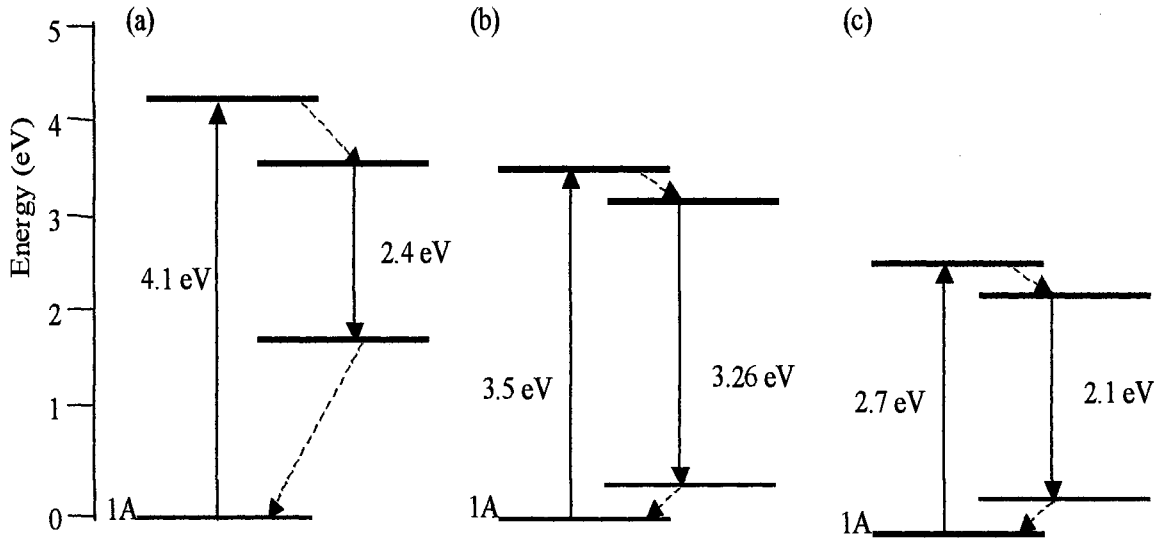

Figure 2-13: Absorption and emission transitions of the F_2 aggregate centers; F_2 (a), F_2^+ (b), F_2^{2+} (c) in Al_2O_3.[72]

the F_2 center absorption is accompanied by a decrease in the F^+ center absorption bands at 255 and 235 nm, a decrease in the F_2^{2+} absorption band at 450 nm, and an increase in the F center absorption at 205 nm and the F_2^+ center absorption at 355 nm. This is interpreted as electrons that are ionized from the F_2 centers are captured by F^+ and F_2^{2+} centers creating an increase in the concentration of F and F_2^+ centers. Also, photostimulation of the F center with 205 nm light can not only increase the F^+ center absorption bands (as noted earlier), but can also increase the absorption of the F_2^+ center, and decrease the F_2^{2+} center absorption. This is interpreted as electrons that are ionized from the F centers being captured by F_2^{2+} centers increasing the concentration of the F_2^+ centers.

The TL emission spectrum from Al_2O_3:C exhibits a strong emission is at 420 nm due to the relaxation of F centers. Also, at the same temperatures, a weaker emission center is present in some samples centered at 326 nm. This weaker emission is associated with the relaxation of an excited F^+ center. The TL emission from an Al_2O_3:Mg is shown in figure 2-14.

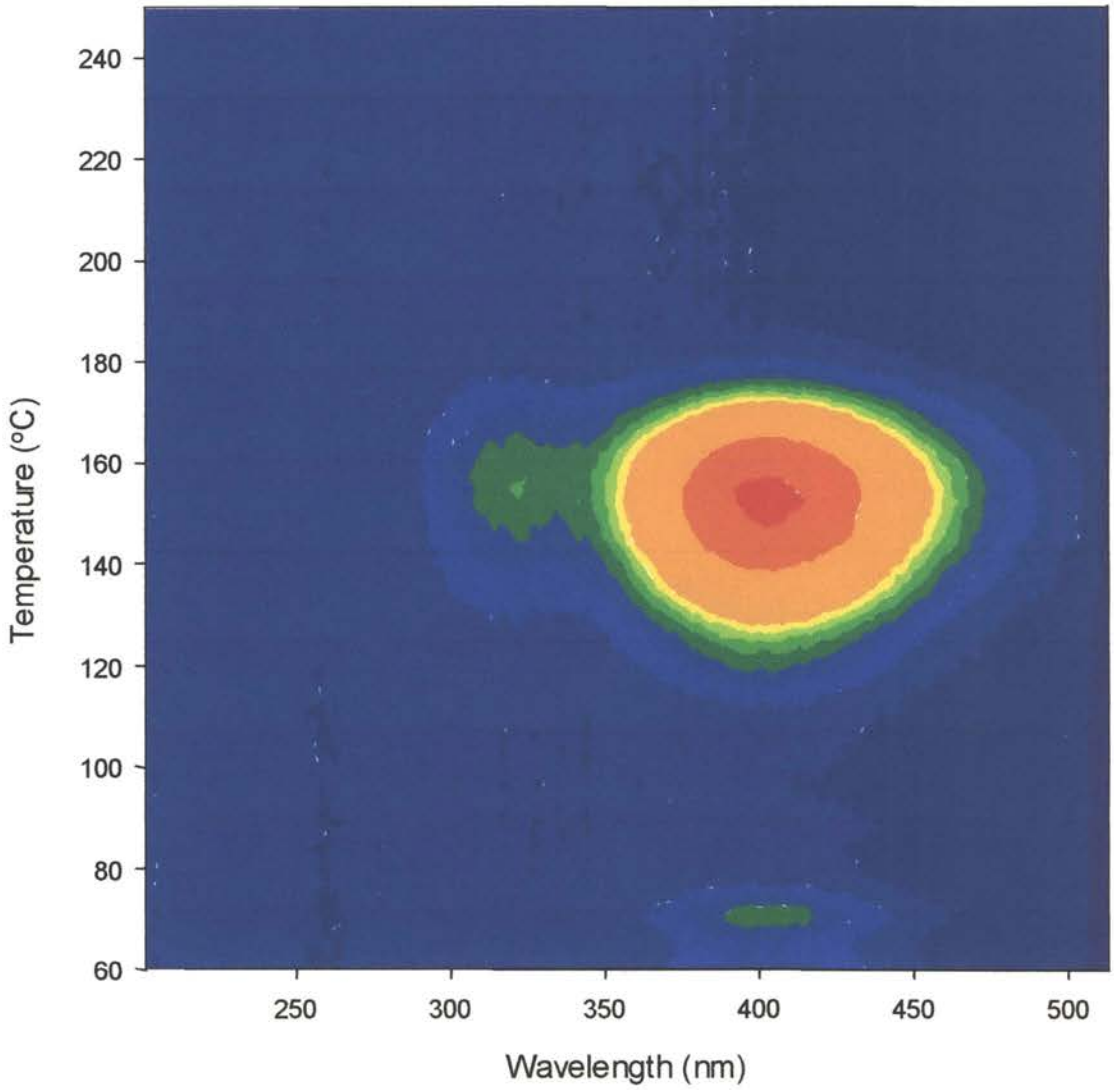

Figure 2-14: TL emission spectra for Al_2O_3:Mg. The main emission band is centered at 420 nm for the 75 and 160 °C TL peak, with a weaker emission band centered at 326 nm for the appearing for the 160 °C TL peak as well.

Chapter 3

3. Characterization of OSL from Al_2O_3 Fibers

3.1 Fibers Used for Research

Al_2O_3:C fibers used for this research were grown by two methods: the Stepanov method and Laser Heated Pedestal Growth (LHPG) method. In each case, the fibers were grown from the melt in the form of single crystal fibers ranging in diameter from 350 to 2000 microns. The fibers produced by the Stepanov method contain certain intrinsic impurities that are unintentionally introduced during the growth process, as well as those intentionally introduced as dopants. Common intrinsic impurities, that occur only in trace amounts, include iron, silicon, calcium, chromium, and titanium.[73] The dopants were added in controlled amounts, and are found in concentrations ranging from as little as ten parts per million to as much as several thousand parts per million.[73] The fiber growth is carried out in a highly reducing atmosphere in the presence of carbon as well as any other desired dopants added to the melt. As the growth proceeds, the presence of carbon in the process catalyses the production of oxygen vacancies in the crystal.

In addition to the fibers grown by the Stepanov method, fibers were also investigated that were grown using the LHPG method. These fibers were grown by melting a bulk Al_2O_3 crystal with a high power CO_2 laser focused onto the starting material creating a localized melting zone, and dipping an Al_2O_3 seed crystal into the melt and pulling the crystal in fiber from the melt.[74] The fibers were pulled in a Helium atmosphere with carbon added to the melt as a dopant.

Both Stepanov and LHPG grown Al_2O_3:C fibers were used for real-time radiation dose measurements. The Stepanov grown fibers were labeled by the growth number, and were given the names: Fiber 1, 4, and 24, 31. The LHPG fiber used for the research was also named for the growth process and was given the name: Fiber D. In addition to the grown fibers, small pellets cut from a bulk Al_2O_3:C rod used for the production of commercial OSL dosimeters, given the name Rod 1, were studied to determine the characteristics best suited for the development of a real-time, fiber optic radiation dosimeter.

3.2 *Photoluminescence Spectra*

The photoluminescence of the Al_2O_3:C fibers was measured using a Jobin-Yvon spectrafluorometer. The fibers were stimulated with light from 225 to 325 nm, and the emission intensity from the fibers was scanned over the wavelength range from 300 to 700 nm. These measurements were performed to gain knowledge of the types and relative concentration of the different luminescent centers present in the fibers. Photoluminescence was first measured with fully annealed samples in which all charge traps in the samples were empty. After this, the fibers were given a saturation dose of UV ($\leq$ 6.0 eV) irradiation from a 50 W mercury lamp. This UV light was used to stimulate trapped electrons from existing defects in the samples to fill electron traps. Since the UV light is not energetic enough to efficiently ionize electron across the band gap, no free holes were created in the valence band to trap in hole traps, and therefore only electron traps were filled. After the photoluminescence was measured for the UV irradiated samples, the fibers were irradiated with ionizing gamma rays from a ^{60}Co source to ensure that all trapping states in the fibers were filled

The photoluminescence spectra for fibers were measured, both before and after irradiation, and the results compared. These spectra from the fibers displayed four major luminescence bands. One was an emission band centered at 326 nm with excitation peaks at wavelengths of 235 and 255 nm. These were due to the relaxation of an excited F^+ center oxygen vacancy. There was also an emission band centered at 420 nm with an excitation peak at wavelengths below 225 nm, which is attributed to the relaxation of an excited F center oxygen vacancy. Photoluminescence spectra from rod 1 which exhibits both F and F^+ center emission bands are shown in figure 3-1. Also, some of the fibers showed a broad luminescence center centered at approximately 560 nm with peak stimulation wavelengths of approximately 225 and 270 nm. The F_2^{2+} emission is thought to appear at stimulation wavelengths of 225 and 270 nm due to the absorption of an as of yet undetermined defect center in the crystal. This center has been shown to exhibit absorption centered at 225 and 270 nm, with an emission band centered at about 450 nm. The 450 nm emission center of this unknown center is subsequently absorbed by the F_2^{2+} center which then produces the emission band centered at about 560 nm.[75] Figure 3-2 shows this broad emission band, which is distorted around 270 nm by the correction for second order effects of stimulation light leaking through the monochromator of the spectraflourometer. This emission band is believed to be caused by the presence of F_2^{2+}oxygen vacancies in the crystal.[76] The F_2^{2+} center is a pair of nearest neighbor F-centers with 2 captured electrons and an overall 2^+ charge with respect to lattice. The final noticeable luminescence band shown in the fibers was a sharp emission line at 693 nm. This is from chromium impurities in the fiber and is from the R2 line of a Cr^{3+} impurity in the Al_2O_3 lattice.[77,78] This emission comes from the $^2E \rightarrow {}^4A_2$ transition of the

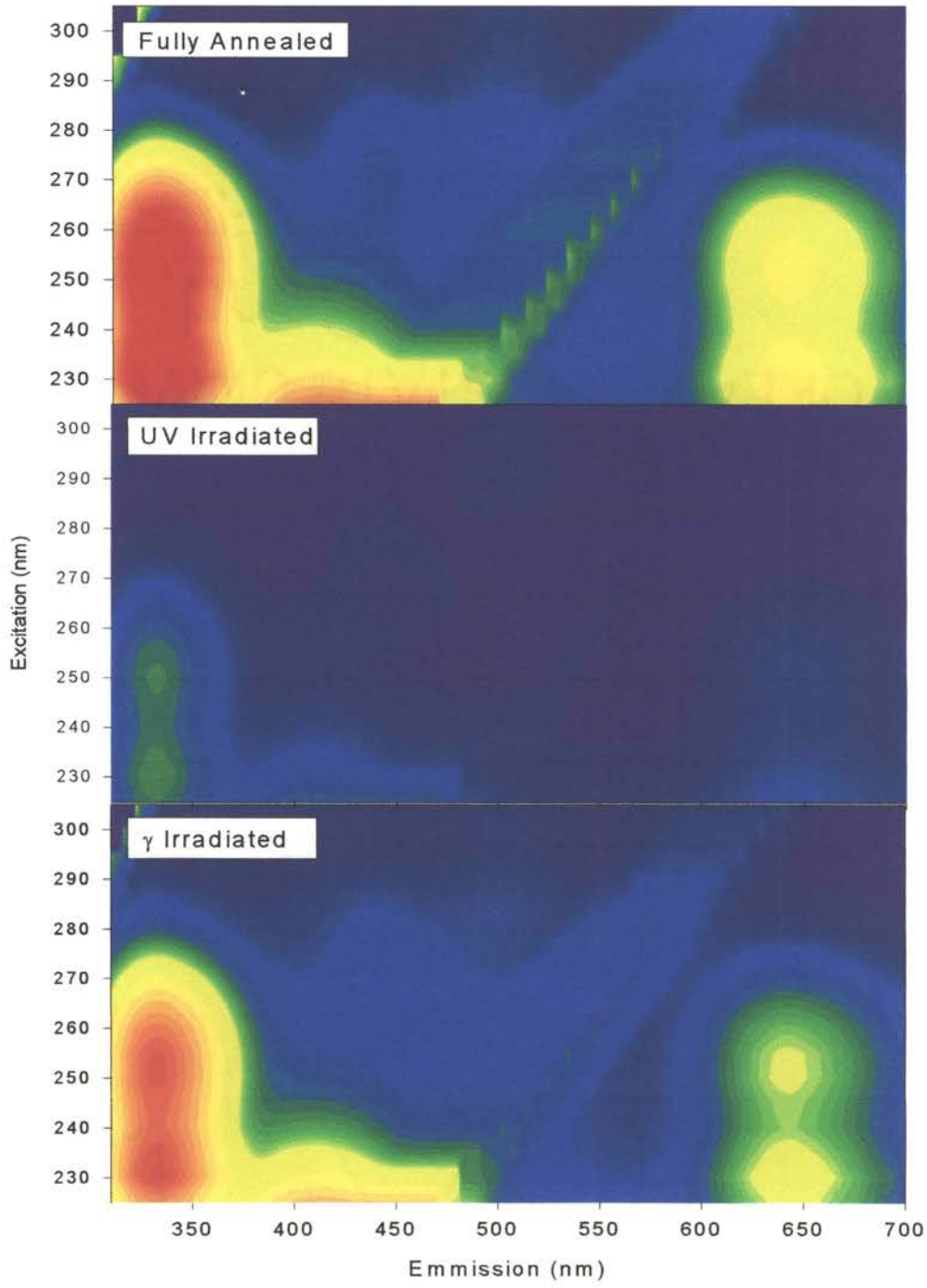

Figure 3-1: Photoluminescence spectra of Al_2O_3 fiber sample Rod 1. Rod 1 shows strong intrinsic F center emission bands centered 420 nm. Also, the spectra show a strong F^+ center emission band centered at 326 nm, as well as peaks centered 652 nm due to the second order effects of the monochromator in the spectrafluorometer.

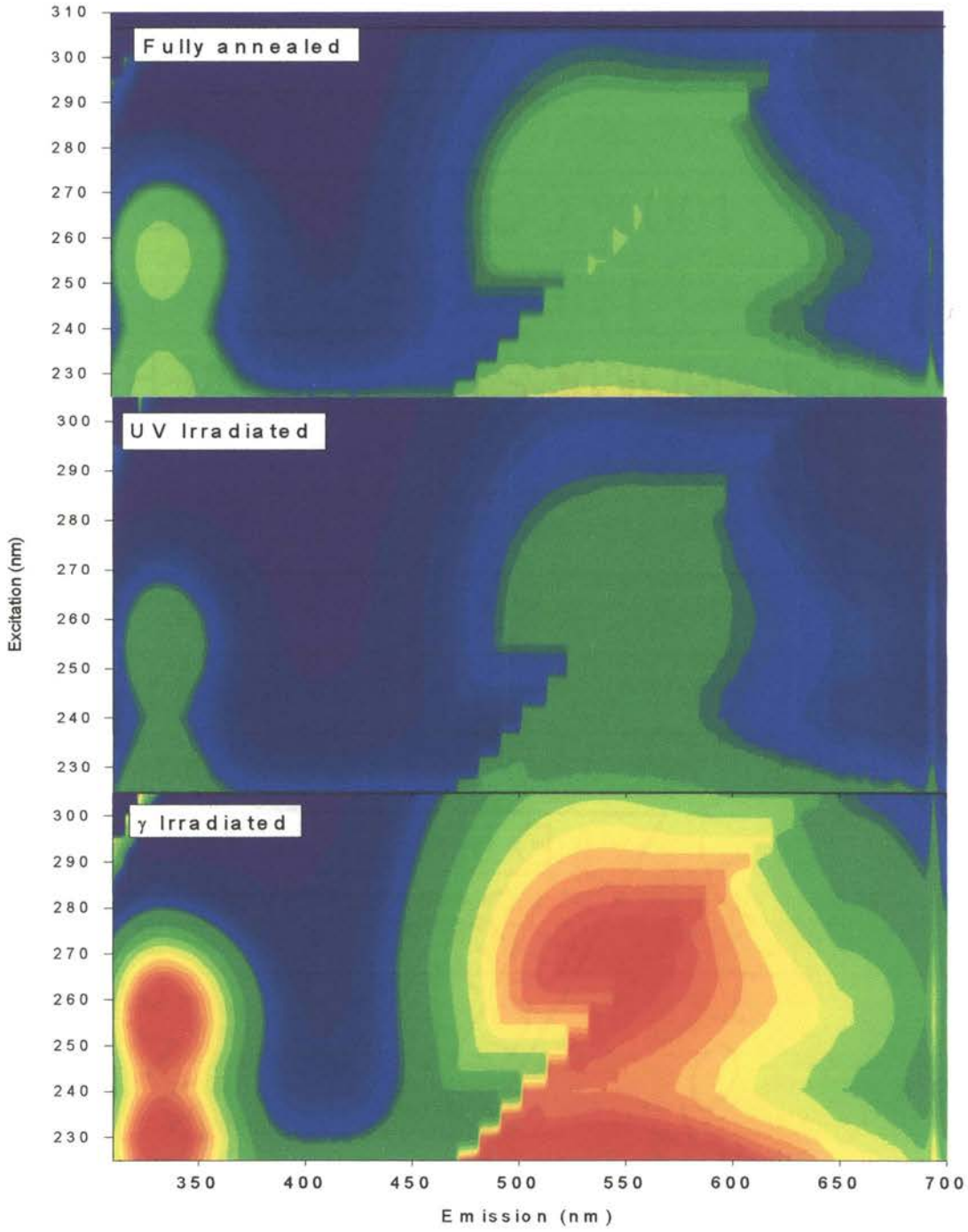

Figure 3-2: Photoluminescence from Al_2O_3 fiber sample fiber 1. Fiber 1 shows a strong F^+ center emission at 326 nm and strong $F^{2+}{}_2$ and Chromium emission at 560 and 694 nm.

excited Cr^{3+} center. An example of F_2^{2+} and chromium emission from fiber 1 is shown in figure 3-2.

The emission spectra were measured for different states of trap filling in the samples. The emission spectra of the fibers showed changes in the intensities of the emission bands following the filling of the electron traps with UV light, and the filling of all charge traps with high energy gamma rays from a ^{60}Co source. The emission bands were seen only to change in intensities. No new emission bands appeared and existing bands did not disappear due to irradiation with gamma rays or UV light. For UV exposure, all the fibers showed a decrease in the intensities of the emission bands due to the F^+, F_2^{2+}, and C^{3+} centers capturing free electrons and thus reducing the concentration of these centers. The intensities of the emission bands for all the fibers increased, from the UV irradiated levels, after irradiation with gamma rays. This increase is interpreted as the capture of holes created by the gamma irradiation by F, F_2^+, and Cr^{2+} centers, causing and increase in the concentration of these centers in the samples.

3.3 OSL from Al_2O_3 Fibers

The OSL from the fibers was measured in a Risoe TL/OSL reader system.[79] For this system, the fibers were irradiated with a $^{90}Sr/^{90}Y$ beta source, and the OSL measured by illuminating the fibers with 527 nm light, and the emission detected by a photomultiplier tube. For the Al_2O_3 fibers, the OSL emission was passed through two U340 band pass filters to separate the emission from the stimulation light before detection.

3.3.1 OSL Decay

The OSL from the fibers was measured to determine the relative OSL decay characteristics for the individual samples. To do this the samples were each given a fixed dose of 10 Gy and the subsequent OSL signal was then readout using the Risoe reader.

The OSL from fiber 1, fiber 4, fiber 31, and rod 1 are shown in figure 3-3. The OSL signal from each fiber shows a slight initial increase followed by an exponential decay. The initial increase arises from the presence of shallow traps that compete for the capture of electron with recombination centers in the sample as discussed in section 2.3.2. The long-lived decay in the fibers shows the presence of competing shallow and deep traps in the samples. These traps cause a slowing of the production of the luminescence by temporarily trapping free charge before re-releasing it (either by optical stimulation or thermal release) into the conduction band where recombination may occur. The presence of these traps causes the OSL decay to be the sum of several different decaying exponential from the competing traps as expressed by equation 2.28 from section 2.3.1. The OSL from the fibers was normalized to the weight of the fibers to show OSL per unit mass and give to a relative sensitivity of each of the fibers of varying sizes. The cut sample rod 1 shows the highest OSL sensitivity, with fiber 31 showing a sensitivity only slightly less. Fiber 1 and fiber 4 showed a much lower sensitivity, with the OSL signal being an order of magnitude less intense than for rod 1.

The OSL decay from fiber 31 is almost straight line with a negative slope, after the initial rise, when plotted on the logarithmic scale, as in figure 3-3. This would indicate a nearly single exponential decay for the OSL signal, which would suggest that

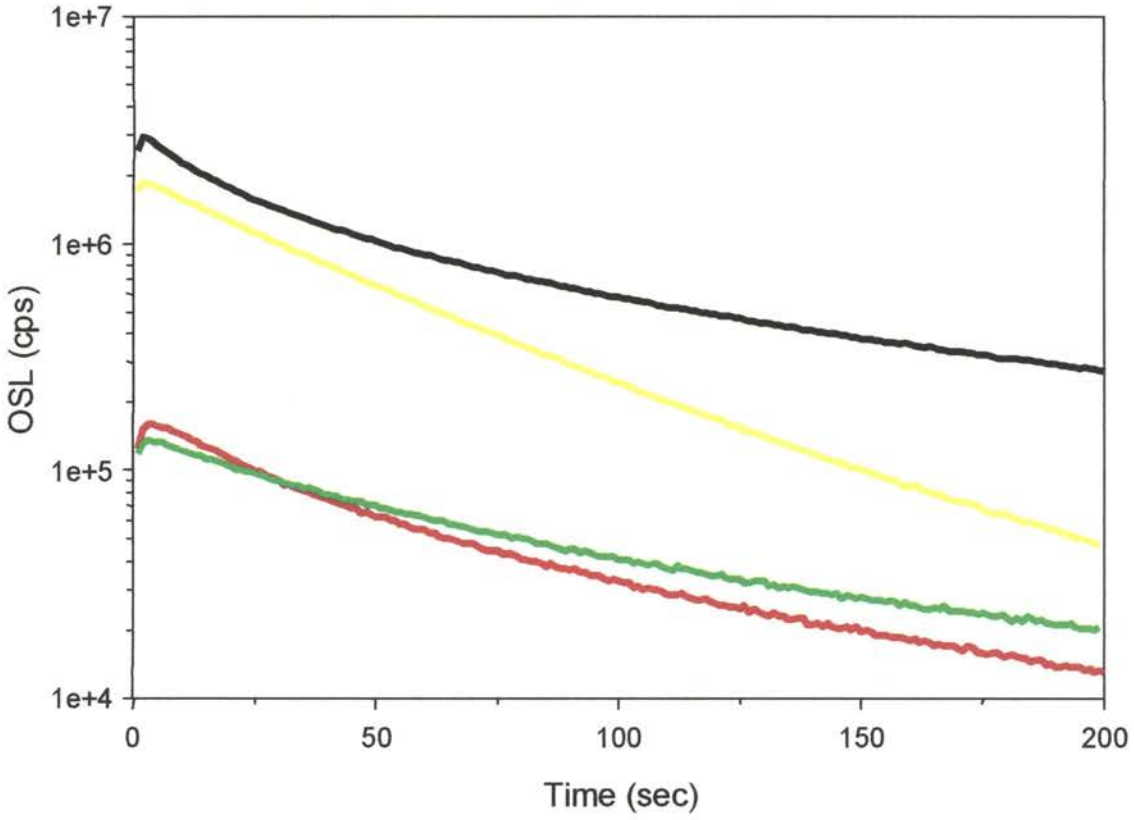

Figure 3-3: OSL decay curve for rod 1 (black), fiber 1 (red), fiber 4 (green), and fiber 31 (yellow). The OSL signals have been normalized by mass to show a relative OSL sensitivity for each fiber.

the OSL is generated almost completely from a single charge trap in the crystal as given by the expression for the simple model of OSL from equation

$$I_{OSL} = n_o f \exp[-ft] = I_o \exp[\frac{-t}{\tau}]. \quad (2.27)$$

By fitting the OSL from fiber 31 to a single decaying exponential of the form of equation 2.27, the optical excitation rate f can be determined. Using this value of f, the photo-ionization cross section for the charge trap can be determined with the use of the expression $f = \phi(\lambda)\sigma(\lambda)$ with $\phi(\lambda)$ defined as the photon fluence rate (photons/m^2/s^2). The photon fluence can be expressed by the equation

$$\phi(\lambda) = \frac{I}{E_{ph} * A * t} \quad (3.1)$$

where I is the intensity of the laser light given in watts, $E_{ph}=h\nu$ is the energy per photon of the simulation light measured in joules, A is the cross sectional area of the region of the sample being stimulated in meters^2, and t is the unit time of the stimulation. By calculating $\phi(\lambda)$ 10 mW of 527 nm light from the LED array of the Risoe reader used for fiber 31, the photo-ionization cross section can be calculated using the value of f determined by the fit of the data and is found to be: $\sigma_o = 4.27 \times 10^{-21}$ m^2. This value is consistent with values of the photo-ionization cross section for single crystal Al_2O_3.[80] The fit of the OSL decay for fiber 31 is shown in figure 3-4.

3.3.2 Dose Response

The OSL response of the Al_2O_3 fibers was measured as a function of dose. The OSL dose responses for fiber 1 and rod 1 were measured on the Risoe TL/OSL reader. For these measurements the following procedure was followed: (1) the samples were

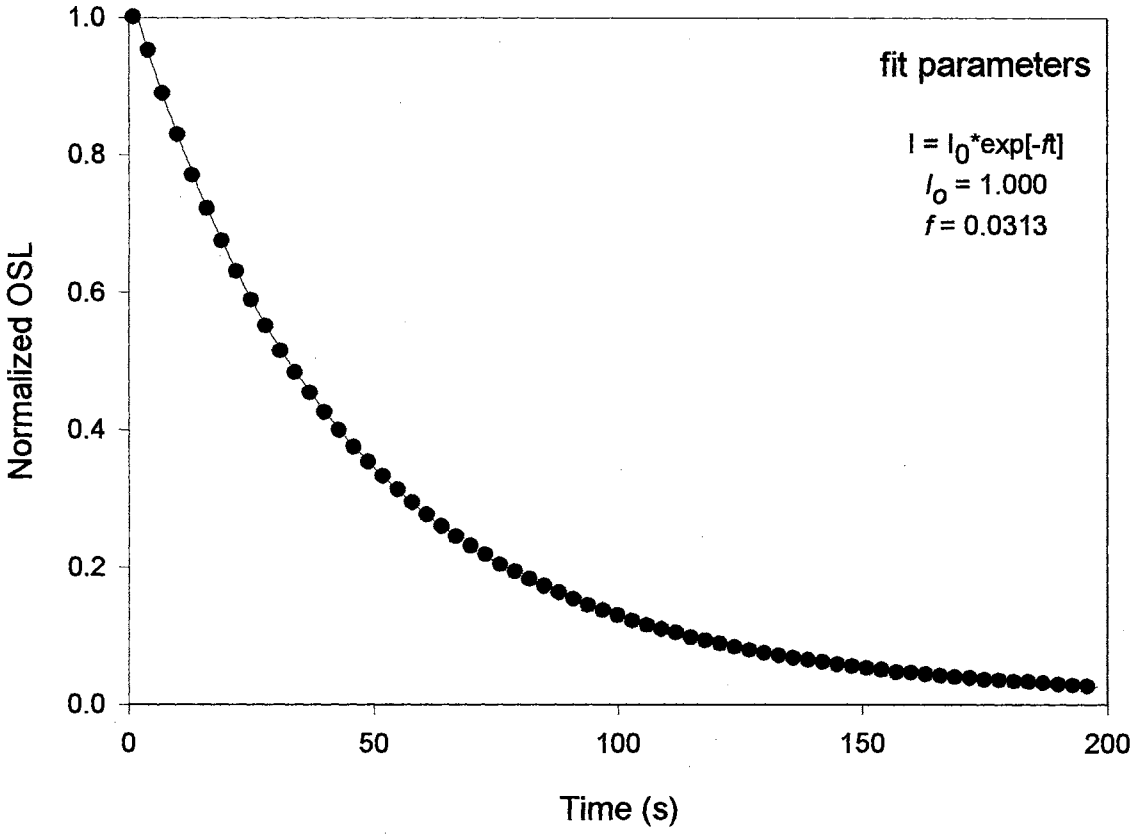

Figure 3-4: OSL decay from fiber 31 (circles) fir to a single decaying exponential function (red line). From the fit, the photoionization cross section for fiber 31 is calculated to be $\sigma_o = 4.27 \times 10^{-21}$ using the value of f determined by the numerical fit of the data.

annealed to empty all charge traps, (2) exposed to a given dose, and (3) the OSL was then read. This process was repeated for doses ranging from approximately 0.1 Gy to 300 Gy.

The dose response curves of the two fibers demonstrate somewhat different characteristic shapes and are plotted as the maximum of the OSL intensity as a function of dose as shown in figure 3-5. Fiber 1 displays a linear OSL response to dose from 0.1 Gy to about 30 Gy. For doses greater than 30 Gy, the OSL is sublinear, up to a dose of about 70 Gy. For dose larger than this, the OSL from fiber 1 was constant due to saturation of the charge traps in the fiber. For rod 1, the dose response was linear through a range from the lower limit of the measurement of about 0.1 Gy to about 10 Gy. For doses greater than 10 Gy, the OSL response of rod 1 showed a supralinear response. That is to say, the OSL response is greater-than-linear for increasing doses given to the sample.[81] This is followed by a sublinear region and saturation of the signal for doses greater than 300 Gy. The supralinear region of the dose response for rod 1 is believed to be due to the filling of competing traps in the sample. The competition process can occur during the irradiation of the sample leading to electrons trapping in the competing traps and lowering the concentration in the main traps responsible for the production OSL, or can occur during the optical stimulation of the sample leasing to freed electrons trapping in the competing traps instead of recombining.[82,83] Both cases lead to an under response of the OSL signal at low doses. As these competitors saturate, more electrons are able to become trapped in the main OSL traps, leading to an increase in the response for increasing dose.[81] This increase in the OSL response is seen as a gradual increase to a greater-than-linear response at higher doses.

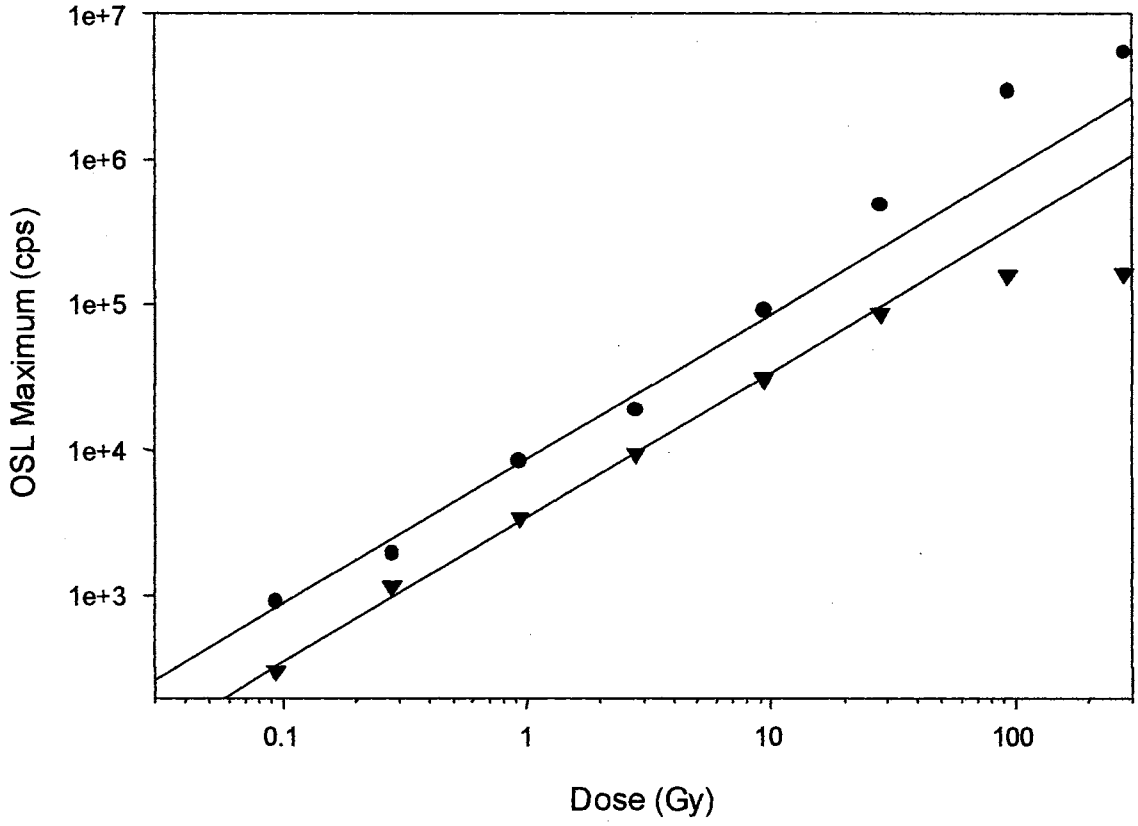

Figure 3-5: The dose response of fiber 1 (triangles) and rod 1 (circles). The solid lines represent the line of linear dose response for each fiber.

3.4 Charge Traps

Since the OSL signal from a crystal is generated from the optical stimulation of trapped charge, it is important to know how easily trapped charge may be ionized from different traps in the sample by the incident stimulation light. The contribution of different traps to the overall OSL signal in the Al_2O_3 fibers was studied to determine the contribution of these different traps to the overall OSL signal. The trapping states were divided into to two types. The first were shallow traps, which were traps that could be measured with TL and included traps that are thermally unstable at room temperature, and the traps that make up the main TL peak that is centered at about 180 °C. The second type were deep traps, which were the traps whose thermal activation energies were greater than that of the main TL peak and thus too high to be efficiently measured with TL due to the thermal quenching process in Al_2O_3.[56]

3.4.1 Shallow Traps

To measure the relative concentrations and optical activeness of the shallow traps, the Al_2O_3 fibers were cooled to –50 °C and irradiated so that thermally unstable traps would become stable and trapped charge would remain in the traps until the TL measurement was taken. The samples were then heated at a rate of 1 °C per second from –50 °C to 250 °C and the resulting emission was passed through two 420 nm band pass filters to select only the F center emission, and the emission detected by a photomultiplier tube. The resulting emission data were recorded as a function of temperature. To determine the contribution to the OSL signal coming from the traps of the low temperature TL peaks, the fibers were again cooled to –50 °C and irradiated. After the irradiation, the samples

were exposed to 532 nm light from a 30 mW Nd:YAG laser for 100 seconds at –50 °C to bleach the charge traps.

The TL glow curves of fiber samples fiber 1, rod 1, fiber D, and fiber 24 are shown in figure 3-6. The fibers had TL glow curves centered at slightly higher temperatures than those found in a standard TLD 500 disk of Al_2O_3 that is used for TLD dosimetry, and the TL peaks were centered at slightly different temperatures.[57] This fact was attributed to the poor thermal contact between the fibers, and the heating plate used for the TL measurements. All the fibers had TL peaks centered between 15 and 30 °C and fibers 1 and 4 also had a TL peak centered at about 60 °C. The fibers all had a main TL peak with the peak temperature occurring in a range from about 175 °C to 200 °C for the different samples. The main TL peak of the different fibers differed in width. For fiber 1, rod 1 and fiber D, the main TL peak is relatively wide spanning a temperature range from about 150 to 250 °C. For fiber 24, the main TL peak is considerably thinner occurring in a temperature range from about 150 to 210 °C. The main peak from fiber 24 seems to occur on the lower temperature side of the main TL peak of fiber 1, rod 1, and fiber D. The glow curves shown in figure 3-6 were corrected for the mass of each fiber in order to give a relative concentration of the traps contributing to each peak in each of the fibers. From figure 3-6, the relative concentrations of thermally unstable traps (20 °C TL peak) to the traps contributing to the main TL peak varies widely from fiber to fiber. Fiber 1 is seen to have a more intense 20 °C TL peak than main TL peak and therefore the relative concentration of such traps is higher for the thermally unstable TL peaks than for the main TL peak. In contrast, rod 1 and fiber 24 have a low temperature TL peak that is less intense than the main TL peak, and fiber D shows almost

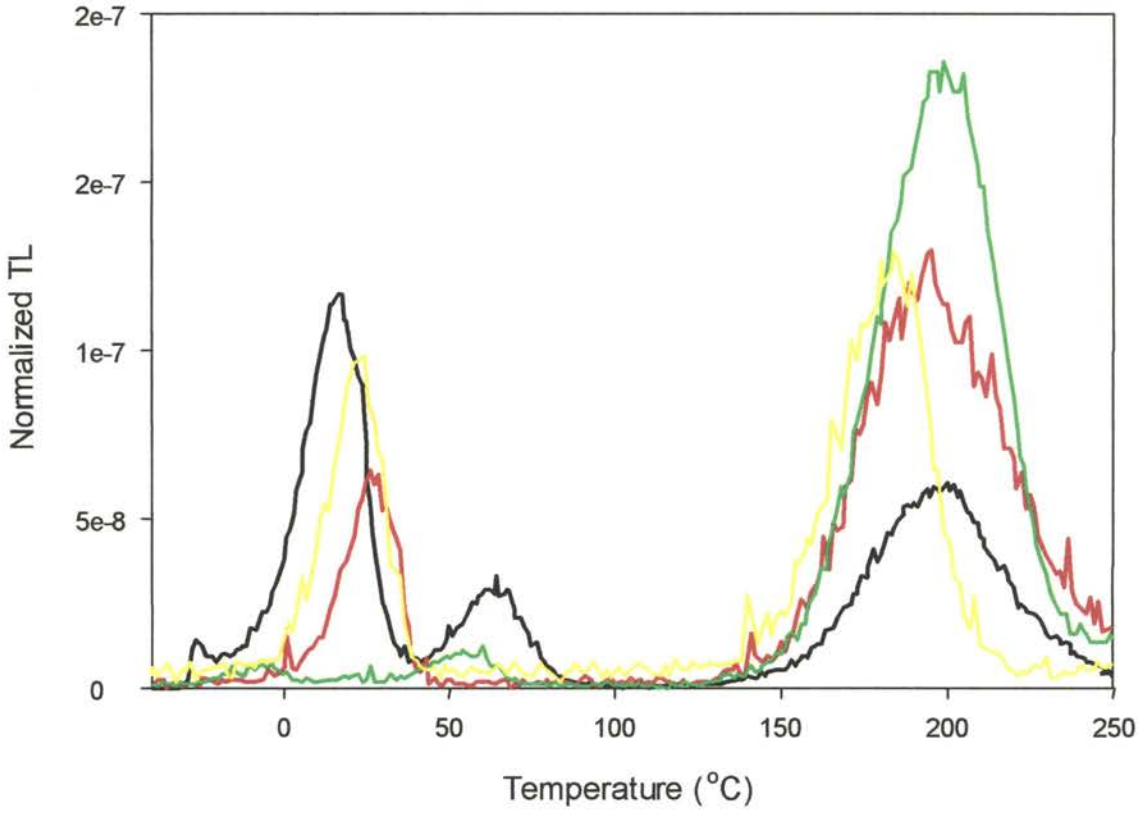

Figure 3-6: TL from fiber 1(black), rod 1 (red), fiber D (green), and fiber 24 (yellow) showing the distribution of shallow trapping states.

no low temperature TL peak and the largest main TL peak of all the fibers.

The TL peaks obtained after bleaching with 532 nm light were compared to the original TL peaks obtained for the fibers. The percentage difference of TL intensities from the original TL peaks and those obtained after bleaching with 532 nm laser light was measured to give a relative measure of the contribution of the TL traps that are bleached during an OSL measurement. The original and bleached TL peaks for fiber 1, fiber 24, and rod 1 are shown in figure 3-7. The main TL peak showed the greatest optical sensitivity, with a large decrease in intensity, and in the case of fiber 1 and rod 1, a change in the shape of the peak with a shift in the TL maximum to higher temperatures. This suggests that the main TL peak of fiber 1 and rod 1 is a convolution of at least two peaks arising from at least two charge traps with slightly different thermal activation energies. Also, the more efficient bleaching at lower temperatures shows that this component has a slightly higher photo-ionization cross-section than the higher temperature component. This leads to a change in the peak shape and a slight shift in the peak maximum to higher temperatures. The main peak of fiber 24 is much thinner than the main peak of fiber 1 and rod 1 and occurs on the lower temperature side. This fact, along with the fact that the peak does not change shape or shift in temperature with bleaching, suggests that its main peak is due to only one charge trap similar the lower temperature component of the main peak for fiber 1 and rod 1. For fiber 1, the 60 °C TL peak showed no decrease in intensity due to bleaching, and is therefore concluded to be completely optically insensitive to 532 nm light. The 20 °C TL peak in fiber 1 and fiber 24 showed a slight optical sensitivity to 532 nm light with a slight decrease in the TL

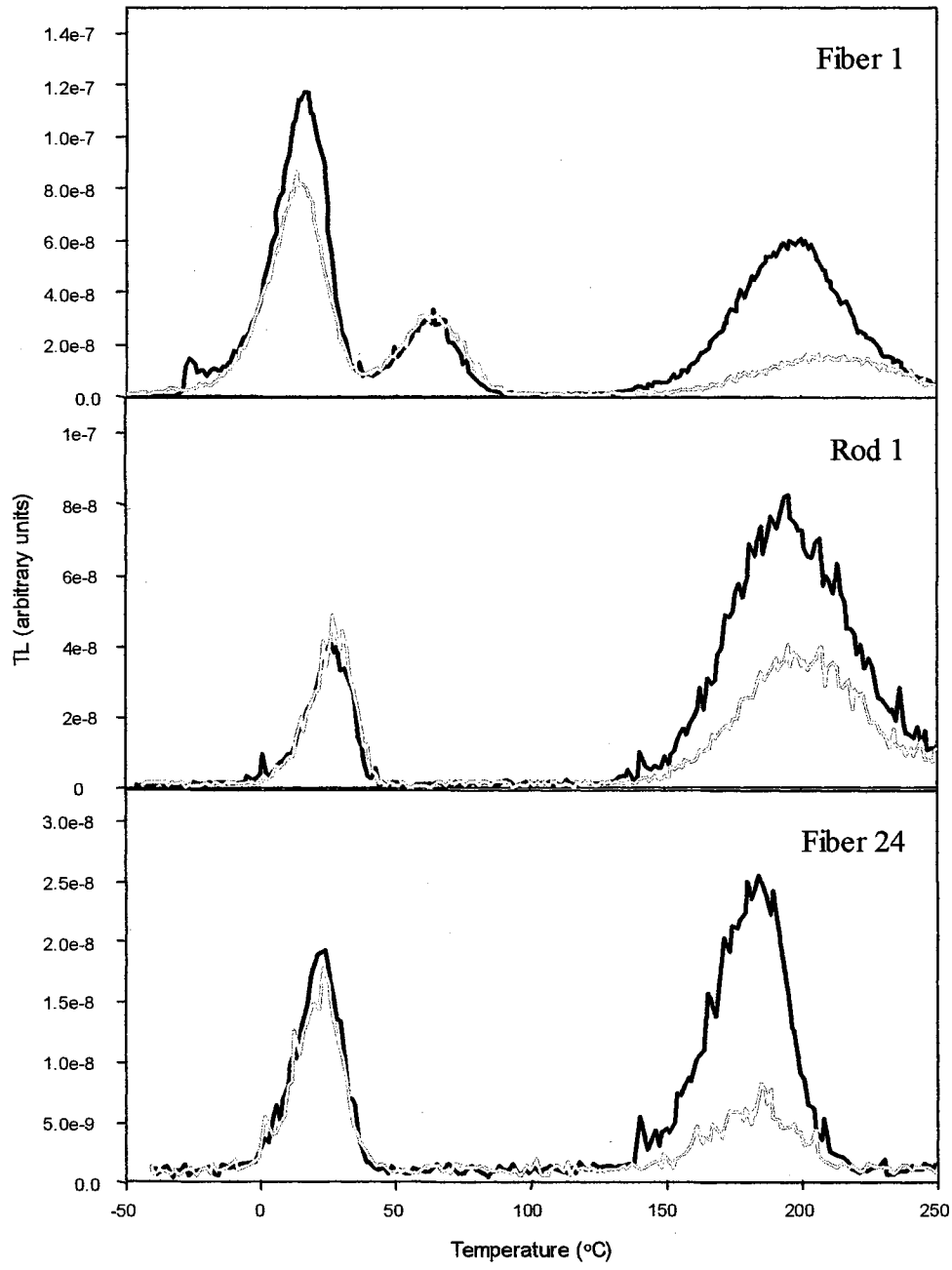

Figure 3-7: Comparison of TL glow curves for fiber 1, rod, 1, and fiber 24 to glow curves obtained after bleaching the irradiated fibers with 532 nm light for 100 seconds at –50 °C.

intensity of the peak due to bleaching. The 20 °C TL peak of rod 1 appeared to be optically insensitive to 532 nm light showing no decrease in intensity.

Each of the TL peaks were normalized to the peak intensity of the original TL measurement, as shown in figure 3-8. In this way the percentage of the remaining signal of each peak after bleaching could be measured. With this normalization, the intensity of the main TL peak in fiber 1 and fiber 24 is reduced by about 80 percent, and by about 60 percent in rod 1 by bleaching with 532 nm light. The 20 °C TL peak intensity in fiber 1 and fiber 24 were reduced by about 25 percent. From this bleaching of the TL peaks, it can be noted that more of the OSL signal generated from the traps responsible for these TL traps comes from the main TL peak, and in particular, the low temperature component of the main peak than from the low temperature peaks.

3.4.2 Deep Traps

The optical activity of the deep traps in the Al_2O_3 fibers was monitored by measuring the OSL signal in the fibers after the shallow traps in the sample were emptied. The fibers were irradiated, and then annealed to 400 °C to empty the shallow traps. The OSL signal was measured after annealing the shallow traps, and thereby only measuring the optical stimulation of charge from the deep traps with the 527 nm light. The fibers were exposed to increasing doses and the OSL from the deep traps measured as a function of dose. A schematic of the experimental procedure used to measure the OSL from the deep traps is shown in figure 3-9. The fibers were next irradiated with ionizing beta particles from $^{90}Sr/^{90}Y$ source to prefill the deep traps. After prefilling of the deep traps, the OSL was measured in the same processes as described in figure 3-9.

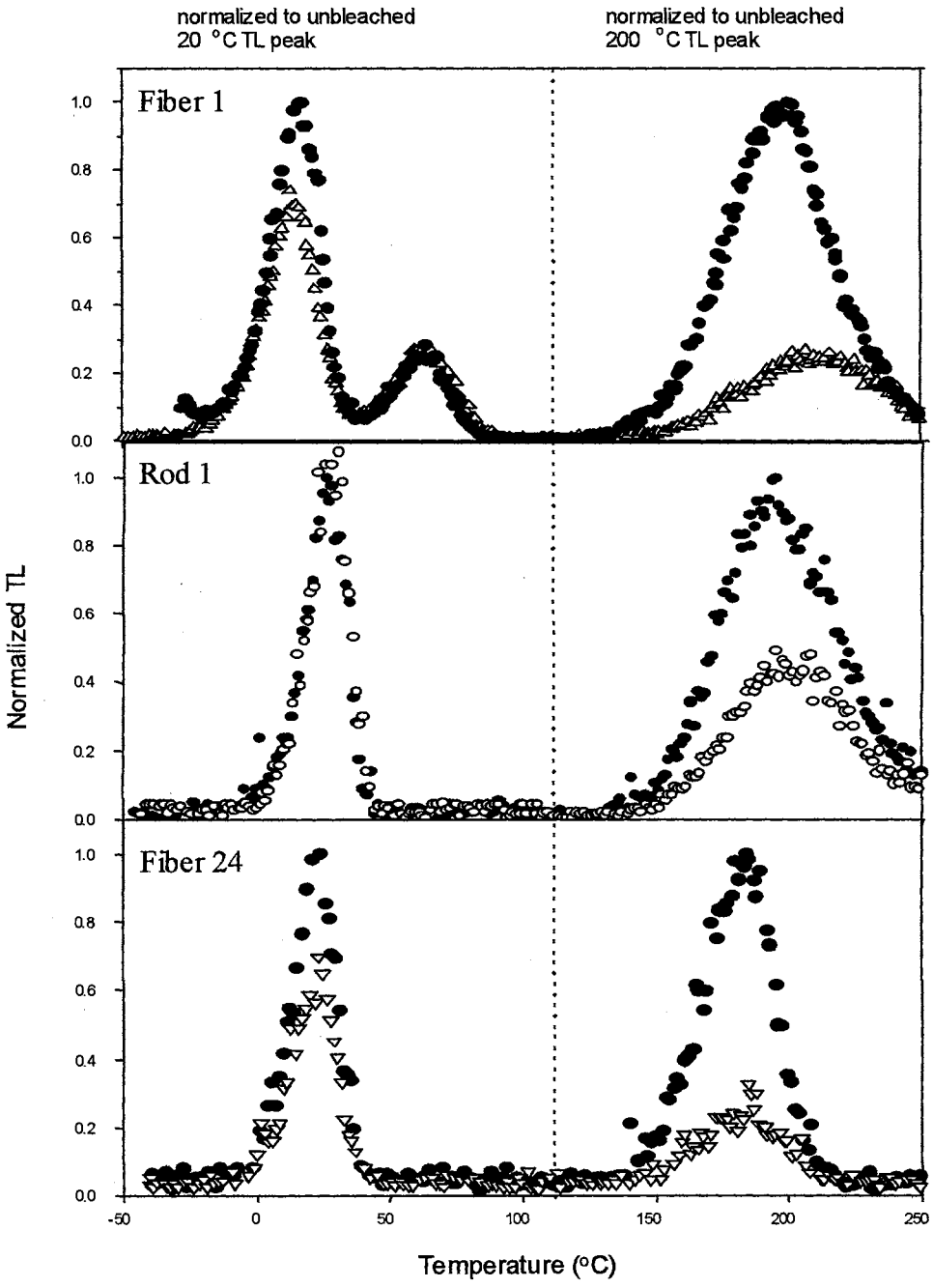

Figure 3-8: Normalized TL for fiber 1, rod 1, and fiber 24 showing the percentage of each TL peak remaining after bleaching with 532 nm light.

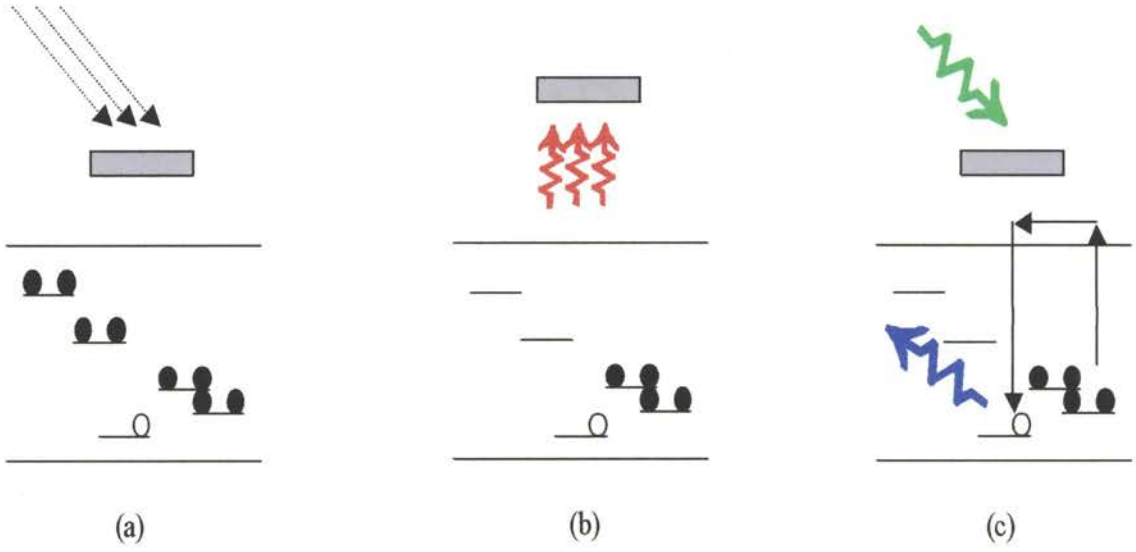

Figure 3-9: The OSL from the deep traps was measured by first (a) irradiating the samples to fill the traps, then (b) annealing to 400 °C to empty the shallow traps and finally stimulating the sample to produce an OSL signal from the deep traps.

The OSL from deep traps was measured as a function of dose in fiber 1 and rod 1 and is shown in figure 3-10. The fully annealed samples showed no OSL signal from the deep traps for small doses. The OSL signal only began to rise above that of background levels for doses of about 10 Gy for rod 1. The OSL from the deep traps for fiber 1 showed no increase above background for dose up to 400 Gy. This leads to the conclusion that rod 1 has a high concentration of optically sensitive deep traps that begin to fill at doses of 30 Gy with saturation of the deep traps occurring at about 400 Gy. Contrary to rod 1, fiber 1 has a low concentration of deep traps, showing no OSL signal from the deep traps up to a dose of about 650 Gy.

Next the fibers were given a saturating dose of ionizing irradiation, and then annealed to remove the charge from the shallow traps, the OSL from the fibers was then read with 527 nm light from the LED array of a Risϕ TL/OSL reader system.[84] After this, the fibers were exposed to 470 nm light from the blue LED array of the Risϕ TL/OSL reader system in order to bleach the charge out of the deep traps and remove the OSL. After bleaching for a set period of time, the OSL from the fibers was read using the 527 nm LED array.

The results of the bleaching of the deep traps in rod 1 and fiber 1 are shown in figure 3-11. The OSL signal for rod 1 and fiber 1 decreases for increasing bleach time with blue light as seen by Walker et al. for the phototransfered of charge from deep trap in Al_2O_3.[85] For both fiber 1 and rod 1, that the OSL from the deep traps can be completely depleted by bleaching with blue light. This shows that for a sample that has been given a large dose, all traps (both shallow and deep) responsible for the OSL signal

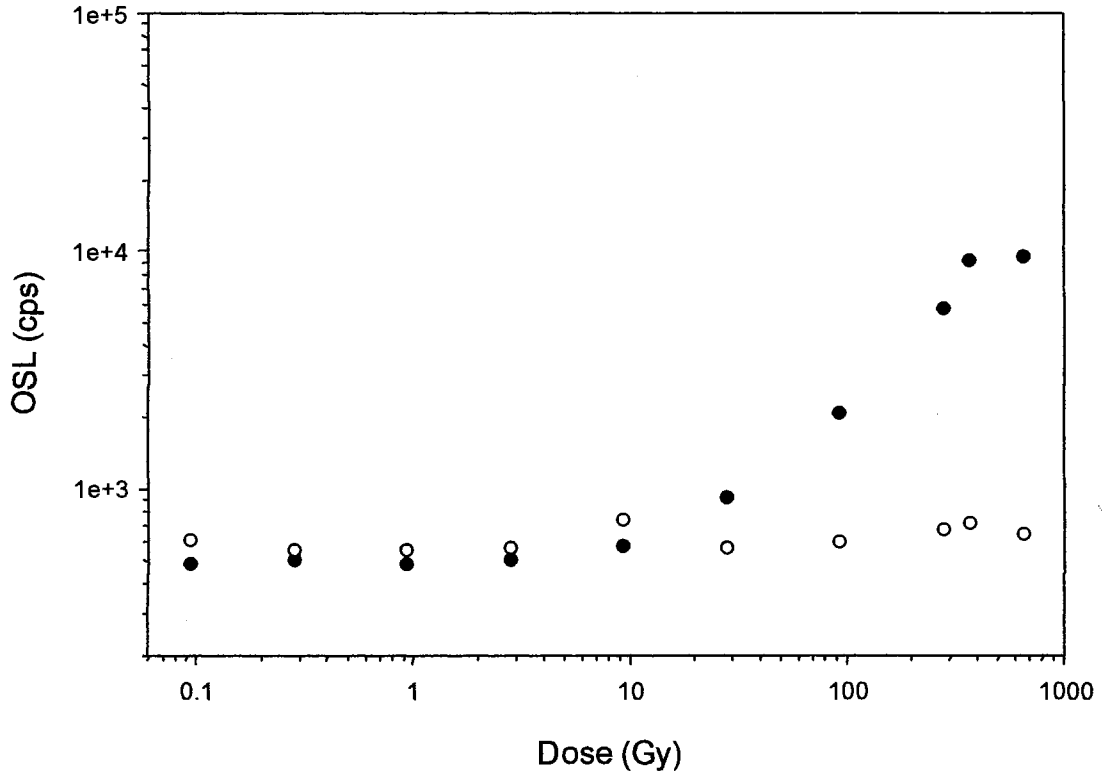

Figure 3-10: OSL stimulated from the deep traps in fiber 1 (open circles) and rod 1 (filled circles) for increasing doses.

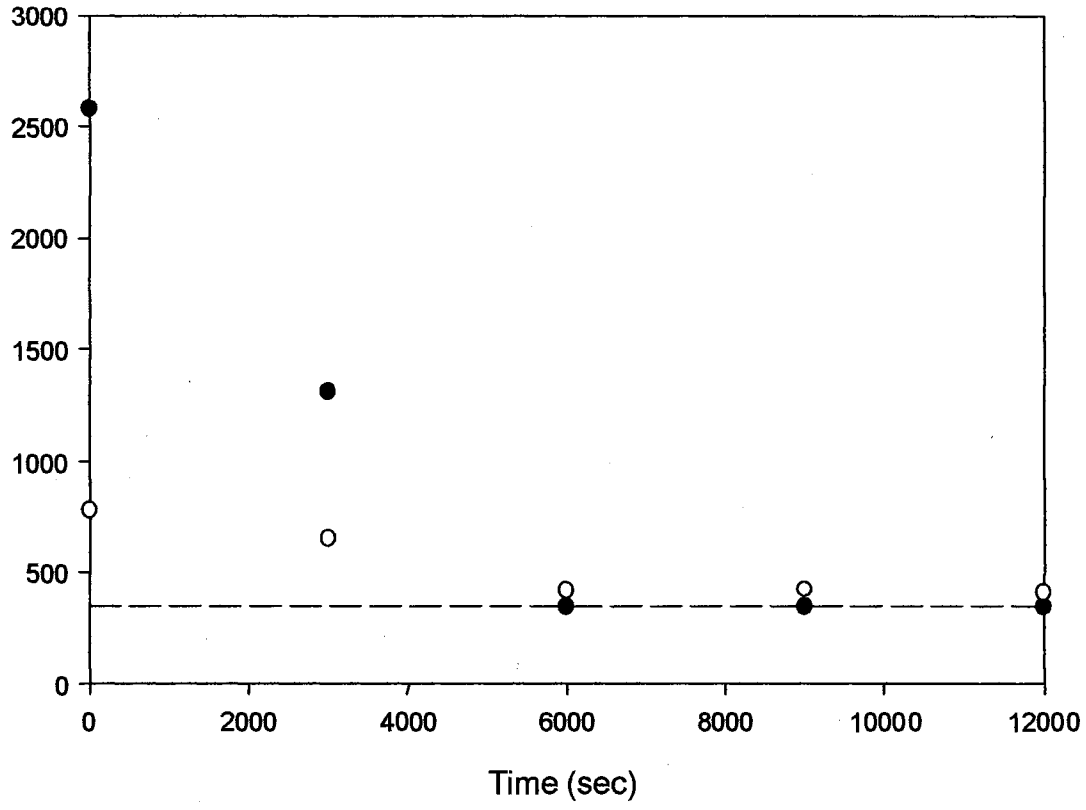

Figure 3-11: Bleaching of the OSL signal from the deep traps for fiber 1 (open circles) and rod 1 (black circles). The signal from the deep traps was completely depleted to the fully annealed background level (dotted line) after about 6000 seconds stimulation with 470 nm light.

can be emptied by bleaching with blue light, and the charge traps in the Al_2O_3 fibers can be reset to their original charge configuration before exposure to radiation.

3.5 OSL Sensitivity Changes

The sensitivity of a sample may be described as the OSL intensity of the sample to a given test dose of radiation (i.e. OSL/unit test dose). For many different materials commonly used for luminescence dosimetry, it has been observed that the sensitivity of a sample may be changed by certain pre-irradiation treatments of the sample.[86,87] Increases in sensitivity can be achieved by removing charge traps that compete with the traps responsible for the OSL signal in the sample. The competitors may be removed either by destroying them, which is typically done by high temperature annealing, or by prefilling them by pre-irradiating the sample before irradiation.

The changes in OSL sensitivity for fiber 1 and rod 1 were investigated by measuring the change in the OSL intensity after the filling of different charge traps in the sample. This was done by exposing the samples to high doses of nonionizing, radiation in the form of UV light, to ionize electrons from defect centers without creating free holes on the valence band in the crystal to fill electron traps. The sample was then annealed to remove trapped charge in the traps responsible for the OSL signal, given a test dose of 3 Gy, and the OSL readout using the green diodes on the Risoe automated reader. After this the sample was annealed at 900 °C to completely empty all charge traps. The sample was then exposed to a high dose of ionizing irradiation (beta) to fill all competing traps (electron and hole traps), and the same procedure, as used for the UV irradiation, was carried out in order to measure the OSL with all competing traps filled.

A comparison of the OSL with different states of filled competitor traps for fiber 1 and rod 1 is shown in figure 3-12. The OSL in figure 3-12 is normalized to the maximum of the signal from the sample with all traps empty prior to irradiation in order to give a relative sensitivity with different traps filled prior to irradiation. The OSL sensitivity of both samples can be increased by more than a factor of two by prefilling the electron traps. This shows that both samples have a large concentration of competing electron traps. These traps compete, during both trap filling and the recombination processes, with the traps responsible for the production of the OSL in the samples. This competition lowers the concentration of electrons trapped in the OSL traps and the number of electrons recombining causing a lowering of the signal intensity when the competing traps are empty. When the samples are irradiated with ionizing irradiation the sensitization is much less for rod 1 with an OSL signal that only increases by about 25 percent, and fiber 1 shows no increase in sensitivity at all. This suggests that ionizing irradiation is filling the competing electron traps, but also filling competing hole traps, that become competitors with the recombination centers responsible for the production of the luminescence. These competing hole traps act as competing recombination centers that are either nonradiative, or produce emission that is outside the measurement window for F center luminescence. This leads to a decrease (or complete removal for fiber 1) of the sensitization effect of the filling of the competing electron traps. Also, from figure 3-12, the initial increase of the OSL signal is seen to increase when the competing electron traps are full, due to an increased efficiency in the trapping of electrons in the shallow traps. The initial increase seem to be larger for fiber 1 than for rod 1 due to the larger concentration of shallow traps relative to the main OSL traps for fiber 1.

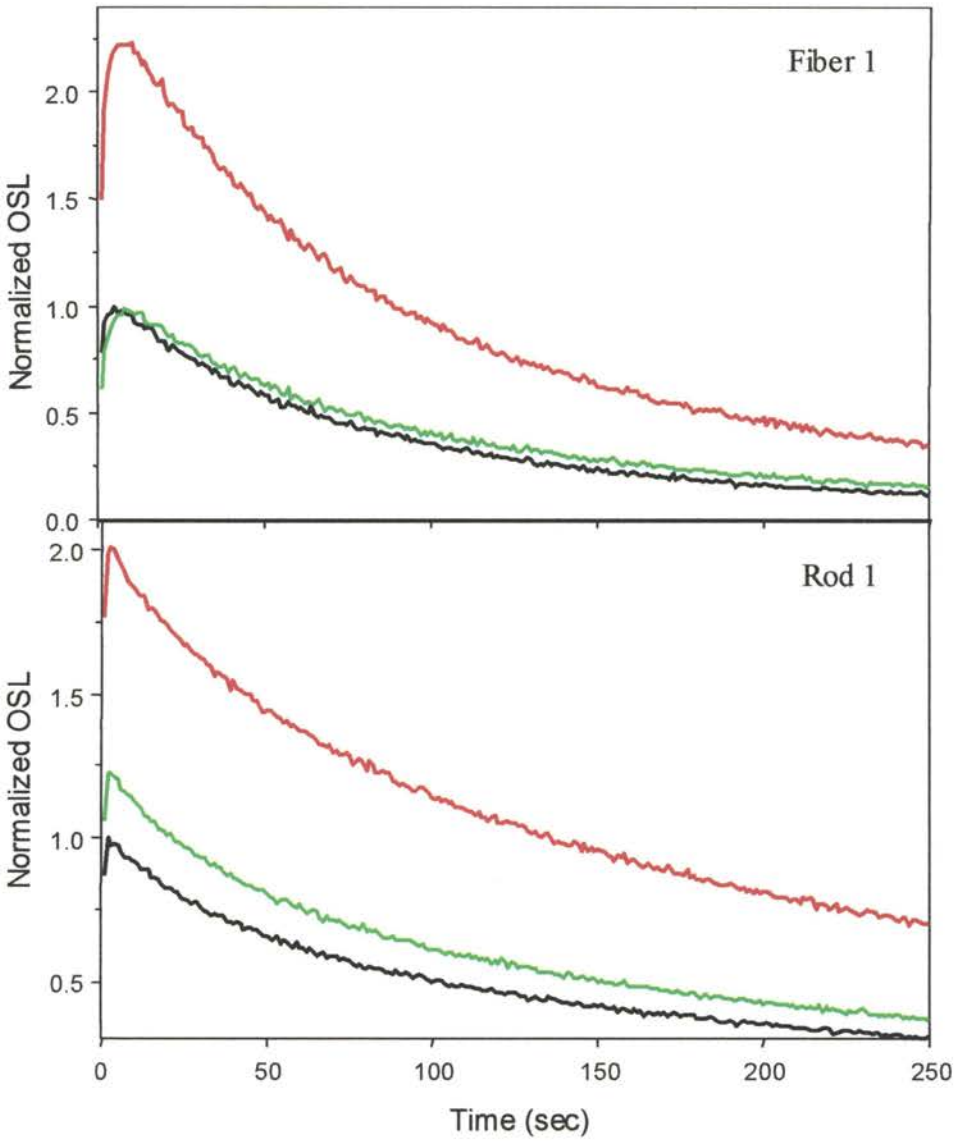

Figure 3-12: Comparison of OSL sensitivity for fiber 1 and rod 1 with all competitor traps empty (black), competing electron traps full (red), and all competing traps full (green). The OSL signals were normalized to the maximum signal for the case of all competing traps empty.

The sensitization of the samples will lead to a higher OSL intensity per unit dose, and thus change the dose response of the fibers. The dose response of the fibers was measured before and after the prefilling of competitor traps in order to measure differences in the intensity and shape of the dose response curves. The sensitized OSL dose response curves are compared to the normal dose response in figure 3-13. The samples both show an increase in intensity with the competing electrons filled. The dose response for both fibers was very similar when all traps were initially empty, and when all competing traps are initially filled. Both samples showed a linear region with saturation at a lower dose for fiber 1. The saturation intensity is however the same for all cases for fiber 1. Filling the competing electron traps extended the range of linearity in rod 1. The dose at which the onset of supralinearity is seen in rod 1 was increased from approximately 3 Gy to about 30 Gy and the OSL saturates for doses above this.

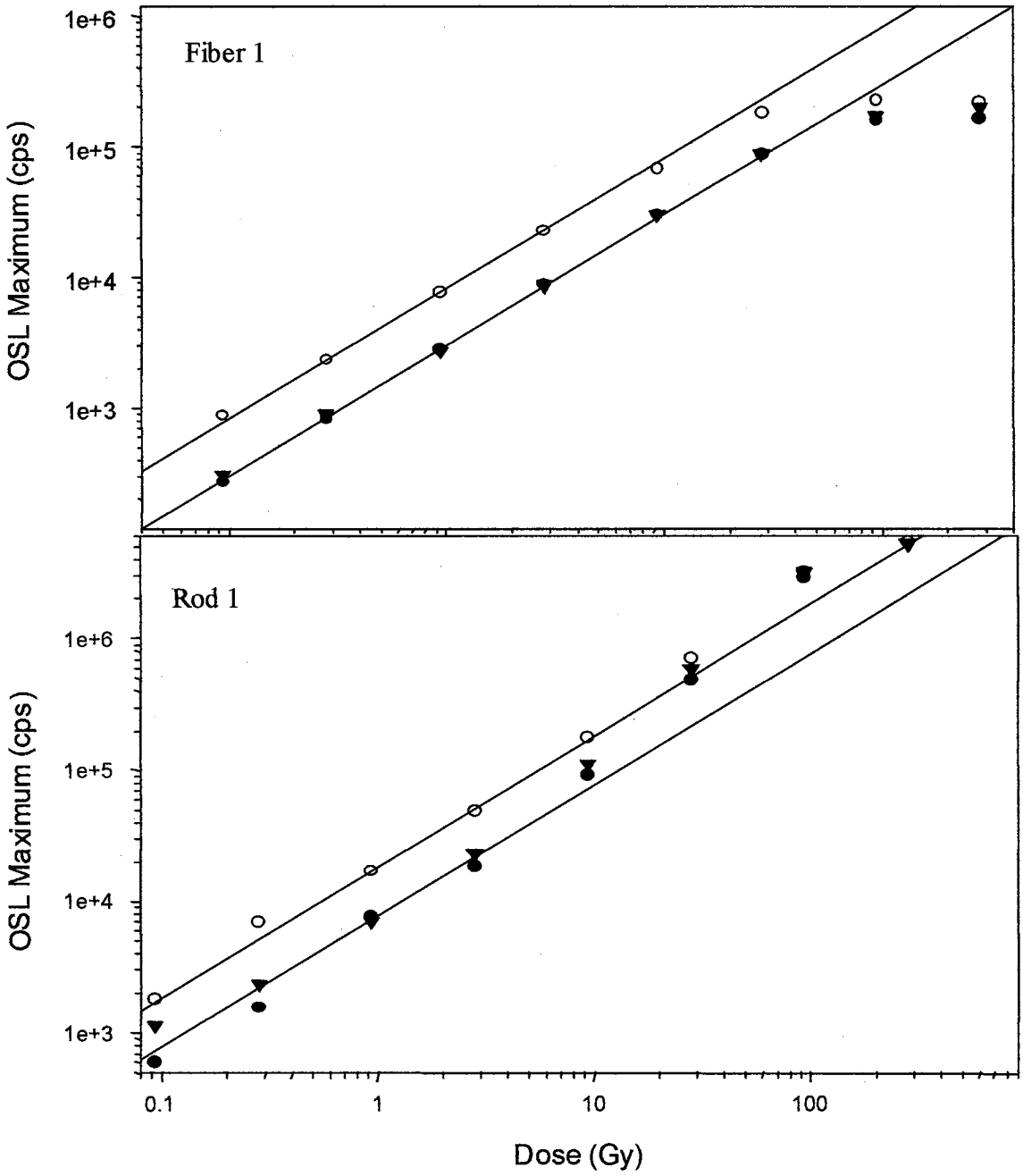

Figure 3-13: Dose response of fiber 1 and rod 1 with all traps initially empty (filled circles), with competing electron traps initially filled (open circles), and with all competing traps initially filled (triangles). The dose response in each instance is compared with the line of linearity (solid lines).

CHAPTER 4

4. Real Time Luminescence in Al_2O_3 Fibers

4.1 A simple Model of Real Time Luminescence

To develop a mathematical description of the OSL signal generated from a sample in real-time during irradiation, both the processes of OSL and RL must be considered. This will be developed in the context of the one trap, one recombination center model as described in chapter two, and illustrated in figure 2.1. To do this, the rate equations for the concentration of electrons in the conduction band for the OSL and RL models must be modified to include both the irradiation and optical stimulation processes separately. The rate equations for the real-time luminescence process can be written as

$$\frac{dn_c}{dt} = \Gamma\Phi + n_t f - n_c A_n (N - n_t) - n_c m A_{mn} \tag{4.1}$$

$$\frac{dn_t}{dt} = -n_t f + n_c A_n (N - n_t) \tag{4.2}$$

$$\frac{dm}{dt} = -n_c A_{mn} m \tag{4.3}$$

where all terms remain the same as defined in chapter two. Equation 4.1 includes terms for both the generation of electrons due to irradiation, and due to optical stimulation. Using the quasi-equilibrium approximation, an expression for the concentration of electrons in the conduction band can be written as

$$n_c = \frac{\Gamma\Phi + n_t f}{A_n (N - n_t) + A_m m}. \tag{4.4}$$

With this expression, and using equation 2.1 an expression for the real-time luminescence intensity (I_{RTL}) can be written

$$I_{RTL} = -\frac{dm}{dt} = A_m m\left(\frac{\Gamma\Phi + n_t f}{A_n(N-n_t)+A_m m}\right). \tag{4.5}$$

This equation can be rewritten into two separate components to give the equation

$$I_{RTL} = -\frac{dm}{dt} = \Gamma\Phi\left(\frac{A_m m}{A_n(N-n_t)+A_m m}\right) + n_t f\left(\frac{A_m m}{A_n(N-n_t)+A_m m}\right). \tag{4.6}$$

By writing the equation for the luminescence intensity in this way, it is readily apparent that the real-time luminescence signal is the sum of the signal produced by recombination with trapped holes at recombination centers of electrons in the conduction band due to the irradiation, or RL, and the signal due to recombination of electrons promoted to the conduction band by optical stimulation, or OSL. Therefore more specifically:

$$I_{RTL} = I_{RL} + I_{OSL} \tag{4.7}$$

where

$$I_{RL} = \Gamma\Phi\left(\frac{A_m m}{A_n(N-n_t)+A_m m}\right) \tag{4.8}$$

and

$$I_{OSL} = n_t f\left(\frac{A_m m}{A_n(N-n_t)+A_m m}\right). \tag{4.9}$$

The luminescence from each component can be modeled separately as functions of time, by solving equations 4.1-4.3 for the concentration of trapped electrons (n_t) as a function of time. Analysis of the RL intensity from equation 4.8 (setting f=0) shows that during irradiation, the concentration of trapped electrons approaches the total number of traps ($n_t \rightarrow N$), and the term in parenthesis in equation 4.8 approaches unity, therefore

the intensity of the RL will approach a constant value ($I_{RL} = \Gamma\Phi$). The RL intensity will therefore start out at an initial value, and rise to a maximum value as the charge traps are all filled. A computer model of the rise to maximum of the RL signal during irradiation is shown in figure 4-1. In contrast, from equation 4.9, when the OSL is measured with no irradiation (setting Φ=0), the concentration of trapped charge will decrease from an initial maximum to zero value ($n_t \rightarrow 0$) due to continued laser stimulation during successive measurements as shown in figure 4-1. Therefore, from equation 4.7, the real-time luminescence signal will be the sum of these two processes and rise from an initial value to a maximum value over time as shown in figure 4-1.

For the case of OSL measurements during irradiation, the signal will not decay to zero, due the continued trap filling due to the irradiation of the sample. During irradiation, the concentration of trapped electrons (n_t) will increase between the OSL measurements, and from equation 4.9, the OSL will initially increase due to the dependence of the OSL signal on n_t. The OSL will increase as long as the overall concentration of trapped electrons in the sample increases. However, as the number of trapped charges reaches a steady state level, due to the filling of electrons traps by irradiation, and depletion of trapped charge during OSL readings, the signal will saturate.

4.2 Real-Time Luminescence Experiments

4.2.1 Experimental Setup

A schematic of the measurement scheme for the real-time luminescence measurements is shown in figure 4-2. The Al_2O_3:C samples were cut into 0.5 cm pieces from Al_2O_3:C fibers ranging from approximately 350 to 800 micron diameter. The pieces were then

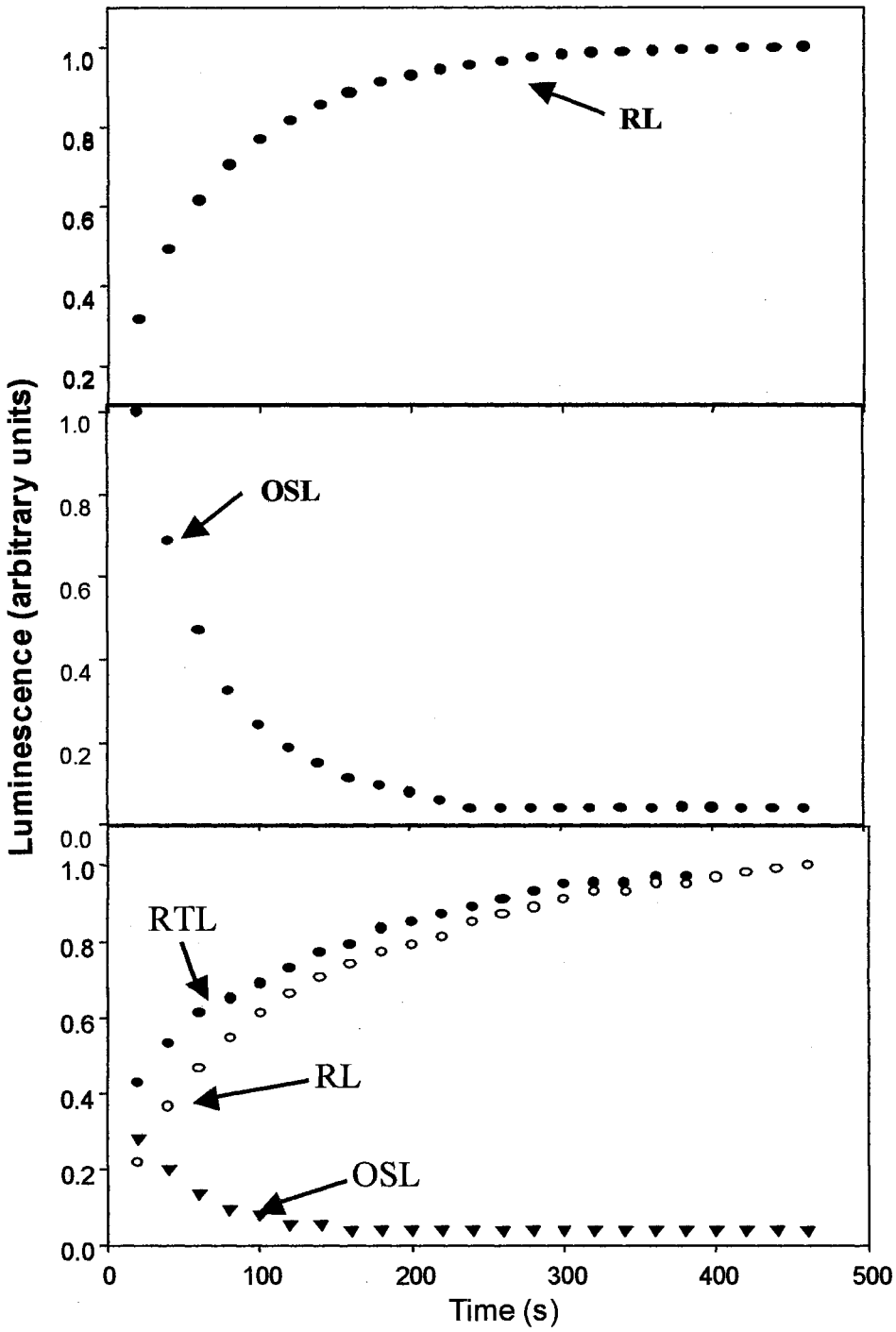

Figure 4-1: The rise to max as a function of time of the RL signal during irradiation of a sample, depletion of the OSL signal as a function of time, and the RTL as the sum of both processes.

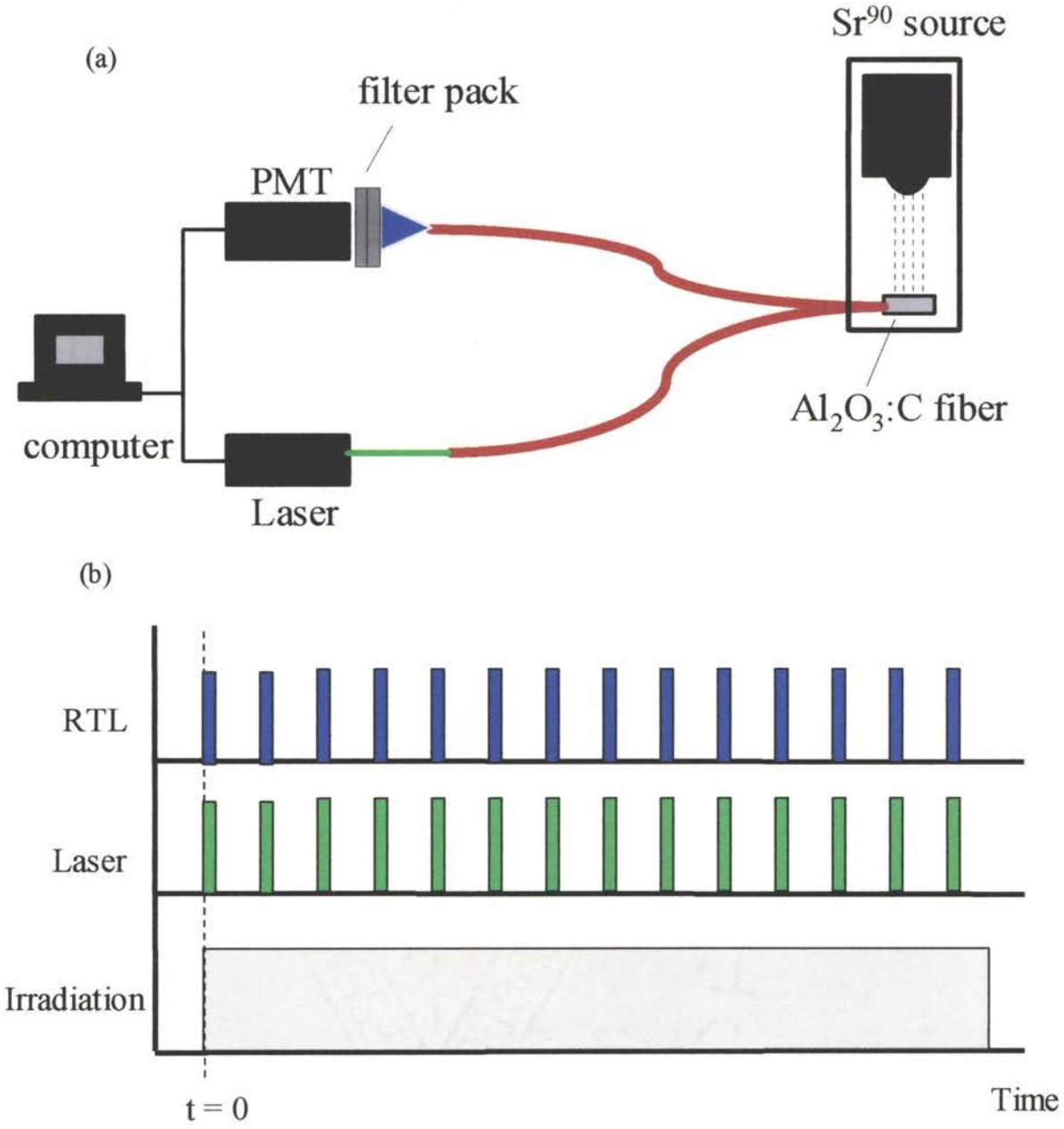

Figure 4-2: Schematic of experimental setup (a) for real-time luminescence measurements with Al_2O_3 fibers, and the measurement parameters (b) used to make the real-time OSL and RL measurements.

polished on both ends and connected to the end of a bifurcated fused silica fiber. The connection was accomplished by coating the end of the fused silica fiber optic cable (with index of refraction, *n=1.45)* with an index of refraction matching gel (with index of refraction n=1.56) between that of the two fibers to increase the efficiency of coupling light between the Al_2O_3 fibers (with index of refraction n=1.77) and the fused silica fiber optic cable. The two fibers were then pressed together at the ends and encapsulated in rigid plastic to solidify the connection between the Al_2O_3:C fiber and the fused silica fiber optic cable. One end of the bifurcated fiber optic cable was then coupled to a 30 mW Nd:YAG laser to provide the optical stimulation to the Al_2O_3:C fiber. The laser power at the sample end of the fiber optic cable was approximately 20 mW as measured by a Melles-Griot model 17049 thermopile powermeter. For these measurements the F center luminescence centered at 420 nm was measured. The luminescence was measured through the other end of the bifurcated fiber by passing it through a filter pack containing a 532 nm laser line rejection filter and two one-quarter inch thick 420 nm interference filters and the intensity of the luminescence was measured by a Thorn EMI model P10PC photomultiplier tube. The Al_2O_3:C fiber was placed inside of a 100 mCi $^{90}Sr/^{90}Y$ source for irradiation with beta particles.

4.2.2 Dose Response of Al_2O_3 Based Fiber Optic Dosimeters

Following the background characterization measurements discussed in chapter 3, OSL and RL data were gathered for fiber 1, fiber D and rod 1. The OSL response to dose of the Al_2O_3:C fiber probes was measured by illuminating the irradiated fiber with laser light for one second. The total OSL signal was measured by summing the luminescence output during the one second stimulation period.

The fiber probes were first inserted into the $^{90}Sr/^{90}Y$ beta source and the OSL dose response measured for doses ranging from 0.05 Gy to 100 Gy. The dose response of the Al_2O_3:C fiber optic dosimetry probes is shown figure 4-3. Fiber 1 and rod 1 exhibited a linear dose response over a dose range greater than four orders of magnitude from approximately 0.05 Gy to greater than 100 Gy. The OSL from fiber D exhibited a linear dose response from 0.05 to about 3 Gy, and saturated for doses above about 3 Gy and showing a slight decrease for doses above 10 Gy. For the arrangement described, the minimum measurable dose for fiber 1 (defined as three times the standard deviation of the background signal from an unirradiated sample) was less than 0.03 Gy.

4.2.3 Dose Rate Dependence of Real-Time Luminescence

Luminescence measurements were taken in real-time during irradiation of the Al_2O_3:C probe. The timing parameters for the real-time luminescence measurements are shown in figure 4-2. For these measurements the fiber probe was inserted into the radiation source and the luminescence measurement was initiated at the same time as the shutter in the radiation source was opened to begin the irradiation. The luminescence was measured at regular intervals by summing the luminescence for one second periods during irradiation. With this measurement system, both the RL and OSL produced by the fiber could be measured by monitoring the luminescence with the laser either turned off (for RL) or turned on (for OSL). The signal measured with the laser turned on is actually the sum of the OSL and RL signals produced by the fibers. Therefore the previously measured RL signal (measured with the laser off) was subtracted from the measured signal with the laser on to give the real-time OSL signal. Real-time measurements were taken in this way for different dose rates of 10 mGy/s, 17 mGy/s, and 34 mGy/s correlating

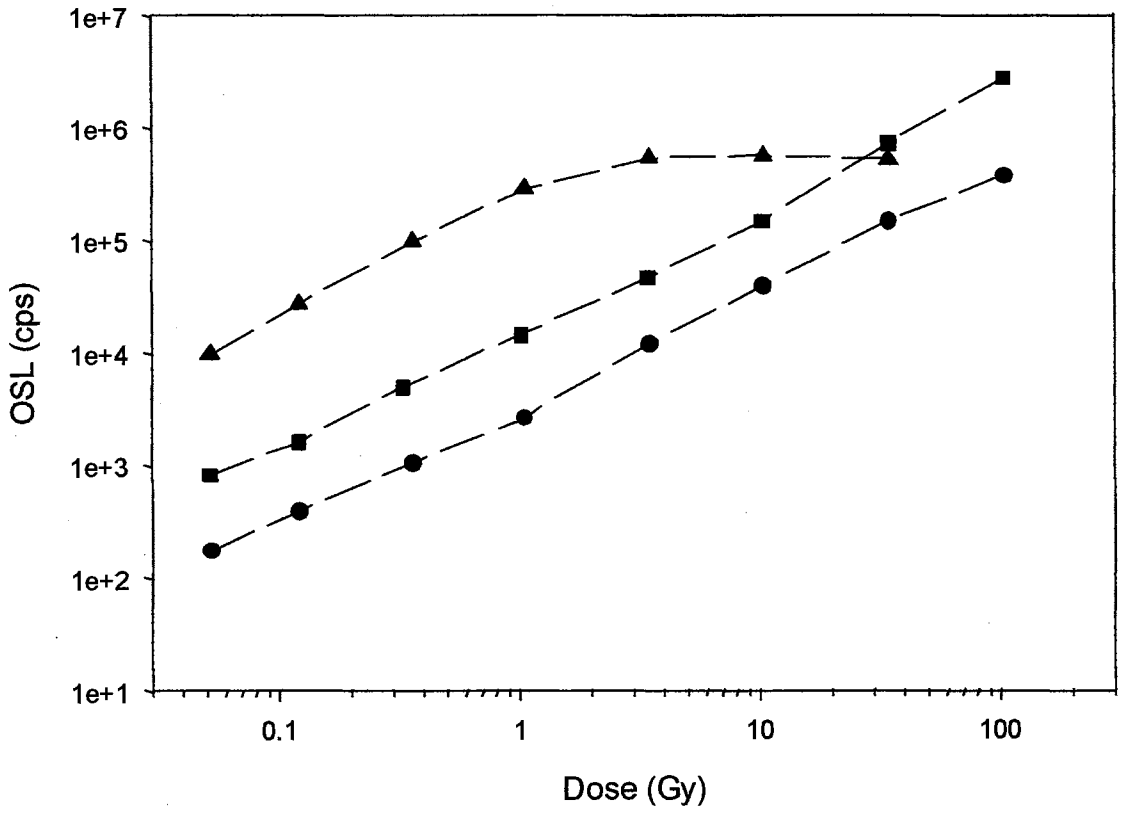

Figure 4-3: OSL dose response from fiber 1 (circles), rod 1 (squares), and Fiber D (triangles) connected to the end of a fiber optic cable. The OSL from the fibers was stimulated and detected down the silica fiber.

to the range of dose rates of a typical radiotherapy treatment.[88]

For the real-time OSL, the determination of absorbed dose from the measured signal will depend on the method of readout used. That is, the signal will behave differently as a function of dose for different methods of readout. The OSL reading can be made with a low power laser beam so that a very small number of the trapped charges are stimulated, and the change in the overall concentration of trapped charge is negligible for each measurement. In this case, the real-time OSL signal will increase with dose in much the same manner as the standard OSL signal. On the other hand, the OSL reading can be made with a strong laser beam so that all trapped charge is stimulated out of the charge traps during the OSL measurement. For this type of measurement, the real-time OSL signal will be constant for measurements at regular intervals as a function of dose.

The RL and OSL signals from fiber 1 for different dose rates are shown in figure 4-4. The RL and real-time OSL both increase to a maximum with the rate of increase and the maximum intensities both increasing with the dose rate. The real-time OSL from fiber 1 is proportional to the dose rate as shown in figure 4-5 with the proportionality being constant throughout the measurement. For both RL and OSL signals, the maximum value of the signal is seen to be linearly proportional to the dose rate, as shown in figure 4-6. This increase with dose rate can be interpreted mathematically from equation 4.6. The real-time luminescence is shown to be linearly dependent to the dose rate from the first term of equation 4.6, as well as from the dose rate dependence of the n_t factor (from equations 4.1 and 4.2) in the second term in the equation. From figure 4.3, the OSL (and therefore n_t) shows a linear dependence on dose over a fixed range of dose. Thus, n_t is linear with dose over this dose range, and therefore for a fixed time interval n_t

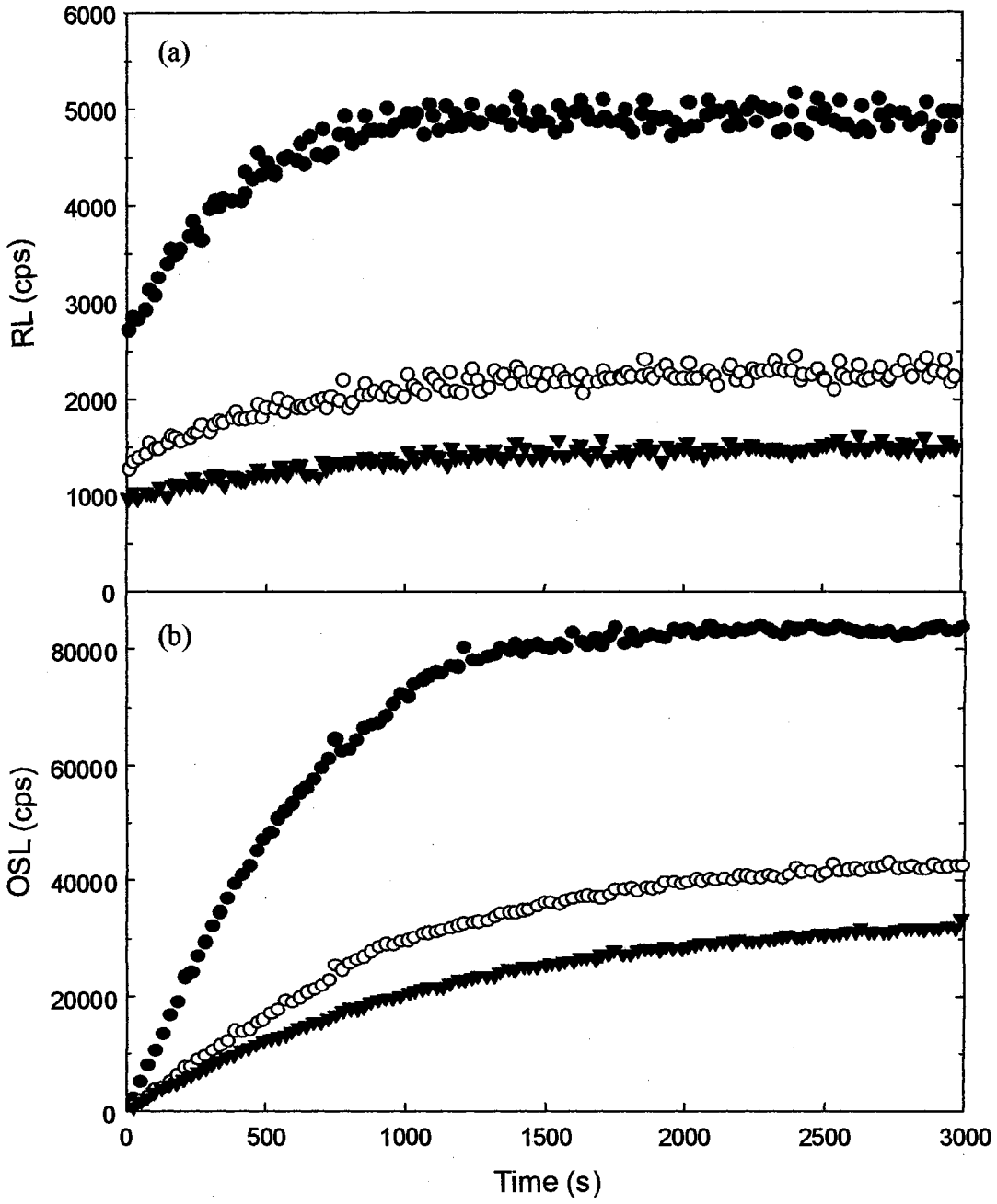

Figure 4-4: The RL (a) and real-time OSL (b) signal from fiber 1. The luminescence is measured as a function of time for 34 mGy/sec (filled circles), 17 mGy/sec (open circles), and 10 mGy/sec (filled triangles) dose rates.

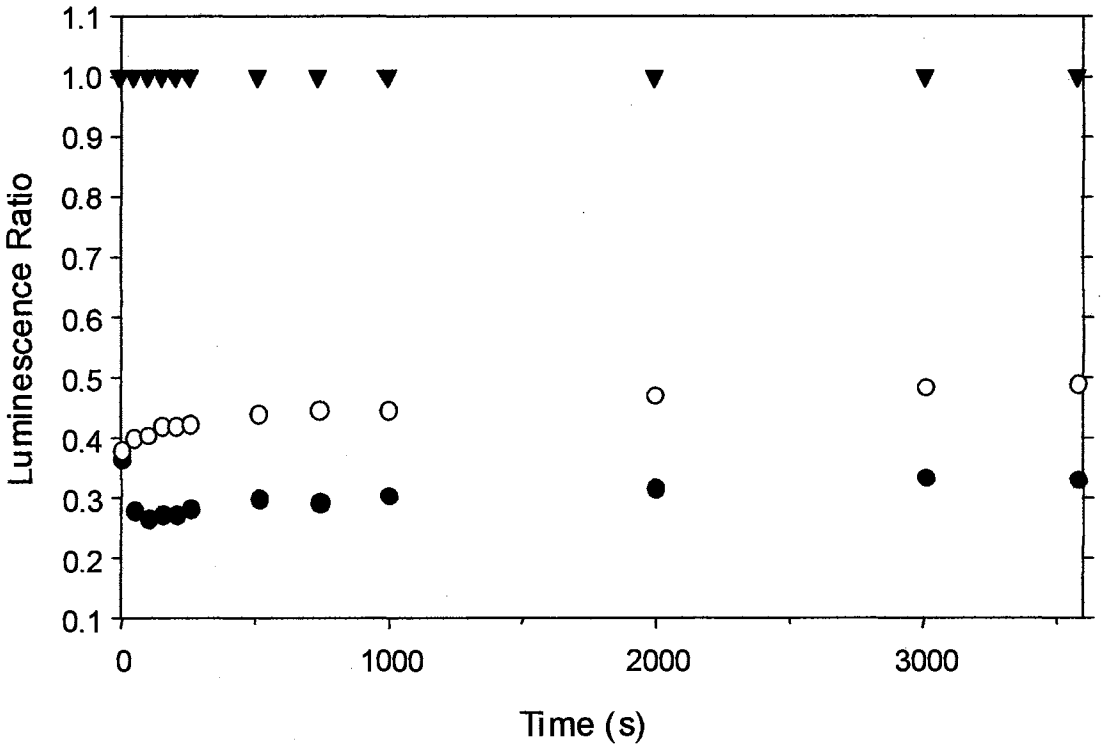

Figure 4-5: The ratio of the real-time OSL at dose rates of 34.4 mGy/sec (triangles), 16 mGy/sec (open circles), and 10 mGy/sec (filled circles) to the real-time luminescence for a dose rate of 34.4 mGy/sec as a function of time during irradiation.

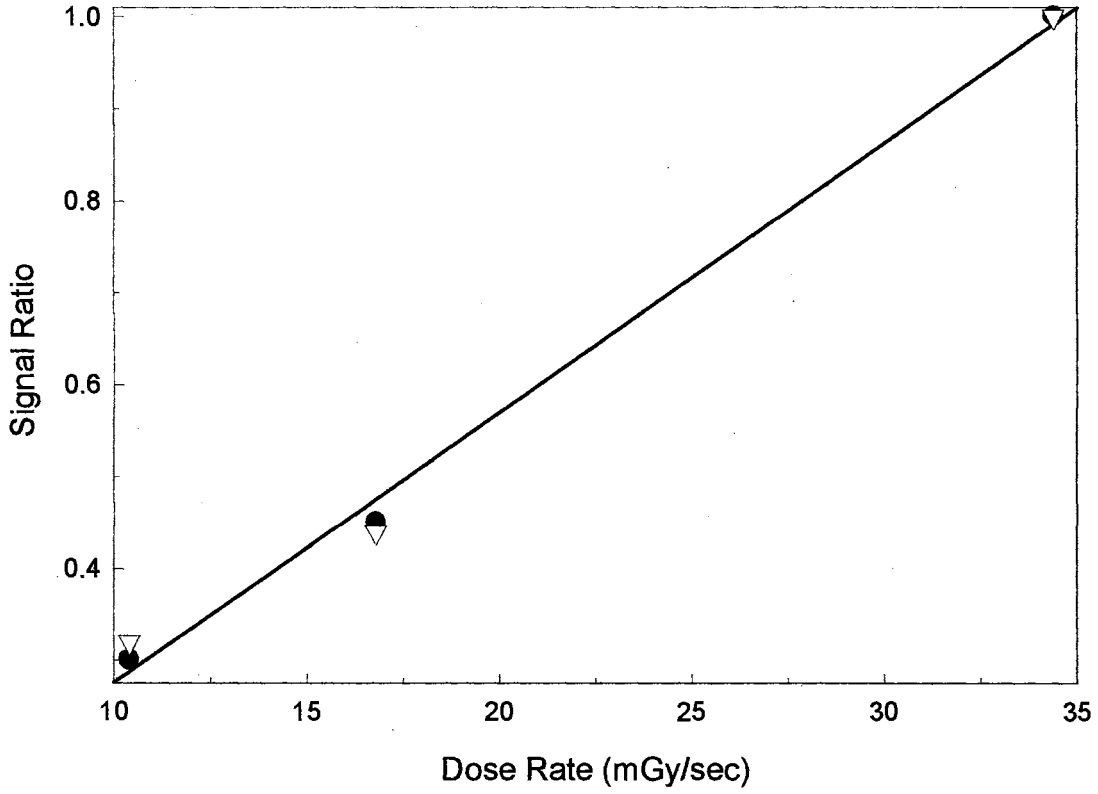

Figure 4-6: Ratio of OSL (circles) and RL (triangles) signal at different dose rates to the maximum at a dose rate of 34 mGy/sec.

is also proportional to dose rate. From this direct proportionality, it can be seen that both the RL (from equation 4.7) and OSL (from equation 4.8) will increase linearly with the dose rate on the range of dose in which the response of the sample is linear with the total delivered dose.

4.2.4 Power Dependence of Real-Time Luminescence

Along with dose rate, the real-time luminescence can be seen to proportional to the laser power used during the read out of the OSL. From the second term of equation 4.6, the OSL part of the real-time luminescence signal would be seen to increase with the laser power used to stimulate the signal. The real-time luminescence from fiber 1 for two different laser powers is shown in figure 4-7. The real-time luminescence increases at a faster rate for higher laser powers, thus reaching the maximum signal in a shorter time period than for lower laser powers. The maximum level of the signal, however, is the same in each case, independent of laser power. The rise to maximum of the real-time luminescence can be understood by looking at equations 4.4 and 4.6. For a nonsaturated sample, the number of traps filled during each equal period between OSL measurements is constant. The number of trapped electrons stimulated into the conduction band, by the laser, is directly proportional to the laser power (f), and to the number of trapped electrons (n_t) in the crystal before the laser is turned on, as seen by equation 2.26. The number of trapped electrons stimulated during the OSL measurement can be given by the equation

$$\Delta n_t^{depl} = n_t * D_f \tag{4.10}$$

where (D_f) is known as the depletion factor for the sample. The depletion factor is the percentage of the trapped charge lost during the OSL measurement, and is dependent on

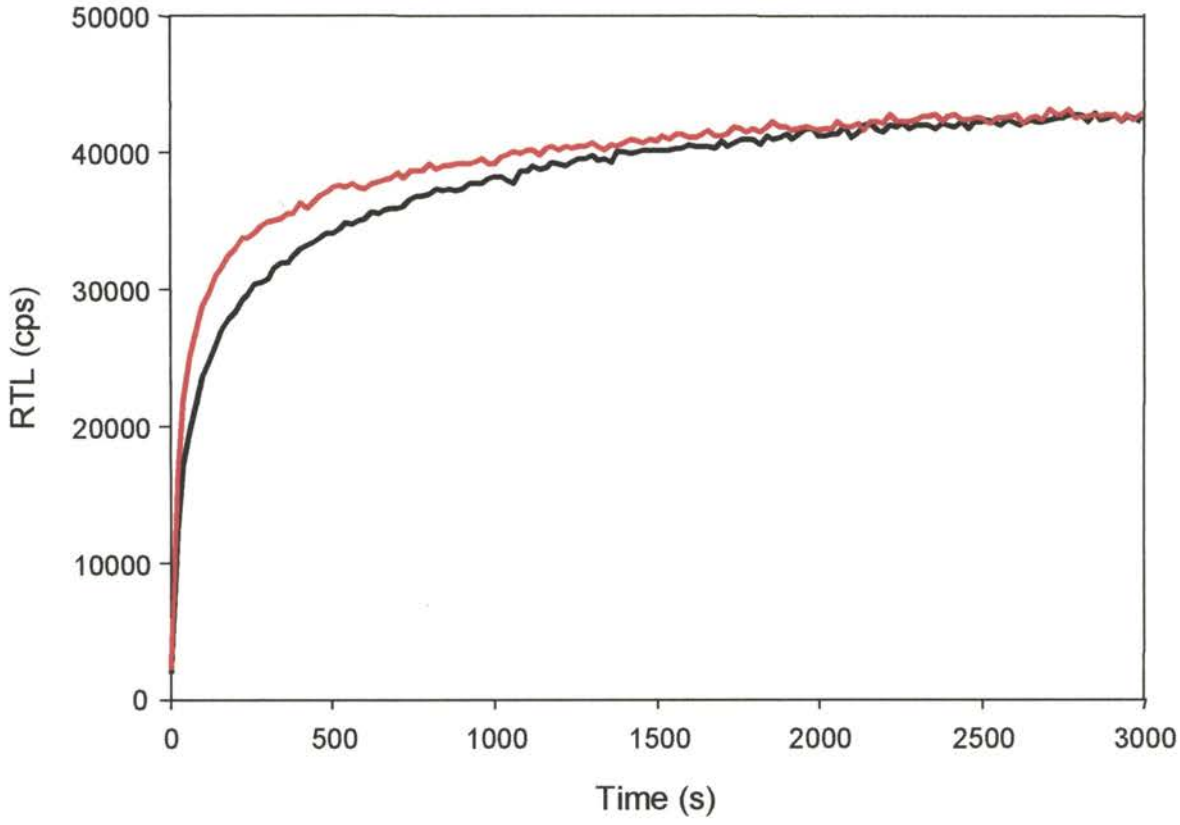

Figure 4-7: Real-Time luminescence from fiber 1 for 50 mW (black) and 100 mW (red) of laser power used to stimulate the OSL.

the laser power (f). According to the simple model of OSL presented in chapter two, the real-time OSL is proportional to the number of electrons stimulated from the traps as given by

$$I_{osl} = \int_0^t \frac{dm}{dt} = \int_0^t \frac{dn_t}{dt} = \Delta n_t^{depl} \tag{4.11}$$

where t is the duration of the laser stimulation during the OSL measurement. During the real-time luminescence procedure, the electron traps are continuously being filled due to the irradiation of the sample, and emptied due to the laser stimulation. A simulation of the concentration of trapped electrons during a real-time luminescence measurement is shown in figure 4-8. As more traps are filled (due to the irradiation), a larger number of electrons are stimulated out of the traps according to equation 4.10. Therefore, the number of electrons stimulated into the conduction band during the laser stimulation continues to increase as long as the number of trapped electrons is increasing and the OSL continues to increase. When the number of electrons traps filled due to irradiation, between measurements equals the number untrapped, due to the laser, the number of electrons stimulated into the conduction band during each OSL measurement reaches a steady state level, and the OSL signal saturates. The competition between the filling and emptying of traps leads to the characteristic rise in the real-time luminescence signal until the processes of trap filling and emptying reach equilibrium, at which point the saturation level of the signal is reached. For a constant dose rate, the equilibrium level between trap filling and emptying will be equal to the number of traps filled between measurements. This leads to the fact that the maximum of the real-time luminescence signal is dependent only on the trap filling between measurements (determined by the dose rate) and not the laser power. Therefore, the real-time luminescence signal maximum is the same no

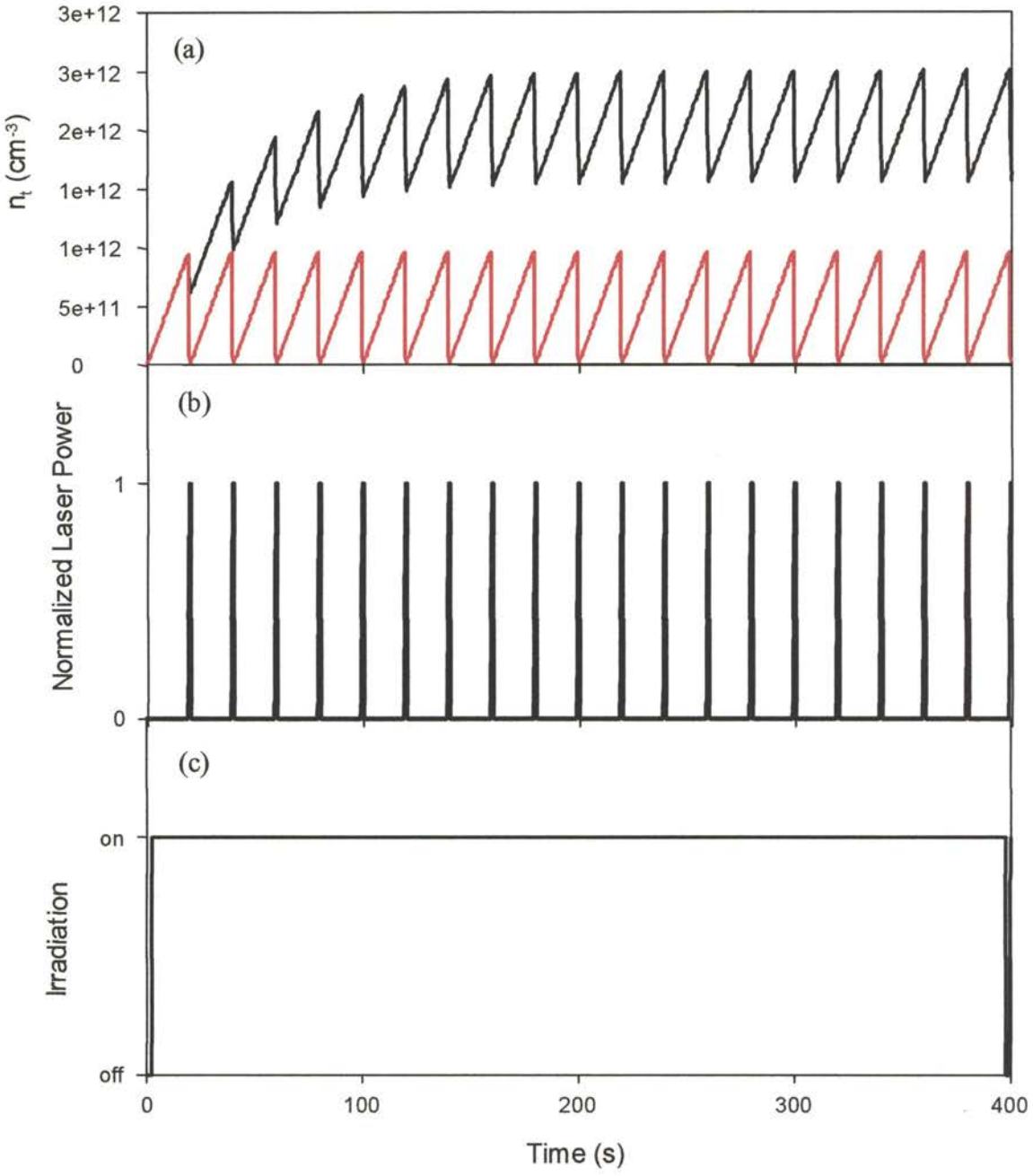

Figure 4-8: Computer simulation of the concentration of trapped electrons (a) for 1 (black) and 10 (red) power units as a function of time during a real-time luminescence measurement with periodic laser stimulation (b) and under continuous irradiation (c).

matter the laser power as seen in figure 4-7. The only difference in the signal for different laser powers is the time required for the signal to reach saturation, is longer for lower laser powers.

4.3 Depletion of Real-Time OSL Signal

4.3.1 Dose Response of Real-Time OSL

During an OSL measurement, the concentration of trapped charge in the sample is reduced each time the sample is stimulated by the laser. This depletion caused by the laser stimulation acts as a competing process for the filling of charge traps during irradiation. This competition results in a lower concentration of trapped charge in the sample for a given dose than would be present if the OSL was not read during irradiation, leading to a reduction of the OSL signal read for a given dose.

A comparison of the standard OSL dose response and the real-time OSL as a function of dose for fiber 1 is shown in figure 4-9. The real-time OSL increases linearly along with the standard OSL signal from about 0.2 Gy up to about 10 Gy. For doses above 10 Gy, the real-time OSL increases sublinearly up to a dose of about 50 Gy were the signal saturates. For doses above 50 Gy, the real-time OSL signal is constant while the standard OSL signal continues to increase linearly through doses of 100 Gy. The onset of the saturated signal of the real-time OSL at lower doses than the standard OSL is due to the depletion of trapped charge during irradiation from the laser stimulation.

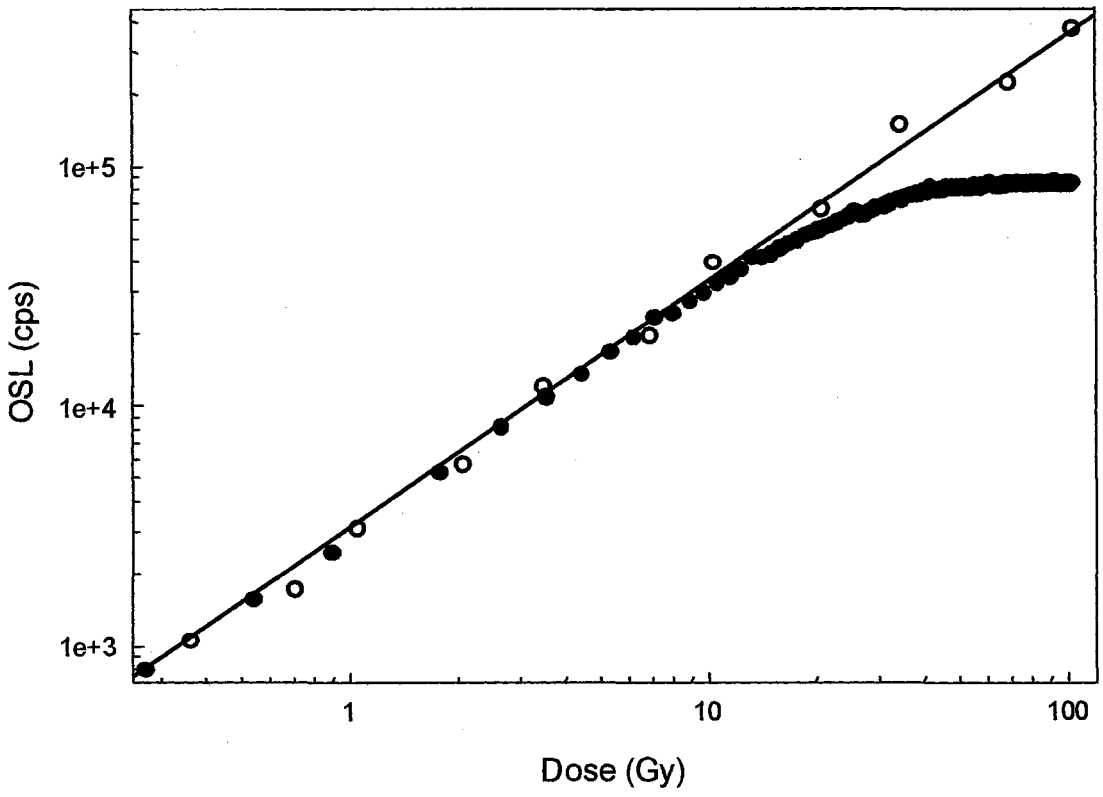

Figure 4-9: Comparison of the OSL dose response (open circles) and the real-time OSL as a function of dose (filed circles) for fiber 1.

4.3.2 Correction of Real-Time OSL for Depletion

The depletion of the real-time OSL signal can be corrected by summing the depletion of trapped charge caused by each laser stimulation period during the real-time luminescence measurement. This can be done by irradiating the sample and taking repeated OSL measurements to determine the depletion factor D_f. For the purpose of the real-time OSL measurements, D_f is measured as the ratio between the first and second OSL measurements at a given laser power. From this type of measurement, the depletion factor for each individual fiber can determined. The depletion correction factor for fiber 1, fiber D, and rod 1 for laser powers ranging from 10 to 330 mW is shown figure 4-10. D_f varies from about 1 percent for about 10 mW of laser power for fiber 1 to about 50 percent for fiber D, and from about 32 percent for fiber 1 for 330 mW of laser power to about 80 percent for fiber D. The depletion factor is seen to exhibit a large variability in magnitude from fiber to fiber. The increase in the depletion for increasing dose is seen to increase asymptotically toward a maximum percentage, which is different for each individual fiber. The absolute maximum for each fiber could not be determined due to limits in the maximum laser power that could be delivered to the fibers with the experimental setup. The depletion for the fibers was found to be independent of the dose delivered to the sample. The depletion as a function of dose delivered to the sample for fiber 1 is shown in figure 4-11.

With the value of the depletion factor, the total depletion of real-time OSL due to the OSL measurement can be calculated according to the equation

$$\Delta = I_{OSL} * D_f . \tag{4.12}$$

where I_{OSL} is the OSL measured from the sample, during the one second laser stimulation,

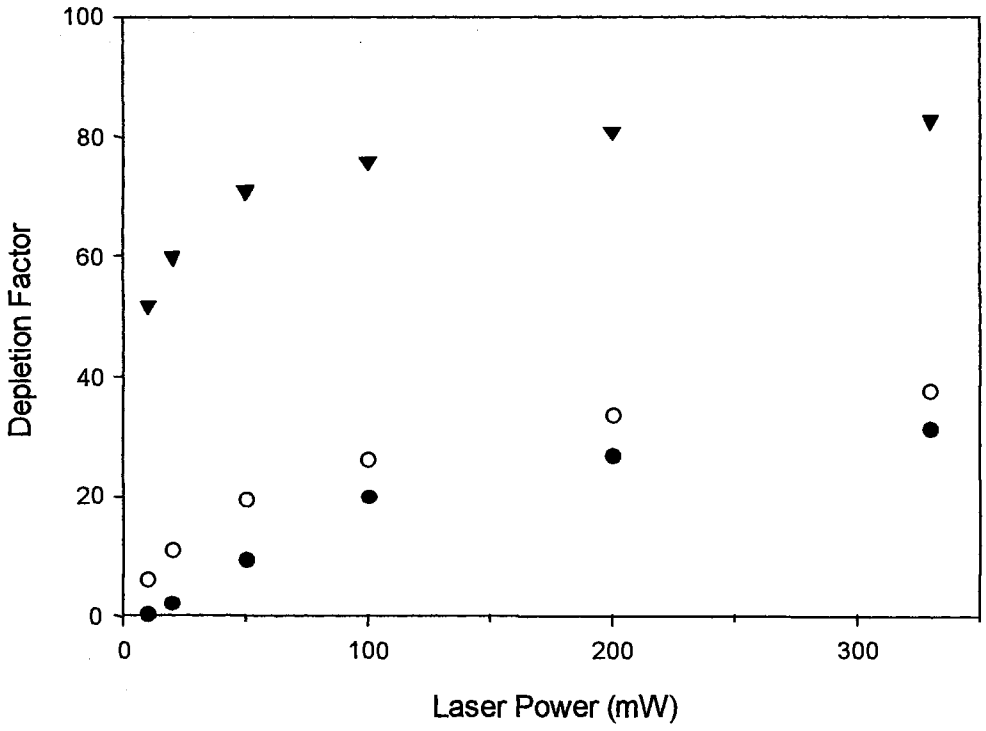

Figure 4-10: The depletion correction factor for fiber 1(filled circles), fiber D (triangles), and rod 1 (open circles) for increasing laser power for fiber 1.

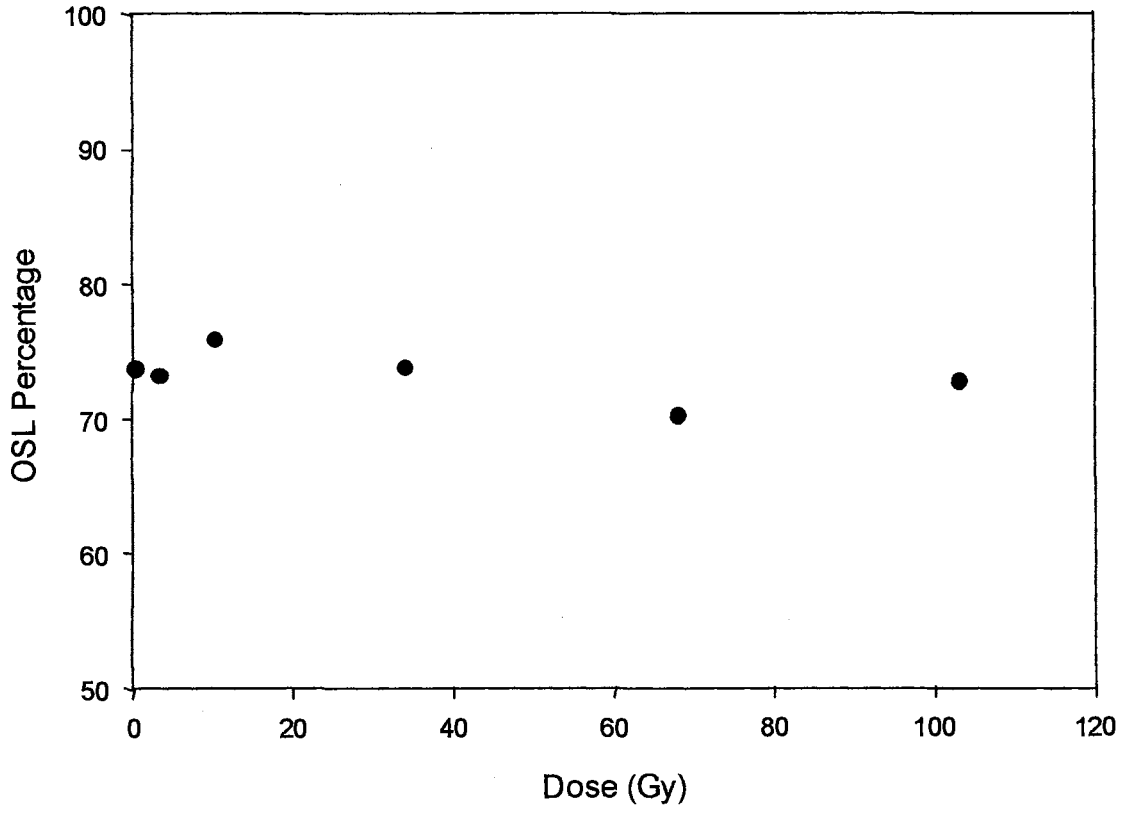

Figure 4-11: The percentage of the OSL signal remaining after one OSL measurement for fiber 1 for increasing doses.

given by equation 4.11. In order to know the total OSL measured from the sample in real-time, the measured signal must be corrected for the depletion of all previous measurements according to the equation

$$C_j = OSL_j + \sum_{i=1}^{j-1} \Delta_i \tag{4.13}$$

where C_j is the total OSL for measurement j from the sample, and OSL_j is the measured intensity from measurement j. This corrected real-time OSL can be plotted as a function of dose to give the total OSL from the sample for a given dose. The corrected real-time OSL from fiber 1 is compared to the standard OSL dose response in figure 4-12. The real-time OSL, after correction for depletion, shows a linear dose response just like the standard OSL from about 0.2 Gy through doses greater than 100 Gy. Therefore, by correcting the measured OSL to obtain the total OSL from the sample, the total delivered dose to the sample can effectively be measured in real-time for doses up to 100 Gy.

The correction procedure is limited by the stability level of the experimental parameters. For example, during the measurement, the output power of the laser could fluctuate, causing a change over time on the intensity of the OSL signal, or the collection efficiency of the photodetection system could change due to thermal effects in the optics induced by the laser light or misalignment due to shock of the system. The correction of collected data will suffer from any fluctuation due to the experimental setup used, and therefore the final corrected value of the OSL may differ from the standard OSL signal which may not of suffered from any systematic fluctuation in the experiment. From figure 4-12, the corrected OSL can be seen to differ from the standard OSL reading by about 25 % at 100 Gy. Also, the correction shown for fiber 1 slightly over corrects the OSL signal in dose ranges from about 10 to 30 Gy, at which point the correction begins

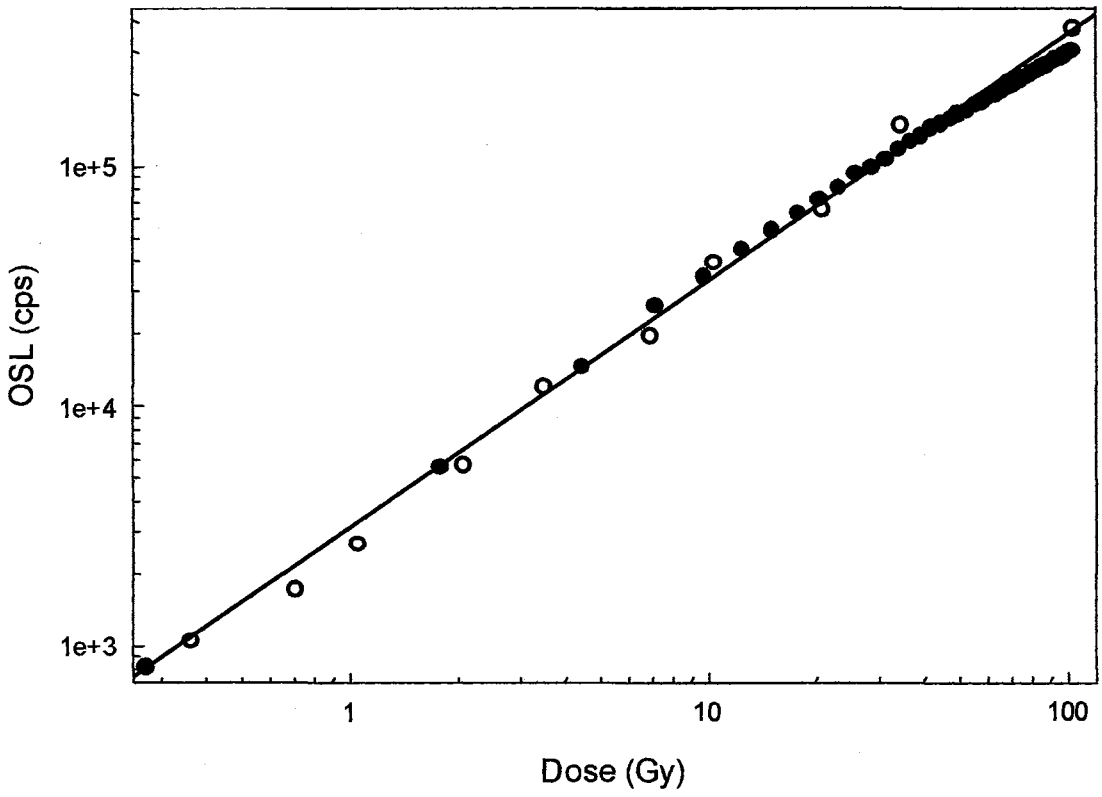

Figure 4-12: Corrected real-time OSL as a function of dose. The measured OSL was corrected for depletion of the signal due to previous measurements.

to under estimate the total OSL. This pattern in the over correction, followed by an under correction can be traced to the time dependent behavior of the laser used for stimulation of the sample. The laser power has been shown to slightly increase in time followed by decrease of the power which continued to a steady state level after about 5000 seconds. It is believed that this time dependent behavior is reflected in the intensity of the real-time OSL leading to the errors in the corrected OSL.

4.3.3 Effects of Deep and Shallow Traps on RL and Real-Time OSL

As discussed in the models of OSL and RL, in chapter two, shallow and deep traps affect the shape and the time characteristics of the two luminescence signals. Addition of optically active, competing shallow and deep traps will affect the real-time luminescence in much the same way as can be seen by adding these two types of traps to the simple model. In the case of this model, the competing deep and shallow traps are considered to be optically active as was seen for the Al_2O_3 fibers in chapter three. With these additions, equation 2.32 for the concentration of electrons in the conduction band becomes

$$\frac{dn_c}{dt} = \Gamma\Phi + n_t f_t + n_2 f_2 + n_3 f_3 - n_c A_n (N - n_t) - n_c m A_{mn} + s_2 n_2 \exp[\frac{-\Delta E_2}{k_b T}] - n_c A_2 (N_2 - n_2) - n_c A_3 (N_3 - n_3) \tag{4.13}$$

where N_2 and n_2 are the total and filled concentration of filled shallow traps respectively, and N_3 and n_3 are the total and filled concentrations of deep traps respectively and f_t, f_2, and f_3 are the optical stimulation rates of the main OSL, shallow and deep traps respectively. With the application of the quasiequillibrium approximation, equation 4.13 can be solved for the concentration of electrons in the conduction band

$$n_c = \frac{\Gamma\Phi + n_t f_t + n_2 f_2 + n_3 f_3}{A_n(N_t - n_t) + A_2(N_2 - n_2) + A_3(N_3 - n_3) + A_{mn} m}. \tag{4.14}$$

From this, the expression for the real-time luminescence from equation 4.5 becomes

$$I_{RTL} = -\frac{dm}{dt} = (\Gamma\Phi + n_t f_t + n_2 f_2 + n_3 f_3 + s_2 n_2 \exp[\frac{-\Delta E_2}{k_b T}]) \left[\frac{A_m m}{A_n(N - n_t) + A_2(N_2 - n_2) + A_3(N_3 - n_3) + A_m m} \right]. \tag{4.15}$$

The real-time luminescence, from equation 4.15, is seen to be composed of an RL and OSL component as well as a component from the release of charge trapped in thermally unstable traps. From the term in square brackets, the rise to maximum of the real-time luminescence is dependent, not only on the filling of the main OSL trap, but also on the filling of the competing shallow and deep traps. The real-time luminescence can be modeled by solving the rate equations numerically, and plotting the real-time luminescence signal as a function of time. Figure 4-13 shows the results of a numerical solution to the rate equations for the simple one-trap, one-recombination center model, and for the model with optically active deep and shallow traps added.[89] For the numerical solution, the real-time luminescence was calculated for three different cases correlating to the trap distributions similar to those found in the Al_2O_3 fibers used in this research: (1) a sample with only an optically active main trap, (2) for a sample with an equal concentration of an optically active main trap and a slightly optically active shallow trap ($\sigma_{ST} << \sigma_{OAT}$), and (3) for a sample with an equal concentrations of the optically active trap, a slightly optically active shallow trap, and a slightly optically active deep trap ($\sigma_{DT} << \sigma_{OAT}$) where σ_{OAT} is the photo-ionization cross section of the main , optically active OSL trap, σ_{ST} is the photo-ionization cross section of the shallow traps,

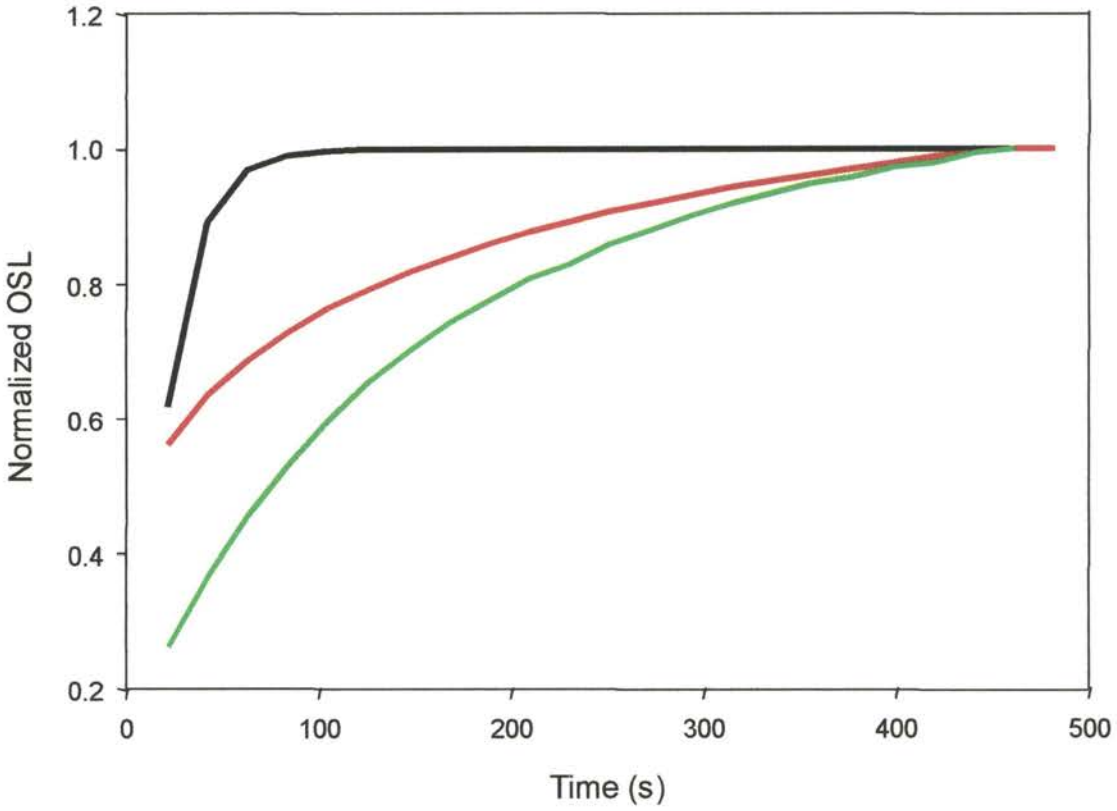

Figure 4-13: Numerical calculation of real-time luminescence for the on-trap, one-recombination center model (black), for the expanded model with shallow traps (red) added, and for the expanded model with deep and shallow traps (green) added.

and σ_{DT} is the photo-ionization cross section of the deep traps. For the model, the photo-ionization cross section of the deep and shallow traps was set with a value much less than that of the main OSL trap. This was done to correlate the parameters for the production of OSL to the parameters seen in the Al_2O_3 fibers in chapter three. From chapter three, the optical activity of the shallow and deep traps from the Al_2O_3 fibers with 532 nm light was much less than that of the main OSL trap. The normalized rise to maximum of the real-time luminescence, shown in figure 4-13, is shown to be greatly dependent on the presence of shallow and deep traps in the sample, with the time required for the signal to reach a maximum increasing with the inclusion of shallow traps and increasing even more for the inclusion of both shallow and deep traps.

This type of behavior in the rise-to-maximum of the real-time luminescence can be seen experimentally for fiber D, fiber 1, and rod 1. As shown from the low temp TL in chapter three, fiber D has a low concentration shallow traps relative to the main OSL traps, and is not believed to have a large OSL signal stimulated from deep traps, due to bleaching data not shown in this thesis. Fiber 1 is seen, from the low temperature TL data presented in chapter three, to have a comparable concentration of shallow traps to the main OSL traps, and a relatively low concentration of deep traps from the bleaching of the deep traps shown in chapter three. Also, from chapter three, rod 1 is seen to have a comparable concentration of shallow traps to that of the main OSL traps, and a relatively moderate concentration of deep traps compared to the main OSL traps as seen from the data for the bleaching of the deep traps. The normalized real-time luminescence signals for a dose rate of 34.4 mGy/s for fiber D, fiber 1, and rod 1 are shown in figure 4-14. From figure 4-14, the real-time luminescence from fiber D rises sharply to maximum in a

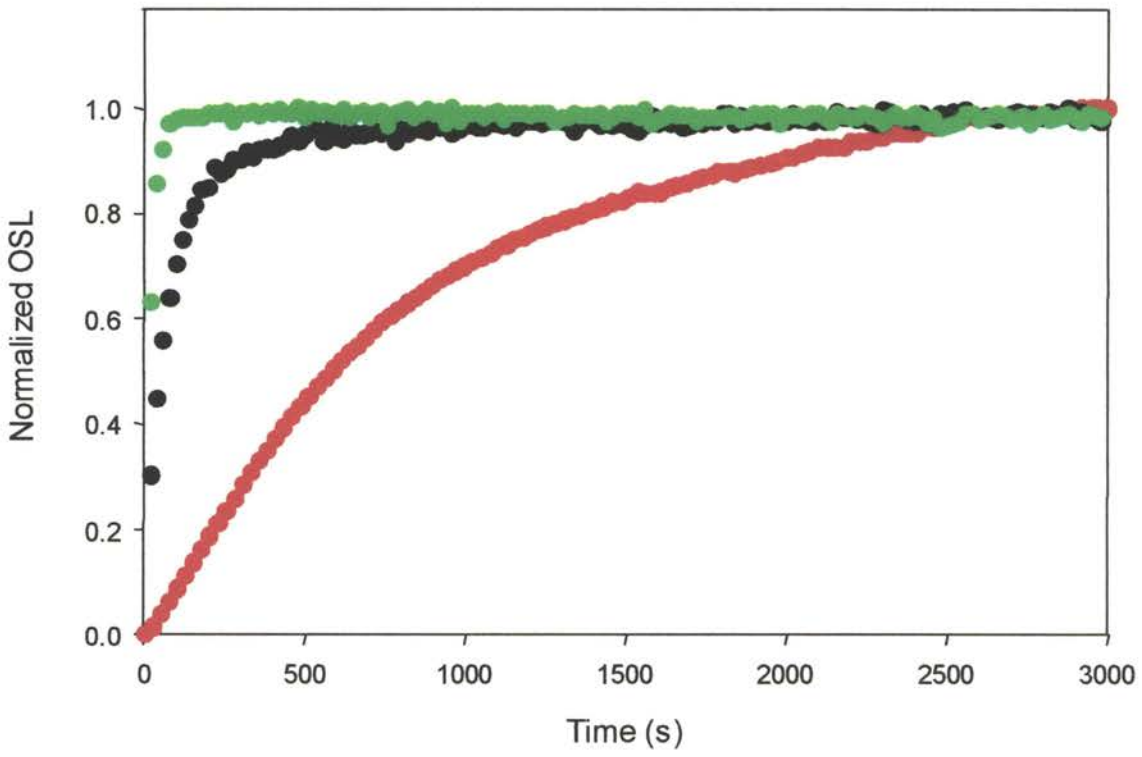

Figure 4-14: The rise-to-max of the real-time luminescence from fiber D (green) with low concentrations of shallow and deep traps and a high concentration of OSL traps, fiber 1 (black) with a low concentration of deep traps and high concentrations of shallow and OSL traps, and rod 1 (red) with high concentrations of shallow, OSL, and deep traps.

period of about 250 seconds. This relatively quick (with respect to the other fibers) rise to maximum of the signal is predicted by the simple model for a sample with only one trap and one recombination center. For fiber 1, with a high concentration of shallow traps, the rise-to-maximum is slightly slowed with the signal reaching a maximum in a period of about 1000 seconds. Rod 1, with a high concentration of both deep and shallow traps has the longest period required for the saturation of the signal, with the maximum being reached after a period of about 2500 seconds. As predicted by the model, the sample with the highest relative concentration of competing traps shows the longest rise-to-maximum time of the signal, and the lower the relative concentration of competing traps, the shorter the rise-to-maximum of the real-time luminescence signal.

The real-time OSL measured in figure 4-14 was taken with a stimulation wavelength of 532 nm. It would be expected, that the stimulation of trapped charge would change with different wavelengths of stimulation.[80] For shorter wavelengths, the efficiency of stimulation of trapped charge would increase, leading to higher OSL intensities for a given power. It should be noted that the signal from not only the main trap, but also the shallow and deep traps would increase for shorter wavelengths of stimulation light. The amount of change would depend on the wavelength dependence of the photo-ionization cross section of each individual trap. Because of this fact, D_f would have to be calculated for each particular stimulation wavelength used for the OSL measurement before any correction to the real-time OSL could be applied.

CHAPTER 5

5. A Real-Time, Fiber Optic Dosimetry System

The method of measurement described in chapter four offers a procedure for the remote measuring of doses in real-time by attaching the Al_2O_3 fibers to the end of a fiber optic cable to produce a dosimetric probe. This would be particularly helpful in several applications, for example, in high dose environments such as nuclear reactors where an accurate dose measurement is needed, but the doses inside the reactor are too high for direct monitoring by a technician. Also, the probe would be helpful in medical radiotherapy treatments where an accurate assessment of the dose delivered to the tumor is needed during the treatment to ensure that the patient does not receive a dose higher (or lower) than prescribed. For this purpose, the fiber optic probes could be inserted into the body through a medical catheter next to the tumor to measure the actual dose delivered to the tumor itself. Still another possible application would be the monitoring of underground nuclear waste storage tanks. In this case, the fibers optic probes would be inserted in the ground around the tanks and periodically monitored to measure radioactivity around the outside of the tanks. In this way, the tanks could be remotely monitored for leaks.

In this project a portable readout system (a "reader") was developed, as well as, a single-fiber, Al_2O_3 fiber optic probe similar to the ones discussed in chapter four for the purpose of making real-time dose measurements. The reader was designed for the purpose of making measurements of both absorbed dose and dose rate delivered to the

Al_2O_3 fibers during irradiation. The reader, along with the single-fiber, Al_2O_3 fiber optic probes compose the two components of a dosimetry system for the measurement of dose in real-time.

5.1 A Portable, Fiber Optic Dosimeter Readout System

The fiber optic dosimetry system was designed to mimic a standard OSL readout systems, as described by McKeever and Akselrod, with all necessary components contained within a portable box that is linked to a computer to control the measurements.[90] Furthermore, the portable reader was designed to be powered by a 12 volt AC adapter from a laptop computer. A schematic of the single fiber reader is shown in figure 5-1. The fiber optic dosimeters were stimulated with 532 nm light from a 30 mW Nd:YAG laser. The laser was powered by 5 volts supplied by the AC adapter from the laptop computer, and was modulated on and off for the OSL measurements by a 5 volt TTL signal from a National Instruments DAQ Card A1-16E-4 data acquisition card installed in the laptop computer. With the TTL modulation, the laser was turned on for one second duration at regular intervals to stimulate the sample for the OSL measurements. The laser light was coupled into the fiber optic cable by an Oriel model # 77644 collimating fiber optic coupler. This coupler was mounted onto an XY translation stage attached to the side of the reader unit to allow for alignment of the fiber coupler with the laser beam in order to ensure maximum coupling of the laser light into the fiber optic cable. The luminescence from the Al_2O_3 fiber was guided back down the fiber where it was collimated by the fiber optic coupler upon exit of the fiber optic cable. After collimation, the beam was directed onto a dichroic beamsplitter to separate the luminescence from any reflected laser light. The collimated beam from the fiber optic

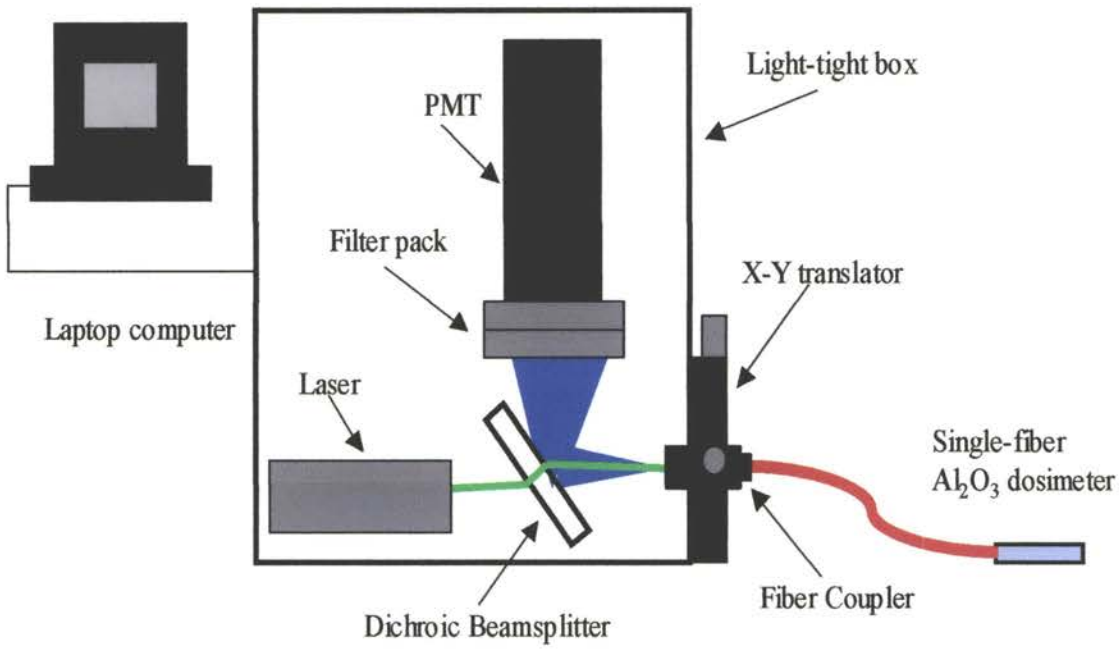

Figure 5-1: A schematic diagram of the single fiber reader used for real-time dosimetry measurements. The laser light is coupled into the fiber probe, and the resulting luminescence that returns down the fiber optic cable is separated from reflected laser light by a dichroic beamsplitter, and measured by a photomultiplier tube (PMT). The OSL readout process is controlled by computer.

probe, was incident upon the beamsplitter at a 45° angle with the luminescence being reflected, and the laser light passing through the beamsplitter. The reflected luminescence was passed through a filter pack consisting of a 532 nm laser line rejection filter, and two one quarter inch thick 420 nm interference filters with a 10 nm full-width-half maximum bandpass window. The luminescence intensity was then detected by a Thorn EMI photomultiplier tube model number P10PC that was powered by 5 volts supplied by the data acquisition board in the laptop. The signal intensity that was measured by the photomultiplier tube was recorded by the same data acquisition card. The timing parameters of the measurements as well as the recording and display of the luminescence signal in real-time were carried out with a computer program written in Labview.

5.2 Al_2O_3-Based Fiber Optic Dosimeters

5.2.1 Assembly of Single-Fiber Dosimeters

The single fiber Al_2O_3 dosimeters were constructed by attaching a 3 cm or 6 cm long piece of an Al_2O_3 fiber that has been polished on both ends to a bare polished end of a 1 or 3 meter long fused silica fiber optic cable of 400 and 600 micron diameter. The Al_2O_3 fibers were either approximately 350 or 550 micron in diameter, and attached to 400 or 600 micron diameter silica fiber optic cables. The single-fiber probes were named according to the length of silica fiber, the diameter and length of the Al_2O_3 fiber. For example, single fiber probe 6-350-3 is a probe with a 6 cm long, 550 micron diameter piece of an Al_2O_3 fiber attached to a 3 meter long silica fiber optic cable. For attachment, the fibers were first aligned in a specially designed micro-alignment system shown in

figure 5-2. The Al_2O_3 fiber was fixed horizontally into place in a microvice, and the bare polished end of the fiber optic cable was clamped horizontally into an XYZ translation stage in order to align the two fibers end to end. The beam from a Picoquant model LDH 4000 blue diode laser was coupled into the back end of the Al_2O_3 fiber. The two fibers are then aligned so that the beam emerging from the Al_2O_3 fiber would be coupled into the silica fiber optic cable. The fiber alignment is accomplished through the micropositioning of the fiber optic cable in three dimensions with through the adjustment of the XYZ translation stage. The optimal alignment is determined when the maximum transmitted intensity of the laser light between the two fibers is achieved. The intensity of the transmitted light was determined by an Ocean Optics SD 2000 fiber optic spectrometer coupled to the other end of the fiber optic cable. After the fibers were aligned for optimal transmission, a permanent connection was made by coating the end of each fiber with a thin layer of Norland NOA 61 UV curing epoxy, and bringing the two ends in contact. The UV epoxy used has an index of refraction of $n = 1.56$ (at 632 nm) to ensure the best possible match between the indexes of refraction of Al_2O_3 (n=1.77) and the silica fibers (n=1.45) to minimize reflections at the interface of the two fibers. The epoxy was then cured with UV light from a 35 W mercury lamp, and after this, the fibers were coated across the connection with an ACE brand resin epoxy to strengthen the connection. A picture of a single fiber Al_2O_3 fiber dosimeter is shown in figure 5-3.

5.2.2 Dose Response of the Single-Fiber Dosimeters

The dose response of a 3 meter long single fiber dosimeter constructed with a 6 mm long, 550 micron diameter piece of fiber 31 was measured using the single fiber readout system

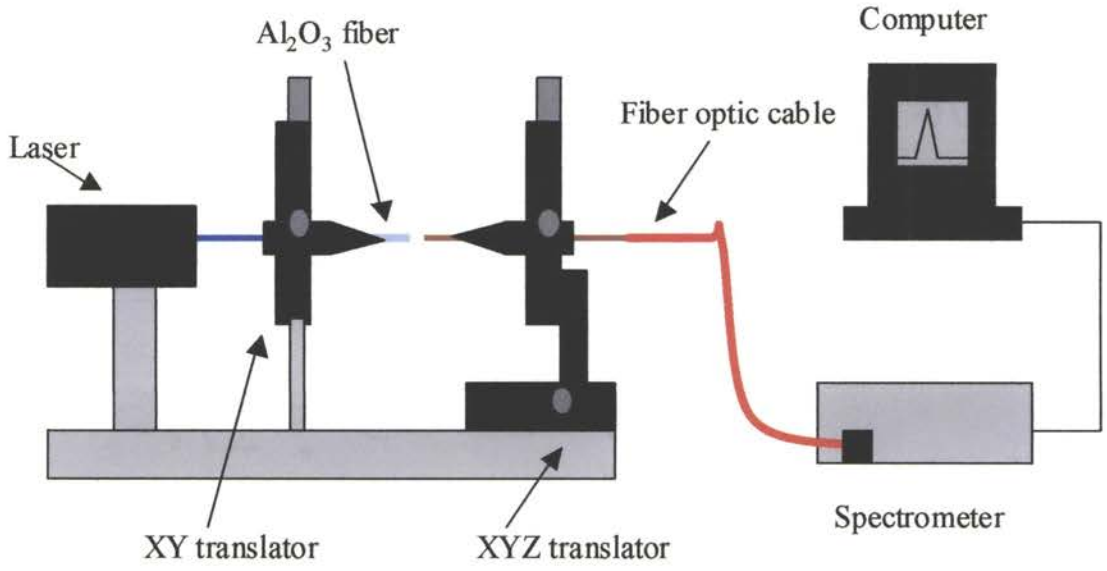

Figure 5-2: A schematic diagram of the fiber optic dosimeter probe assembly system. A blue diode laser was coupled through the Al_2O_3 fiber. The Al_2O_3 fiber and a fused silica fiber optic cable were aligned using an XYZ translation stage to maximize transmission of the laser light into the fiber optic cable. The intensity of the laser light coupled into the fiber was measured using an Ocean Optics spectrometer.

Figure 5-3: A single-fiber Al_2O_3-based dosimeter. Pictured is a 6 mm long, 550 micron diameter piece of fiber 31 attached to a 3m fused silica fiber optic cable. A close up of the tip of the dosimeter is shown in the inset.

described in section 5.1. For these measurements, the standard dose response was measured in the same way as was described in section 4.2.2. The fiber was irradiated with a known dose, and then stimulated for one second with an Nd:YAG laser. The resulting OSL signal was then integrated for the duration of the stimulation. After this, the signal was bleached to background level with the laser before irradiating again. This procedure was carried out over a range of doses from 0.0005 to 52 Gy. The minimum measurable dose (described as the dose corresponding to the zero dose background signal plus three times the standard deviation of the measured signal) with the single fiber dosimeter and the readout system was approximately 0.004 Gy. The single fiber dosimeter showed a linear response over the dose range from about 0.005 Gy to about 10 Gy. For doses above 10 Gy, the dose response saturates. The dose response of the single fiber dosimeter is shown in figure 5-4. The dose response does not show any supralinearity in the dose ranges before saturation as was seen for rod 1 in section 3.3.2. It is believed that any supralinear response of fiber 31 was removed by exposure to UV light during the assembly procedure of the probe. This exposure is believed to fill competing electron traps, increasing the sensitivity of the fiber and producing a linear response over the entire range of doses up to saturation as was also seen for rod 1 in section 3.5.

5.2.3 Angle Dependence of OSL

The OSL response of the single fiber dosimeters was measured as a function of the angle of incidence of the dosimeter relative to the irradiation beam. For these experiments, the fiber dosimeters were irradiated with a fixed dose of 140 kVp (~ 37 keV peak energy) x-rays from a General Electric diagnostic X-ray machine. For each measurement, the fibers

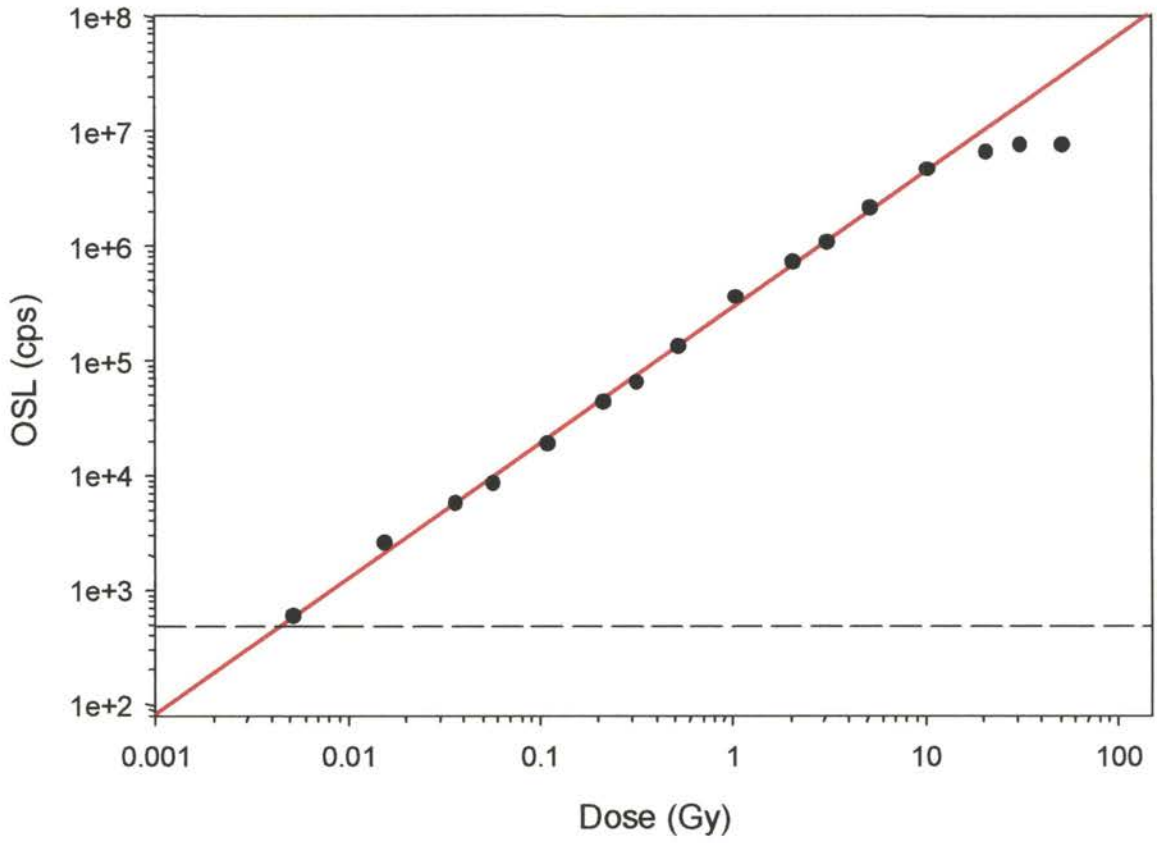

Figure 5-4: Dose response of a single fiber Al_2O_3 dosimeter with constructed with fiber 31. The dosimeter shows a linear response from about 0.005 Gy to about 10 Gy with a minimum detectable dose (dashed line) of about 0.005 Gy.

were positioned at a fixed angle relative to the X-ray beam with perpendicular being 0° and parallel being 90°. The fibers were irradiated with a one second pulse of x-rays (~ 10 mGy), and the OSL measured with the single fiber reader. The fiber was then bleached to a zero dose background, and the procedure was repeated at a different angle.

Figure 5-5 shows the percentage of OSL/unit dose at a 0° angle of incidence for angles of incidence from 0° to 90°. For fiber 31 and fiber D, the OSL/unit dose is constant for angles of incidence up to 45°, and up to 60° for fiber 1. For angles greater than this, the OSL signal progressively decreases for increasing angles. This fall off in signal is due to a the decrease in the amount of material being irradiated by the x-ray beam as the angle of incidence increases, and the fibers become parallel to the beam. The penetration depth of low energy x-rays in Al_2O_3 is much less than the length of the fibers, and as the angle of incidence approaches 90°, the amount of material falls off greatly due to the short depth of penetration of the x-rays. For fiber D and fiber 31, the OSL signal begins to drop off at a smaller angle than for fiber 1. This difference in the difference in the angle at which the OSL response begins to decrease is believed to be due to the difference in sizes of the fibers, with fiber D and fiber 31 having smaller diameters than fiber 1.

5.2.4 Real-Time Luminescence with Single Fiber Dosimeters

The RL and real-time OSL from the single fiber probes were measured using a $^{90}Sr/^{90}Y$ beta source at the Risoe National Labs in Roskilde, Denmark. For these measurements, the fiber dosimeters were inserted into the irradiation chamber beneath the source, and irradiated at dose rates of 0.3, 1.0, and 3.0 mGy/s for 300 seconds. The RL was recorded during the irradiation, and following this measurement, the luminescence

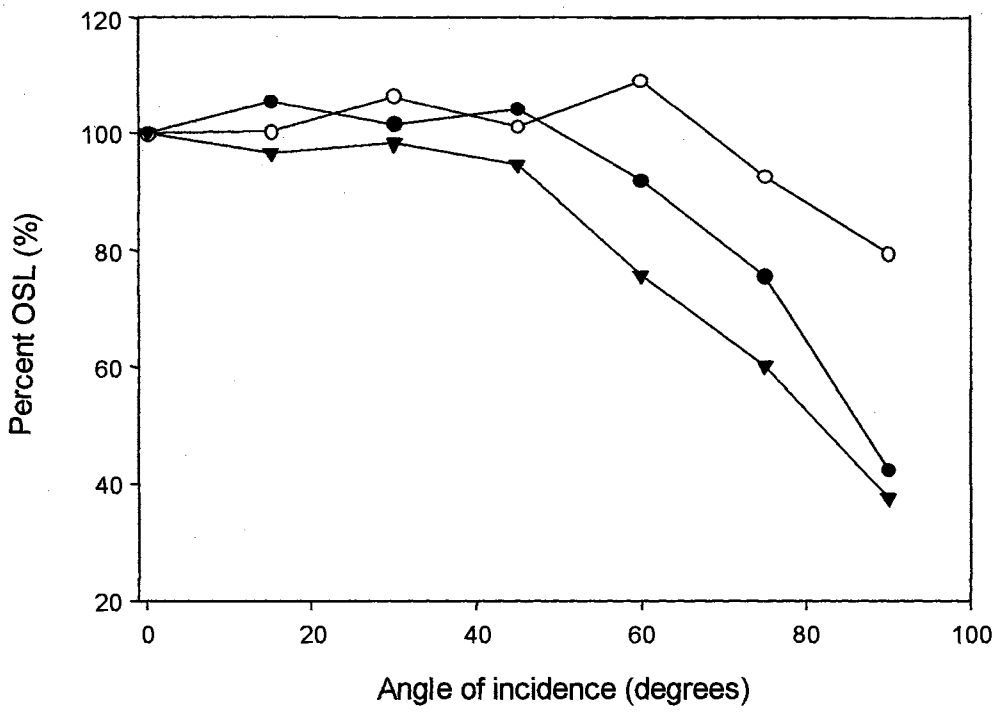

Figure 5-5: The angle dependence of the OSL signal/unit dose as a function of angle of incidence with the irradiation beam. Fiber D (triangles) and fiber 31 (closed circles) show a constant OSL signal/unit dose for angles up to 45° and for fiber 1 (open circles) shows a constant response for angles up to 60°. Above these angles, the OSL/unit dose falls off with increasing angle.

was read, and the sample was "zeroed" to background by bleaching. Following the RL measurements, the real-time OSL was measured and the RL signal was subtracted from the measured real-time luminescence to obtain the real-time OSL signal.

The RL signal from fiber dosimeter 3-550-3 for the three different dose rates is shown in figure 5-6. The intensity of the RL signal is seen to be proportional to the dose rate as discussed in section 4.2.3. In each measurement, the RL signal increases linearly with dose rate due to the fact that for the low dose rates used for the measurements, the total absorbed dose that the dosimeter has received during each measurement is well below the saturation dose for the sample, and the rate of trap filling is still linear with dose. This in turn means that the increase in the RL is linear with time. From this it can be seen that at these low dose rates, the slope of the RL signal versus time is linearly proportional to dose rate. Figure 5-7 shows the RL signal normalized to its initial value, with this signal fit to a straight line. The slope of the line for the RL at 3.0 mGy/s is approximately 10 times the slope for the RL for 0.3 mGy/s dose rate, and is approximately 3 times that of the slope for the RL at 1.0 mGy/sec dose rate.

The real-time luminescence was measured and the RL signal measured with the single fiber probe was subtracted to give the real-time OSL signal from the single fiber probe. The real-time OSL from fiber dosimeter 3-550-3 shows a rise to max behavior as discussed in section 4.2.3 and as is shown in figure 5-8. The maximum intensity of the real-time OSL, as well as the rate of increase of the signal, are seen to increase with dose rate for the single fiber probes.

The real-time OSL signal from the single fiber probes can be corrected for depletion to produce a linear response of the real-time OSL to dose by the method

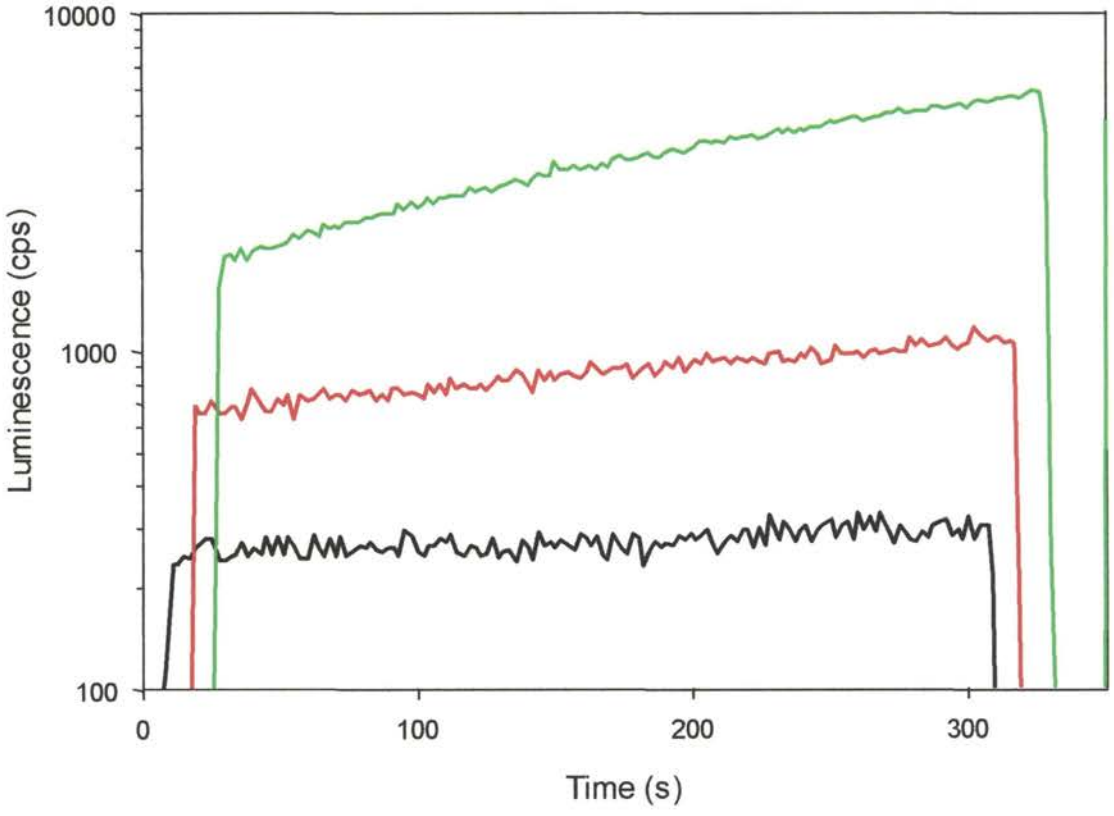

Figure 5-6: RL from single fiber dosimeter for 0.3 (black), 1.0 (red), and 3.0 (green) mGy/s. The RL signal is proportional to the dose rate.

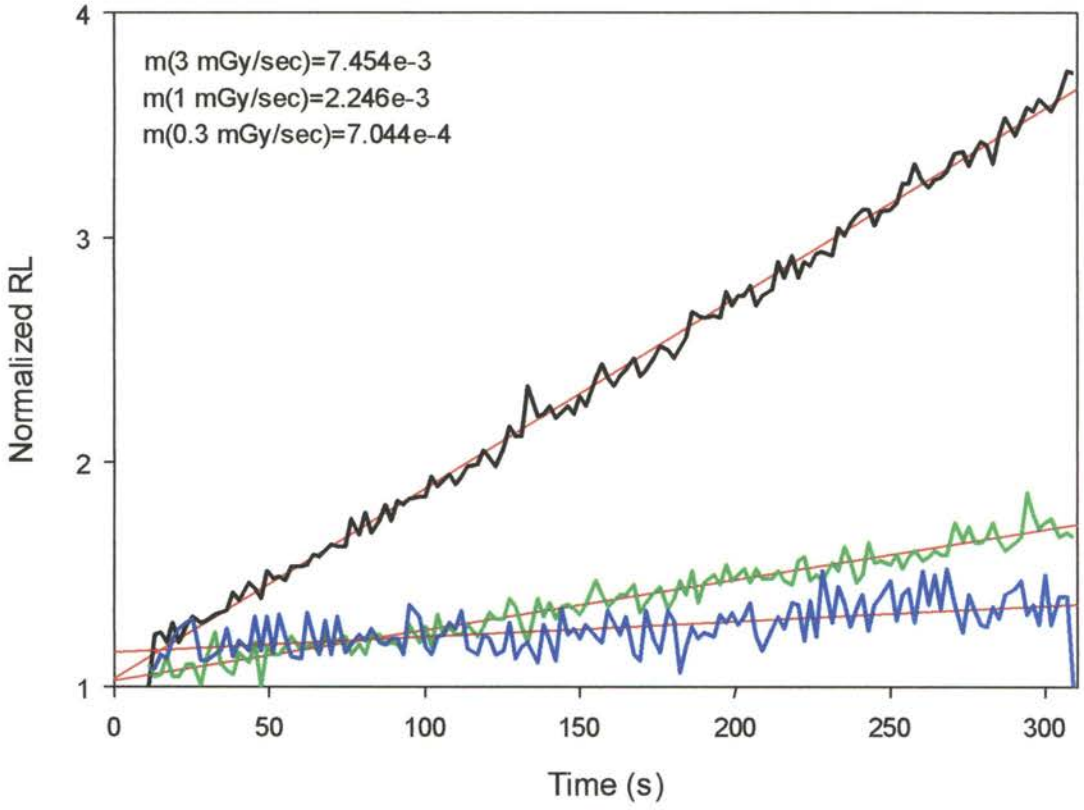

Figure 5-7: Normalized RL signal for 0.3 (blue), 1.0 (green), and 3.0 (black) mGy/s dose rate fit to straight lines (red). The slope (inset) of the RL signal is seen to be linearly proportional to the dose rate.

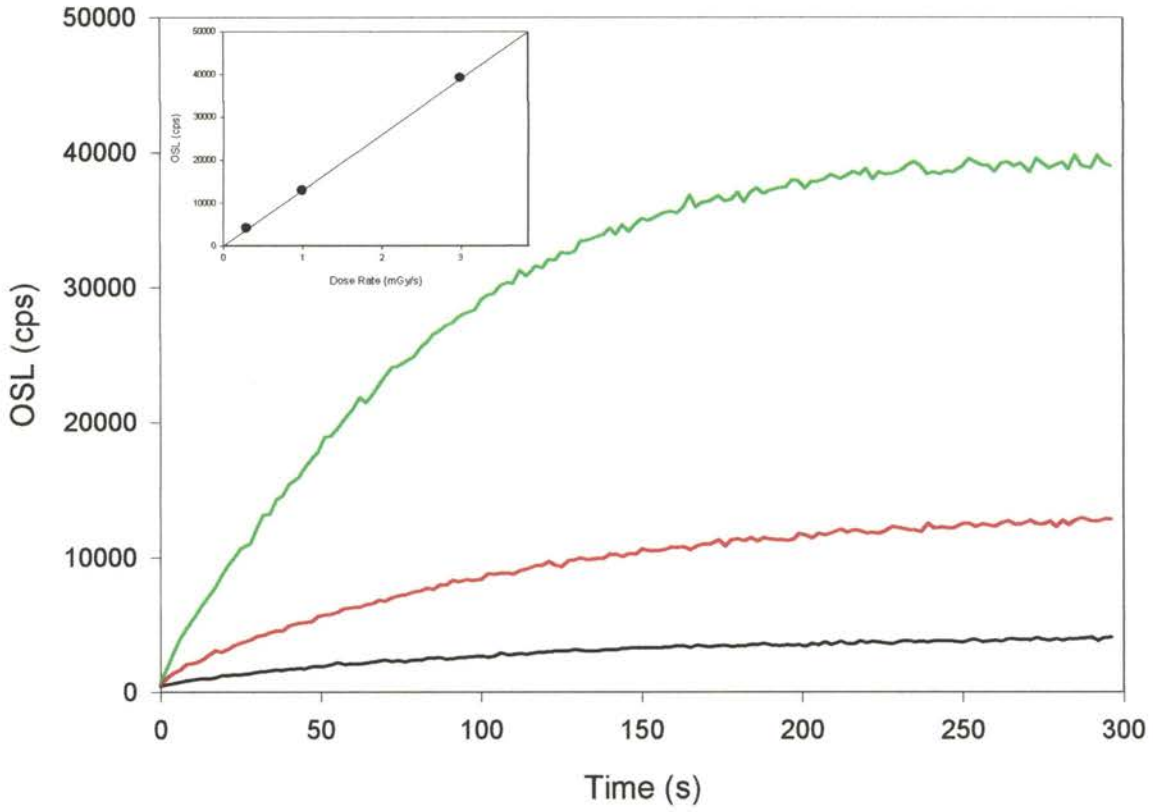

Figure 5-8: The real-time OSL for 0.3 (black), 1.0 (red), and 3.0 (green) mGy/s dose rates. The real-time OSL signals rise to a maximum value, with that maximum value being increasing linearly with dose rate as shown in the inset.

described in section 4.3.2. The depletion factor (D_f) for fiber 31 for a laser power of about 18 mW delivered to the sample from the single fiber reader was measured to be approximately 0.28. Using this value, the correction of the real-time OSL for the lost signal yields a linear dose response that is in agreement with the OSL signal obtained for a standard OSL dose response for the single fiber probe as seen in figure 5-9.

5.3 Clinical Testing of Single Fiber Dosimetry System

The single-fiber dosimeters were tested in a clinical setting with a variety of different sources used for diagnostic and therapy purposes. With these sources, the RL and OSL signals from the single-fiber dosimeters were measured using the single-fiber reader described in section 5.1. From these readings, the relative sensitivity of several single fiber dosimeters of different sizes was measured, and the luminescence and Cerenkov radiation (discussed later in this chapter) produced in the silica fiber optic cables was measured for different energies of incident irradiation.

5.3.1 Calibration of Sensitivity for Single Fiber Dosimeters

After assembly of the fiber dosimeters, the relative sensitivity of each was measured using a ^{137}Cs calibration source. The RL and OSL from fiber dosimeters with different sized pieces of fiber 31 were measured and the relative intensities of the signals compared. The samples were placed inside of a medical water phantom (a 12x24x24 cm plexiglass container filled with water with apertures to insert the dosimeters at different depths), which was placed in the ^{137}Cs beam. The samples were given a dose of 500 mGy at a dose rate of 0.425 mGy/s. During irradiation the RL was measured for each sample and upon completion of irradiation the laser was turned on, and the OSL was

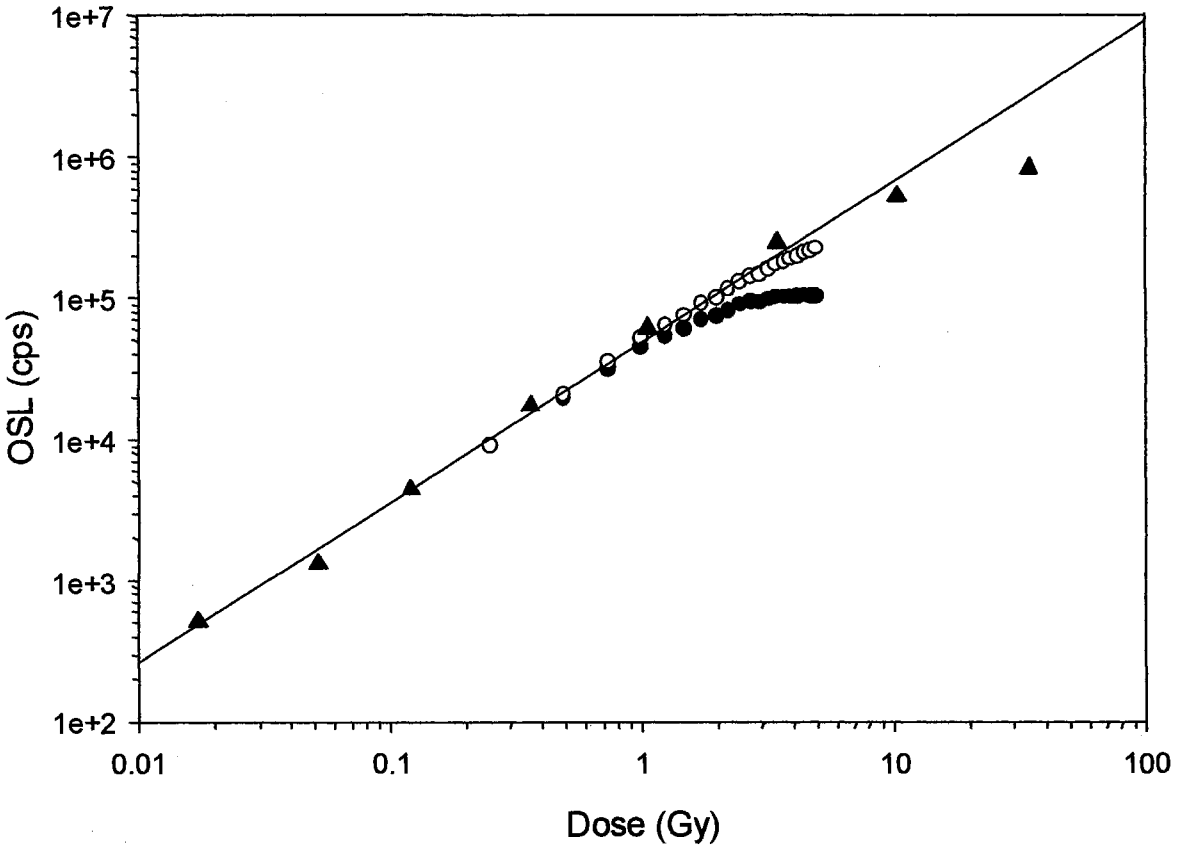

Figure 5-9: Comparison of the real-time OSL (filled circles) to the standard OSL (triangles) as a function of dose. The real time OSL signal can be corrected for the depletion of the OSL signal due to laser stimulation giving a linear response as a function of dose for the real-time OSL signal.

measured by integrating the signal for one second as the signal was bleached to background.

The relative sensitivities of the single fiber dosimeters are shown in figure 5-10. The three different-single fiber dosimeters studied in these measurements were: a 6 mm long, 550 micron diameter piece of fiber 31 attached to a 3 meter, 600 micron diameter fiber optic cable (6-550-3), a 3 mm long, 550 micron diameter piece of fiber 31 attached to a 3 meter, 600 micron diameter fiber optic cable (3-550-3), and a 6 mm long, 350 micron diameter piece of fiber 31 attached to a 3 meter long, 400 micron diameter fiber optic cable (6-350-3). These fibers all showed similar RL intensities with the signal being greatest for the dosimeters 6-550-3 and 6-350-3. The RL signal from these two fibers is approximately twice that from 3-550-3. The OSL from these samples however, showed a much greater range in the maximum intensity of the signal. The maximum of the OSL signal is lowest for 3-550-3 and the intensity for 6-350-3 is approximately twice this level. The maximum of the OSL from 6-550-3 is approximately one order of magnitude greater than the maximum from 3-550-3 and 6-350-3.

5.3.2 Clinical Measurements

The response of the single fiber dosimeters and readout system were tested in a clinical environment at the Lünd University hospital in Malmö, Sweden. For these measurements, the fiber dosimeters were exposed to varying dose rates of x-rays and electrons of different energies using the hospitals' Varian 2100C CLINAC linear accelerator used for patient radiotherapy. For each of the measurements, the fibers were given a typical dose for a single radiotherapy treatment of 500 mGy, for a range of dose rates corresponding to those typical of radiotherapy treatments.[88] The dose rate

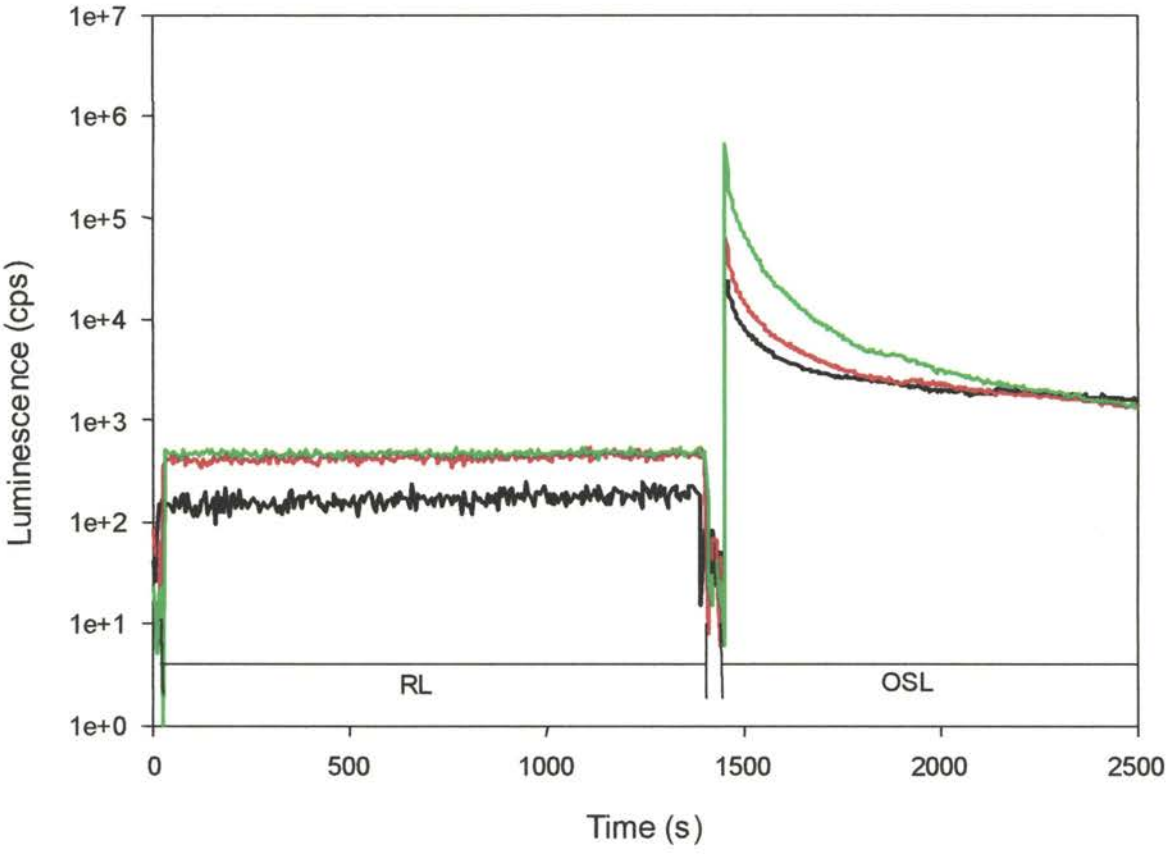

Figure 5-10: Relative sensitivity of three single fiber dosimeters in a medical ^{137}Cs calibration facility. Shown are the relative RL and OSL signal for dosimeters constructed with pieces fiber 31 that are 3 mm long, 550 micron diameter (black), 6 mm long, 550 micron diameter (red), and 6 mm long 350 micron diameter (green).

dependence of the fiber dosimeters was measured for dose rates of 12, 40, and 53 mGy/s using 6 MV (2 MeV peak energy) photons from the linear accelerator to irradiate the fiber dosimeters. The dependence of the RL and OSL signal on the energy of the incident irradiation was measured by irradiating fiber dosimeter 6-550-3 with a dose of 500 mGy at a dose rate of 40 mGy/sec for 0.66 MeV photons from a ^{137}Cs calibration beam, 6 MV (2 MeV peak energy) photons, 18 MV (6MeV peak energy), and 20 MeV electrons from the linear accelerator. All of the clinical experiments were performed by placing the fiber dosimeters inside of a Gammex RMI 457 solid water phantom during irradiation, in order to simulate the dose received by a patient during treatment.[91]

Cerenkov radiation in a medium of refractive index *n* results from a charged particle passing through that medium with a velocity greater than the phase velocity of an electromagnetic wave in the medium.[92] The Cerenkov radiation produced in the fibers was measured for each measurement. For each irradiation, a significant Cerenkov signal was measured due to the energies of the incident irradiation being above the Cerenkov threshold for silica fibers of 190 keV.[93] The emission band of the Cerenkov irradiation appears in two main bands centered at 400 and 450 nm for silica fibers.[94,95] Since these emission bands lie in the wavelength range of the measured Al_2O_3 F center emission (420 nm), the signal measured during an RL measurement will actually be the combination of the Cerenkov radiation and the radioluminescence signal. Therefore, in order to accurately measure the intensity of the RL signal the Cerenkov radiation must be measured and subtracted from the total measured signal to yield the intensity of the RL. To do this, the Cerenkov radiation was measured by placing a bare silica fiber (with no Al_2O_3 fiber attached to it) into the solid water phantom, and measuring the luminescence

signal for each energy of incident irradiation and dose rate. A plot of the intensity of the Cerenkov radiation for the different energies of incident irradiation used is shown in figure 5-11. For the clinical luminescence measurements, the cerenkov radiation represents a significant percentage of the total signal. For these measurements, the Cerenkov signal was only present for the RL measurements since the OSL was measured after completion of the irradiation. The Cerenkov signal also demonstrates a significant energy dependence with the signal for 6 MeV photons being an order of magnitude greater than the two lower energies.

The energy dependence of the dosimeters was measured using fiber probe 6-550-3 for the different energies of incident irradiation. For each measurement, the RL was measured during the irradiation, and the OSL was readout afterwards. For each measurement, the OSL signal was completely bleached to background before the next measurement was made. Figure 5-12 shows the RL and OSL response for the different irradiation energies. In figure 5-12, the average of the RL during the measurement is plotted for each energy, and the maximum of the OSL intensity is plotted for each energy. Both the RL and OSL signals display an energy dependence over the range of energies studied. The response appears to show a decrease in the response of both the RL and OSL between 2 MeV and 6 MeV. For the OSL this is a decrease of about 12.5 % of the total signal, and a decrease of about 33 % for the RL signal. The energy dependence of the RL and OSL Al_2O_3 is expected to be relatively flat over the range of energies tested.[96] The measurements of the RL and OSL for different energies were all performed at the same dose rates and irradiating the fibers with the same total dose. The fibers were tested for a change in sensitivity to 6 MV photons for the last experiment performed with

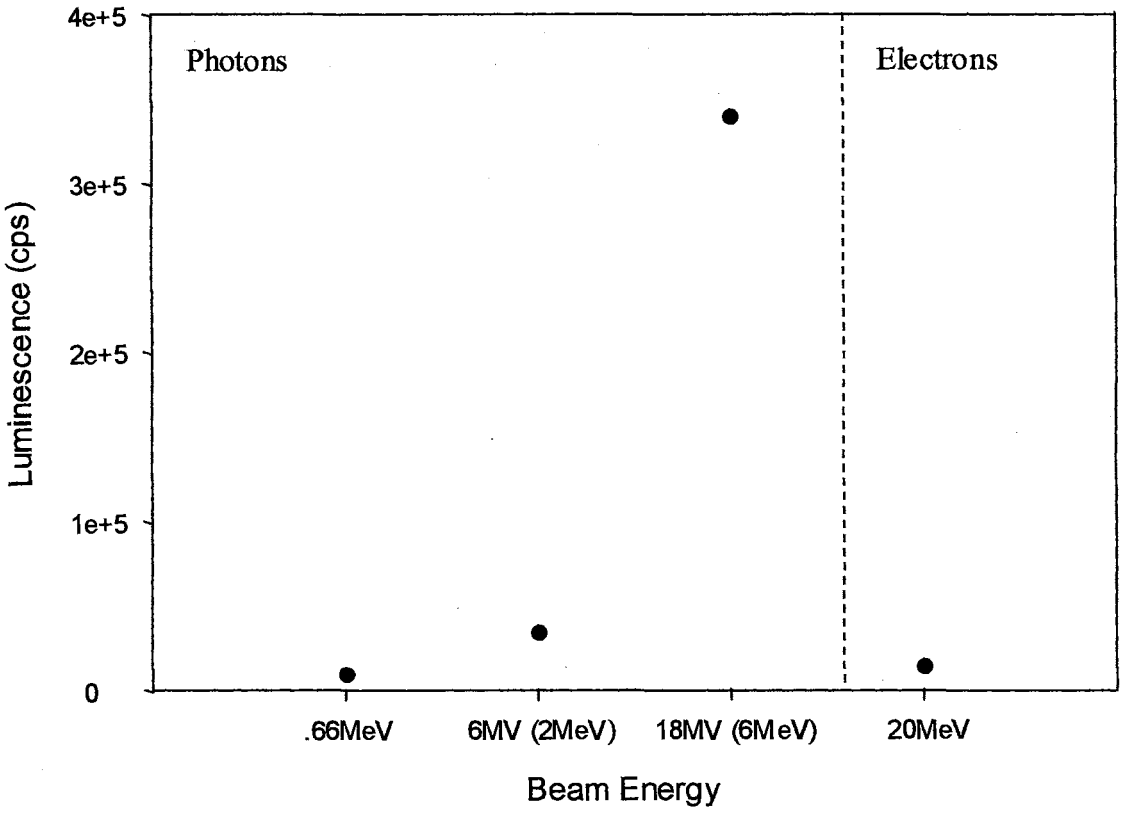

Figure 5-11: The Cerenkov radiation intensity in a bare silica fiber with no Al_2O_3 fiber attached to it for different energies of incident irradiation.

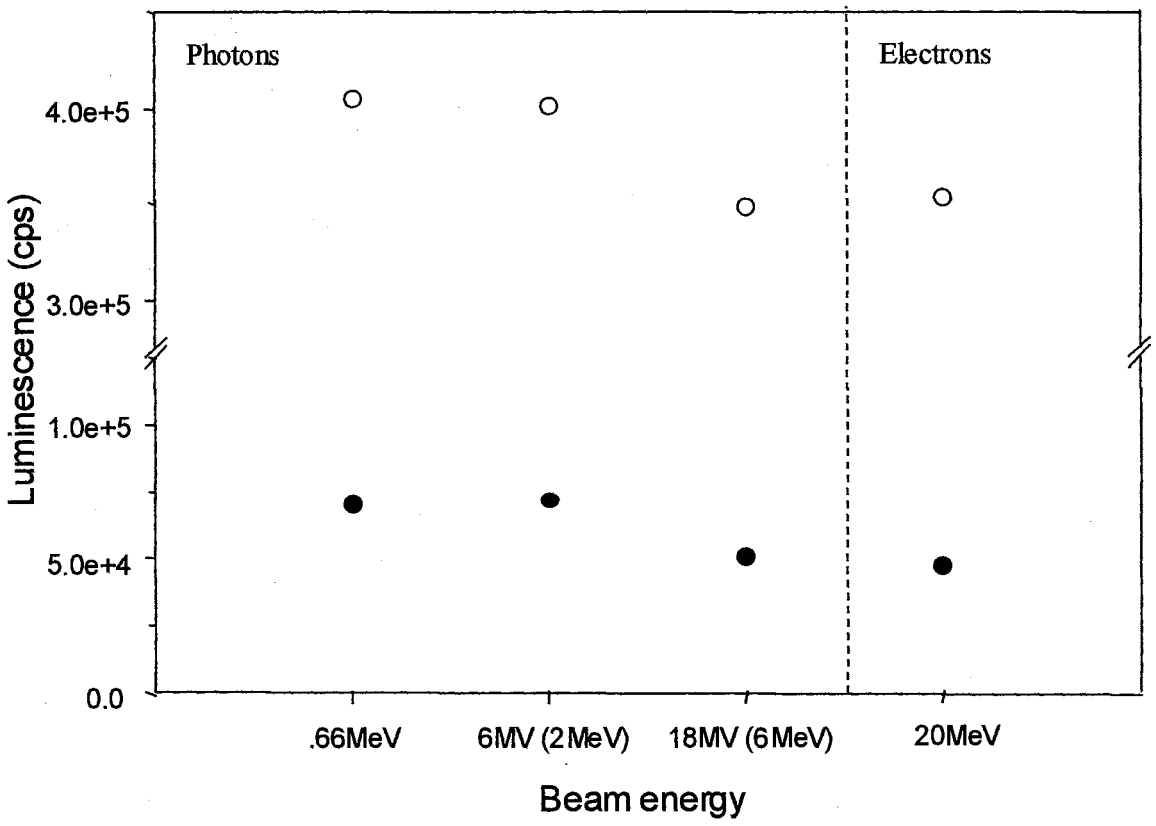

Figure 5-12: Energy response of RL (filled circles) and OSL (open circles) for the single-fiber dosimeter for a range energies used for clinical radiotherapy treatments.

the LINAC. The results of the RL and OSL from these measurements were compared. The differences in the RL and OSL signals from the first measurement to the last was less than 3 %, which is much less than the change seen in the RL and OSL signals for different energies.

The dose rate dependence of the fiber dosimeters was measured using fiber dosimeter 6-550-3 for the each dose rate investigated. The single-fiber dosimeters were inserted into a $^{90}S/^{90}Y$ beta source at the Risoe National Laboratory, and RL and OSL measured for different dose rates. For the dose rate measurements, the RL was measured during the irradiation, and the OSL was readout immediately after the irradiation had finished. Figure 5-13 shows the RL and OSL arbitrarily normalized to the signal measured at a dose rate of 53 mGy/s. The RL increases linearly with dose rate over the range of dose rates tested. This result is in agreement with the measurements made with the $^{90}Sr/^{90}Y$ source in the OSU laboratory discussed in section 4.2.3. Also, the OSL measurement is constant for the constant dose delivered to the sample at each different dose rate.

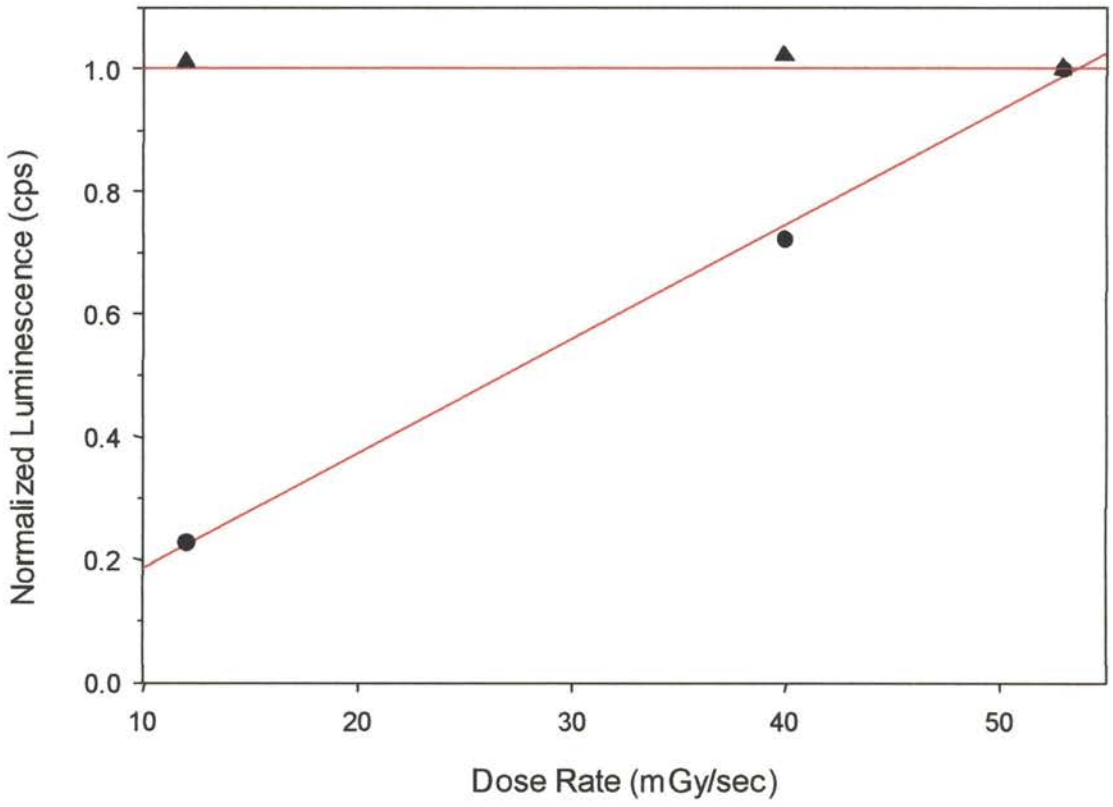

Figure 5-13: The dose rate dependence of the RL (circles) and OSL (triangles). The RL shows good agreement with an increasing line with a slope of unity (red line) and the OSL show good agreement with a flat line with a zero slope (red line).

CHAPTER 6

6. Conclusions and Future Work

6.1 Summary

The results of a detailed study of the luminescence and radiation dosimetry properties of Al_2O_3 fibers has been presented in this thesis. The fibers were grown by either the Stepanov or the Laser Heated Pedestal Growth methods. The photoluminescence spectra of the fibers were measured to gain an understanding of the emission centers present in both the annealed and irradiated samples. Within these samples, emission due to F and F^+ centers (neutral and singly charged oxygen vacancies) was observed from both the irradiated and unirradiated samples. Also in some samples, emission due to Cr^{3+} impurities was present, as well as an emission band centered at 540 nm thought to be due to F_2^{2+} vacancy centers (a doubly charged cluster of two oxygen vacancies).

The OSL (measured at the emission wavelength of the F center) of the samples was measured after irradiation. The OSL signal showed an initial increase up to a maximum signal followed by decay of the signal. The initial increase in the OSL is caused by the large concentration of shallow traps in the samples that act as competitors to the recombination process as discussed in section 2.3.2. The beta dose response of the OSL signal showed a linear response over ranges varying from a lower limit of about 0.005 Gy to a maximum limit of about 10 to 30 Gy depending on the sample.

The charge trapping states in the fibers were investigated through the measurement of TL and OSL. All the fibers, except fiber D, contained a large

concentration of shallow, thermally unstable charge traps, and all fibers (including fiber D) contained a large concentration of thermally stable traps related to the main TL peak centered between 180 and 200 °C depending on the sample. It was inferred, that all the samples contained a large concentration of thermally disconnected, deep electron and hole traps. The main contribution to the overall OSL signal from the shallow traps was seen to come from the charge traps responsible for the main TL peak in the samples by comparing the size of the TL peak after bleaching of an irradiated sample to that from an irradiated sample. Also, the contribution to the overall OSL from the deep traps in the samples was monitored by measuring the OSL signal from the fibers after the shallow and main OSL traps had been thermally emptied. The OSL signal from the deep traps varied greatly from sample to sample with the percentage of the overall signal coming from the deep traps being almost 0 % for fiber 1 and about 10 % for rod 1.

Changes in the sensitivity (as defined by the OSL resulting from a standard beta test dose) was tested for each fiber. The OSL sensitivity was measured for each fiber with all traps empty, with deep electron traps filled, and with all deep traps filled. The OSL sensitivity increased when the deep electron traps were filled. Also, the supralinear behavior of rod 1 disappeared with all the deep electron traps full giving rod 1 a linear dose response up to a dose of about 30 Gy. This effect was interpreted as being due to the reduction of competition during trap filling and recombination.

The luminescence produced by the fibers in real-time during irradiation was also studied. The real-time luminescence was modeled and found to be the sum of the RL and OSL signals produced by the Al_2O_3 fibers. To measure the real-time luminescence signals, the Al_2O_3 fibers were attached to the single end of a bifurcated

silica fiber optic cable, with the other ends of the fiber optic cable connected to a laser and a photomultiplier tube. Both the RL and real-time OSL signals were seen to exhibit a signal that increases over time to a maximum value, with the maximum value dependent on the dose rate. For the range of dose rates investigated, both the RL and real-time OSL maximum increased linearly with dose rate. The real-time OSL signal initially increased linearly with the measurement time, but the signal saturates at a maximum level due to the simultaneous depletion of trapped charge during the measurement process. The maximum level of the real-time OSL was determined to be related to the number of charge traps emptied by the laser stimulation during the OSL measurement as well as being related to the number of charge traps filled during irradiation between successive OSL measurements. Saturation of the real-time OSL signal was determined to be reached when the number of charge traps emptied by each OSL measurement is equal to the number filled by irradiation between measurements. From this, the maximum level of the real-time OSL was shown to be independent of the laser power. The percentage of charge depleted by the laser stimulation was determined for each fiber, and with this information, the real-time OSL was corrected for the depletion caused by each measurement. When the real-time OSL was corrected for this depletion, the signal was found to be linear over the same dose range as the standard OSL signal (i.e. measured after the same dose increment).

The Al_2O_3 fibers were used to produce fiber optic dosimeter probes composed of a single (silica) fiber optic cable with a piece of an Al_2O_3 fiber connected to the end. The Al_2O_3 fibers were connected to the fiber optic cables with an index of refraction matching epoxy to minimize the lass due to reflection at the interface of the two fibers. Along with

these fiber optic probes, a portable, single-fiber OSL measurement system was developed in order to measure the luminescence signals from the fiber dosimeters in real-time. The single-fiber dosimeters showed similar characteristics to the bifurcated experimental setup used in the initial tests of real-time luminescence signals. The single-fiber dosimeters had a linear dose response over a dose range from about 0.005 Gy to 10 Gy. The maxima of the RL and real-time OSL signals were found to increase linearly with dose rate. Furthermore, the slope of the RL signal was found to increase linearly in the low dose region of the measurement, and the slope of the signal was seen to increase with dose rate.

The single-fiber dosimeters were then tested in clinical environments by irradiation with diagnostic x-ray and radiotherapy equipment. The dependence of the OSL signal on the angle of incidence of the radiation beam was measured using 140 KVP (37 keV peak) diagnostic x-rays. The angular dependence was seen to be similar for several different Al_2O_3 fibers, with the OSL signal remaining constant for angles of incidence between 45° and 60° and a decrease in the OSL per unit dose for angles greater than this. The fibers were exposed to high energy x-rays and electrons from a clinical linear accelerator to test the response of the fiber dosimeters to different beam energies and dose rates typically used for radiotherapy. The Cerenkov radiation produced in the fibers optic cables due to the high energy particles used for irradiation was also measured. This signal was subtracted from the measured RL signals. The maximum RL and OSL signals from the fiber dosimeters varied by about 25 % over the range of energies tested. The OSL and RL response was a maximum for the lower energy x-rays, and decreased for higher energy x-rays and electrons.

6.2 Future Work and Concluding Remarks

The investigation of the OSL properties of the Al_2O_3 fibers used in this work was a broad based study of many of the material properties important for the production of the OSL signal. However, much work still needs to be done to fully understand many of the OSL properties of the Al_2O_3 fibers. The processes of trap filling and emptying that lead to the linear and supralinear dose response is not fully understood in Al_2O_3. A comprehensive study of this material similar to the study of thermoluminescence in LiF and quartz is necessary to fully understand the interaction between filling and emptying of traps, and competition between trapping and recombination that leads to the different types of dose response curves seen for different Al_2O_3 fibers.[81,86,97] Also, the changes in sensitivity in the material should be better investigated to fully understand the interaction between the prefilling of certain traps and their relationship to the OSL sensitivity of the sample.

A full spectroscopic investigation of the Al_2O_3 fibers is currently underway in order to gain an understanding of the exact types of defects and vacancy centers present in the sample. This will include an investigation of the 540 nm emission seen in fiber 1 in order to explain the appearance of this band when stimulating the sample with 225 and 270 nm light.

The development of the single-fiber dosimeters and the portable OSL reader has led to the ability to measure doses delivered in real-time. The development of a clinically viable real-time dosimeter for use in the real-time measurement of doses delivered to a patient during radiotherapy is the focus of current research at Oklahoma State University, and of collaborators at the Risoe National Laboratories in Denmark. This includes work to optimize the construction techniques used to produce the fiber probes and work to

optimize the single-fiber reader. Also, a method of calibrating the fiber dosimeters and readers to accurately measure the actual dose delivered during the treatment is currently under development at Oklahoma State University in cooperation with the College of Veterinary medicine and St. Francis Regional Medical Center in Tulsa. The long-term goal of this continuing project is the development of a dosimeter probe for use in applications such as the measurement of doses delivered to a patient during radiotherapy and the measurement of environmental radioactivity levels.

REFERENCES

[1] Roesch W.C. and Attix F.H., In *Radiation Dosimetry, Vol.1: Fundamentals* (eds. Attix F.H. and Roesch W.C.) Academic Press (New York) (1968).

[2] Randall J.T. and Wilkins M.H.F., *Proc. Roy. Soc. Lond.*, **184**, 366 (1945a).

[3] Garlick G.F.J. and Gibson A.F., *Proc. Phys. Soc.*, **60**, 574 (1948).

[4] Daniels F., Boyd C.A., and Saunders D. F., *Science*, **117**, 343 (1953).

[5] Horowitz Y., *Thermoluminescence and Thermoluminescent Dosimetry*, vol. 2, CRC Press (1984), Boca Raton Florida.

[6] McKeever S.W.S., *Thermoluminescence of Solids*, Cambridge University Press, Cambridge, (1985).

[7] Trowbridge J. and Burbank J.E., *Am. J. Sci.*, Ser. 4, **5**, 55 (1898).

[8] Curie M., *Radioactive Substances*, Greenwood Press (Westpoint) (1961).

[9] Wick F.G., and Gleason J.M., *J. Opt. Soc. Am.*, **9**, 639 (1924).

[10] Lyman T., *Phys. Rev.*, **48**, 149 (1935).

[11] May C.E. and Partridge J.A., *J. Chem. Phys.*, **40**, 1401 (1964).

[12] Cameron J.R., Suntharalingam N., and Kenney G.N., *Thermoluminescence Dosimetry*, University of Wisconsin Press (Madison) (1968).

[13] McKeever S.W.S., Mosovitch M., and Townsend P.D., *Thermoluminescence Dosimetry Materials: Properties and Uses*, Nuclear Technology Publishing, Ashford England (1995).

[14] Huntley D.J., Godfrey-Smith D.L., and Thewalt M.L.W., *Nature*, **313**, 105 (1985).

[15] Aitken M.J., *Quarter. Geochron.*, **13**, 503 (1994).

[16] Anatov-Romanovskii V.V., Kerium-Marcus I.F., Poroshina M.S., Trapeznikova Z.A., in *Conference of the Academy Sciences of the USSR on Peaceful of Atomic Energy*, USAEC Report AEC-tr-2435 (pt. 1), 239 (1956).

[17] Braunlich P., Shafer D., and Sharmann A., in *Proceedings of the 1st International Conference on Luminescence Dosimetry*, USAEC, **183**, (1967).

[18] Sanborn E.N., and Beard E.L., in *Proceedings of the 1st International Conference on Luminescence Dosimetry*, USAEC, **183**, (1967).

[19] Rao R.P., DeMurcia M., Gasiot J., *Radiat. Prot. Dosim.*, **6**, 64 (1984).

[20] Yoder R.C., Salasky M.R., *Health* Physics, **72**, S18 (1997).

[21] Miller S.D., Endres G.W.R., McDonald J.C., and Swinth K.W., *Radiat. Prot. Dosim.*, **25**, 2010 (1988).

[22] Akselrod M.S. and McKeever S.W.S, *Radiat. Prot. Dosim.*, **81**, 167 (1999).

[23] Paymal J., Bonnaud M., and Le Clerc P., *J. Am. Ceram. Soc.*, **43** No. 8, 430 (1960).

[24] Evans B.D., Sigel Jr. G.M., Langworthy B.J., Faraday J.B., *IEEE Trans. Nucl. Sci.*, **NS-25**, 1619 (1978).

[25] Beuker H. and Haesing F.W., *SPIE 2425*, 106 (1994).

[26] Griscom D.L., Gingrich M.E., Freibele E.J., *Radiat. Eff.*, **65**, 62(1982).

[27] Marshal C.D., Speth J.A., and Payne S.A., *J. Non-Cryst. Solids*, **212**, 59 (1997).

[28] Marrone M.J., *Appl. Phys. Lett.*, **38** No. 3, 115 (1981).

[29] Henschel C., and Kohn O., *IEEE Trans. Nucl. Phys.*, **47**, 699 (2000).

[30] Takada E., Hososno Y., Kakuta T., Yamazaki M., Takahashi H., and Nakazawa M., *IEEE Trans. Nucl. Sci.I.*, **45** No. 3, 556 (1999).

[31] Justus B.L., Merritt C.D., Pawlovich K.J., Huston A.L., and Rychnovsky S., *Radit. Prot. Dosim.*, **84**, No. 1-4, 189 (1999).

[32] Jones S.C., Sweet J.A., Braunlich P., Hoffman J.F., and Heglund J.E., *Radiat. Prot. Dosim.*, **47**, No. 1-4, 525 (1993).

[33] Braunlich P. F., *US Patent 4,638,163* (1987).

[34] Roy O., Magne S., Gaucher J.C., Albert L., Dusseau L., Bessiere J.C., Ferdinand P., *12th International Conference on Optical Fiber Sensors OFS 97*, Wiliamsburg VA, (1997).

[35] Lindmayer J., *U.S. Patent 5,030,834*, (1991).

[36] Miller R.W., Huston A., Ning H., Worley S., Bevels T., Justus B., and Altemus R., *Radiation and Oncology Sciences Program*, U.S. Navy research report, (1999).

[37] McKeever S. W. S., and Chen R., *Theory of Thermoluminescence and Related Phenomena*, World Scientific, Singapore (1997).

[38] Bube R.H., *Photoconductivity in Solids*, John Wiley & Sons, New York (1967).

[39] Bohm M. and Scharman A., *Phys. Stat. Sol.*, (a)**4**, 99 (1971).

[40] Chen R., Kriastianpoller N., Davidson Z., and Visocekas J., *Luminescence*, **23**, 293 (1981).

[41] Rasheedy M.S., *J. Phys.: Condensed Matter*, **5**, 633 (1993).

[42] Bull R.K., McKeever S.W.S., Chen R., Mathur V., Rhodes J.F., and Brown M.D., *J. Appl. Phys.*, **19** 1321 (1986).

[43] Sunta C.M., Ayta W.E.F., Chubaci J.F.D., and Watanabe S., *Radiat. Meas.*, **35**, 47 (2002).

[44] Lewandowski A.C., and McKeever S.W.S., *Phys. Rev. B*, **43**, 8163 (1991).

[45] Sunta C.M., Watanabe S., *Mater. Sci. Forum 239-241*, **1997a**, 745, (1997).

[46] Dussel G.A. and Bube R.H., *Phys. Rev.*, **155**, 764, (1967).

[47] Kelly P.J. and Braunlich P., *Phys, Rev. B*, **1**, 1587, (1970).

[48] Levy P.W., *Nucl. Tracks Radiat. Meas.*, **10**, 547 (1985).

[49] Levy P.W., in *The Encyclopedia of Physics*, Lerner R.G. and Trigg G.L. editors, 2nd Edition, VCH Publishers, New York, 1264, (1991).

[50] Yukihara E.G., *Doctoral Thesis*, University of Sao Paulo, Sao Paulo Brazil, (2000).

[51] Grimmeiss H.G. and Ledebo L. A., *J. Appl. Phys.*, **46**, 2155, (1974).

[52] Grimmeiss H.G. and Ledebp L.A., *J. Phys.*, **8**, 2615, (1975).

[53] Bailey R.M., Smith B.W., and Rhodes E.J., *Radiat. Meas.*, **27**, No. 2, 123, (1997).

[54] McKeever S.W.S., Botter-Jensen L., Agersnap Larsen N., and Duller G.A.T., *Radiation Measurements*, **27**, No. 2, 161 (1997).

[55] Kotov V.S., Milman I.I., Kirpa V.I., Lesz J., *Radiat. Prot. Dosim.*, **55**, 279 (1994).

[56] Akselrod M.S., Agersnap-Larsen, N., Whitley V., McKeever S.W.S, *Journ. App. Phys.*, **84**, No. 6, 3364 (1998).

[57] McKeever S.W.S., Akselrod M.S., Colyott L.E., Agersnap-Larsen N., Polf J.C., Whitley V.H., *Radiation Measurements*, **84**, No. 1-4, 163 (1999).

[58] Stoneham A.M. and Hayes W., *Defects and Defect Processes in Nonmetallic Solids*, Wiley Interscience Publications, New York City, New York (1985).

[59] Kitis G., Papadopoulus S., Charalambous S., Tuyn J., *Radiat. Prot. Dosim.*, **55**, 183 (1994).

[60] Agersnap-Larsen N., *Docterate of Philosohpy Thesis*, Niels Bohr Institute, University of Copenhagen (1997).

[61] Evans B.D. and Staplebrook M., *Phys. Rev. B.*, **18**, No. 12, 7089 (1978).

[62] Summers G.P., *Advances in Ceramics: Structure and Properties of MGO and Al_2O_3 Ceramics*, **10**, 25 (1983).

[63] Brewer J.D., Jefferies B.T., and Summers G.P., *Phys. Rev. B*, **24**, 6074 (1981).

[64] Caufield C.P and Cooper R., *Phys Rev B.*, **47**, 55 (1993).

[65] Vainshtein I.A. and Kortov V.S., *Physics of the Solid State*, **42**, No. 7, 1259 (2000).

[66] Whitley V.H., *Doctorate of Philosophy Thesis*, Oklahoma State University, (2000).

[67] Lee K.H. and Crawford J.H., *Phys. Rev. B*, **15**, No. 8, 4065 (1977).

[68] Akselrod M.S. and Gorelova E.A., *Radiat. Prot. Dosim.*, **21**, 143 (1993).

[69] Welch L.S., Hughes A.E., and Pells G.P., *J. Phys. C: Solid State Phys*, **13**, 1805 (1980).

[70] Pogatshnik G.J., Chen Y., and Evans B.D., *IEEE Trans. Nucl. Sci.*, **NS-34**, 1709 (1987).

[71] Pogatshnik G.J., Chen Y., and Evans B.D., *J. Liminescence*, **40**, 315 (1988).

[72] Evans B.D., Pogatshnik G.J., and Chen Y., *Nucl. Instr. And Meth. In Phys. B*, **91**, 258 (1994).

[73] Akselrod M.S., Kortov V.T., and Gorelova E.A., *Radiat. Prot. Dosim.*, **47**, 159 (1993).

[74] Yen W.M., *Preparation of Single Crystal Fibers,* in Insulationg Materials for Optoelectronics, Aquello-Lopez F. (Ed.), (Singapore: World Scientific), (1995).

[75] Whitley V.H., *private communications*, Oklahoma State University, (2002).

[76] G.J. Pogatshnik, Y. Chen, B.D. Evans, *IEEE Trans. Nucl. Sci.*, **6**, 1709-1712 (1987).

[77] T. Toyodo, T. Obikawa, T. Shigenari, *Mat. Sci. Eng. B*, **B54**, 33-37 (1998).

[78] G. Molnar, J. Borosay, M. Benabdesselam, P. Iacconi, D. Lapraz, K. Suvegh, A. Vertes, *Phys. Stat. Sol A*, **179**, 249-260, (2000).

[79] Botter-Jensen L. and Mejdahl V., *Nucl. Radiat. Protect.*, **6**, 193 (1984).

[80] Whitley V.H. and McKeever S.W.S., *J. Appl. Phys.*, **87**, 249, (2000).

[81] Chen R. and McKeever S.W.S., *Radiat. Meas.*, **23**, 507, (1994).

[82] Rodine E.T. and Land P.L., *Phys. Rev. B*, **4**, 2701, (1971).

[83] Mische E. and McKeever S.W.S., *Radiat. Prot. Dosim.*, **29**, 159 (1989).

[84] Botter-Jensen L. and Mejdahl V., *Nucl. Radiat. Protect.*, **6**, 193 (1984).

[85] Walker F.D., Colyott L.E., Agersnap-Larsen N., and S.W.S. McKeever, *Radiat. Meas.*, **26**, No. 5, 711, (1996).

[86] Chen R., Yang X.H., and McKeever S.W.S, *J. Phys. D: Appl. Phys.*, **21**, 1452 (1988).

[87] Mayhugh M.R. and Fullerton G.D., *Health Phys*, **28**, 297 (1975).

[88] Powell, S.N., and Suit, H.D., *Radiation Biology for Radiation Oncologists*, in Clinical Radiation Oncology, 2nd edition, Wang C.C. (Ed.), (New York: Wiley-Liss), (2000).

[89] Yukihara, E.G. and J.C.Polf, *private communications*, Oklahoma State University (2002).

[90] McKeever S.W.S. and Akselrod M., *Radiat. Port. Dosim.*, **84**, No. 1-4, 317 (1999).

[91] Chiu-Tsao S.T., Andersen L.L., O'Brein K., and Sanna R., *Med. Phys.*,**17**, 817 (1990).

[92] Jackson J.D., *Classical Electrodynamics*, 3rd Ed., John Wiley & Sons, New York City, New York, (1999).

[93] Jelly J.V., *Cherenkov Radiation and Its Applications*, Pergamon, London, England (1958).

[94] Khanlary M.R., Townsend P.D., and J.E. Townsend, *J.Phys. D: Appl. Phys.*, **26**, 371 (1993).

[95] Beddar A.S., Mackie T.R., and Attix F.H., *Phys. Med. Biol.*, **37**, no. 4, 925 (1992).

[96] Akselrod M.S., Kortov V.S., Kravetsky D.J., and Gotlib V.I., *Radiat. Prot. Dosim.*, **47**, 119 (1990).

[97] Horowitz Y.S., *Nucl. Instr. and Meth. in Phys. Res. B*, **184**, 68 (2001).

VITA 2

Jerimy Clifford Polf

Candidate for the Degree of

Doctorate of Philosophy

Thesis: A STUDY OF OPTICALLY STIMULATED LUMINESCENCE ON Al_2O_3 FIBERS FOR THE DEVELOPMENT OF A REAL-TIME, FIBER OPTIC DOSIMETRY SYSTEM

Major Field: Photonics

Biographical:

Personal Data: Born in Liberal, Kansas, on June 30, 1974, the son of Dewey and Sherrilyn Polf.

Education: Graduated from Liberal High School, Liberal Kansas in May 1992; received Bachelors of Science degree in Applied Physics form Oklahoma State University, Stillwater, Oklahoma in May 1998, received Masters of Science degree in Photonics at Oklahoma State University in May 2000. Completed the requirements for the Doctor of Philosophy degree with a major in Photonics at Oklahoma State University in August 2002.

Experience: Employed in the field of construction from 1992 until 1994 and due to this experience decided to go to college. Employed as an undergraduate Physics teaching and research assistant from 1996 to 1997, and a graduate research assistant for Dr. Stephen McKeever from 1998 to present.

Professional Memberships: Optical Society of America, Society of Physics Students, Phi Kappa Tau National Fraternity, and the Stillwater "Groovers."